uc3m | Universidad Carlos III de Madrid

DOCTORAL THESIS

Analysis, simulation and operation of advanced converter-based railway power supply systems for high-speed lines

Author:

Daniel Serrano Jiménez

Supervisor:

Prof. Dr. Javier Sanz Feito

Electrical Engineering, Electronics and Automation

Leganés, 2018

Acknowledgment

Firstly, I would like to express my gratitude to my supervisor Prof. Dr. Javier Sanz for his support and guidance during the realization of this thesis. Thank you for your strong determination to open new lines of research. It has been an honor and pleasure to work with you.

I would also like to extend my gratitude to the company ELECTREN S.A., for its technical advice and financial aid provided. I wish to thank particularly Felipe Moya for making possible this cooperation between the university and the industry.

Thank you to the Electrical Engineering Department of the Universidad Carlos III de Madrid for giving me the opportunity to grow professionally and personally. Thank you to Maria Angeles Moreno, my supervisor during my degree thesis, and Manuel Garcia, my supervisor during my master thesis. Thank you to Lars Abrahamson and Luleå University of Technology for welcoming me during my research stay.

Thank you to my doctorate fellows, Miguel Angel Garcia, Margeris Jiménez, Ayman Esmat, Francisco Arredondo, Jesús Serrano, Victor Primo, Pablo Tapetado and Miguel Carpintero. This work without all of you would have been much more difficult. Thank you also to Cristina Vega for your kindness. I would like to make an especial recognition to Sandra Castaño for giving me the strength when I needed the most.

Thank you to my family and friends for supporting me in the most difficult moments and for understanding my absences during these four years. Thanks Patricia and Sergio for always believing that this work was possible. Thanks Isabel, Jon and Mónica for showing me what friendship means. Finally, I would like to thank you to David, for bringing the happiness to my life and staying with me despite the difficulties in the path.

Abstract

Railway is a key player in the construction of more efficient and environmentally friendly transport systems. Within the different railway modalities, high-speed lines seem to be attracting special attention due to their velocity, reliability, safety and comfort. At present, these lines are typically electrified by means of conventional transformer-based substations that must be connected to utility grids with high short circuit capacity because of their high energy consumption and their single-phase nature. This fact involves a significant increase in the cost of the electrical installation that seriously limits their advancement.

In this situation, researchers are proposing new electrical power supply systems based on modern electronic power converters capable of minimizing the principal drawbacks of conventional transformer-based configurations. One of the most promising ones are the so-called advanced systems that combines the use of reversible and totally controllable converter substations with a continuous catenary scheme. These systems enable not only to balance the load, and thus reducing the short circuit capacity of the utility grid needed, but also to perform an optimal control of the power flows within the railway grid. This latter aspect involves a real qualitative leap in railway electrification that allows to align them with the current electrical power system transformation towards smart grids.

The development of simulation tools becomes therefore a crucial factor for the progress of these new electrical power supply configurations. Railway simulation is a complex task due to the singular characteristics presented in these systems that has been aggravated with the new difficulties brought by the advanced schemes. In this context, the thesis proposes a new simulation tool capable of determining with great detail the operation of both conventional transformer-based and advanced converter-based configurations. Using a decoupled model, the tool is divided into two parts.

The first part is devoted to the simulation of the traffic system. It determines the consumption and position of the trains over the time considering the topographic profile of the line, the kinematic limitations of the sections and the dynamic characteristics of the motor and the brake. The second part is devoted to the electrical system simulation. It determines the voltage and current distributions of the conductors, as well as the power flows of both railway grid and electrical grid. To this end, a multiphase power flow based on a modified nodal analysis has been implemented, that includes a mathematical representation capable of integrating the AC and the DC equations. Finally, the power flow has been solved using the complete version of the Newton-Raphson method and a new initialization procedure has been proposed.

The next topic addressed in the thesis has been the study the operation of the advanced systems. In contrast to conventional transformer-based ones, the operation of the advanced systems is determined by the type of control implemented. In this respect, the thesis has developed a control strategy based on the droop approach and valid for both alternating current and direct current. This strategy distributes the electrical power according to the distance between the trains and the substations, but it is capable of increasing or decreasing the degree of cooperation between traction substations depending on the conditions of the utility grid without the need of communication between their elements. In the case of alternating current, it is necessary a communication system that synchronizes the angles of the converters. Finally, the effectiveness of the control strategy has been validated by the simulation tool previously described and compared with the operation of the conventional transformer-based systems for a simple electrical scheme.

Finally, the simulation of a complete high-speed line has been carried out, specifically the Spanish line connecting the cities of Madrid and Valencia. This analysis has made it possible firstly to verify the robustness of the simulation tool and the effectiveness of the control system for larger and more complex systems. Secondly, it has allowed to analyze the feasibility and potential of advanced converter-based systems over conventional transformer-based systems for the electrification of high-speed lines.

.

Resumen

El ferrocarril es un actor clave en la construcción de sistemas de transporte más eficientes y respetuosos con el medio ambiente. Dentro de las diferentes modalidades de ferrocarril, las líneas de alta velocidad parecen estar atrayendo una especial atención debido a su rapidez, fiabilidad, seguridad y confort. En la actualidad, estas líneas están normalmente electrificadas mediante subestaciones transformadoras que por su alto consumo y su carácter monofásico deben ser conectadas a redes eléctricas con potencia de cortocircuito altas. Este hecho implica un aumento significativo del coste de la instalación eléctrica que limita seriamente su avance.

Ante esta situación, los investigadores están proponiendo nuevos sistemas de alimentación eléctrica basados en modernos convertidores electrónicos de potencia capaces de minimizar las principales limitaciones de las configuraciones convencionales basadas en transformadores. Uno de los más prometedores son los denominados sistemas avanzados que utilizan una combinación de subestaciones convertidoras reversibles y totalmente controlables junto con un esquema de catenaria continua. Estos sistemas permiten no sólo equilibrar completamente la carga, y por tanto reducir la potencia de cortocircuito necesaria de la red, sino también realizar una gestión óptima de los flujos de potencia dentro de la red ferroviaria. Este último aspecto supone un verdadero salto cualitativo dentro de la electrificación ferroviaria que permiten alinearlos con la tendencia actual dentro de los sistemas eléctricos de potencia hacia redes inteligentes.

La simulación de los sistemas ferroviarios se convierte por tanto es un aspecto determinante para el desarrollo de estas nuevas configuraciones. Se trata de una tarea compleja debido a las características singulares de los sistemas ferroviarios a las que se deben sumarse las dificultades planteadas por los sistemas avanzados. En este contexto, se ha desarrollado una herramienta de simulación capaz de determinar con gran nivel de detalle el funcionamiento tanto de las configuraciones convencionales basadas en transformadores como de las avanzadas basadas en convertidores. Utilizando un modelo desacoplado, la herramienta se divide en dos partes.

La primera parte se encarga de la simulación del tráfico ferroviario, mediante la cual se determina el consumo y posición de los trenes de a lo largo del tiempo teniendo en cuenta el perfil orográfico de la línea, las limitaciones cinemáticas de las secciones y las características dinámicas del motor y freno. La segunda parte se encarga del sistema eléctrico calculando las distribuciones de tensión y corriente de los conductores, así como los flujos de potencia tanto de la red ferroviaria como de la red eléctrica. Para ello se ha implementado un flujo de potencia polifásico basado en un análisis nodal modificado con una formulación capaz de integrar las ecuaciones de corriente continua y alterna. Finalmente, el flujo de potencia se ha resuelto utilizando la versión completa del método de Newton-Raphson y se ha propuesto un nuevo procedimiento de inicialización.

El siguiente tema abordado en la tesis ha sido la operación de los sistemas avanzados. A diferencia de los sistemas convencionales basados en transformadores, la operación de los sistemas avanzados viene determinada por el tipo de control implementado. En este aspecto, se ha desarrollado una estrategia de operación basada en el concepto de droop y valida tanto para corriente alterna como corriente continua. Esta estrategia distribuye la potencia de acuerdo con la distancia entre los trenes y las subestaciones, pero a la vez es capaz de aumentar o disminuir el grado de cooperación dependiendo de las condiciones de la red sin necesidad de comunicación entre las subestaciones. En el caso de corriente alterna, es necesario, sin embargo, un sistema de comunicación que sincronice los ángulos de los convertidores. Finalmente, la efectividad de la estrategia de control ha sido validada mediante la herramienta de simulación anteriormente descrita y comparada con la operación de los sistemas convencionales basados en transformadores para un esquema eléctrico sencillo.

Finalmente, se ha realizado la simulación de una línea de alta velocidad completa, concretamente la línea española que una las ciudades de Madrid y Valencia. Este análisis ha permitido en primer lugar comprobar la robustez de la herramienta de simulación y la efectividad del sistema de control ante sistemas más grandes y complejos. En segundo lugar, ha permitido analizar el factibilidad y potencial de los sistemas avanzados basados en convertidores frente a los sistemas convencionales basados en transformadores en la electrificación ferroviaria de líneas de alta velocidad.

Contents

List of figures

List of tables

Chapter 1

Introduction

1.1 Context and motivation

The transport system is a key player in the development of every society that is undergoing a rapid transformation over the last years driven by the globalization and the steadily increase of the population. In this context, the countries are forced to undertake ambitious transport policies capable of maximizing people mobility while minimizing the negative impact on the environment. To this end, the European Union, in the White Paper on Transport [1] outlined a roadmap composed of forty initiatives based on three fundamental goals: developing of new sustainable fuels and propulsion systems, promoting the use of more energy efficient means of transport and increasing the efficiency of the current transport modes with information systems.

Among these initiatives, the use of electrical railway over other modes of transport is clearly emphasized. As it states, its inherent efficiency, high capacity and reduced carbon emissions make electrical railway one of the key actors for the development of more sustainable transport systems. Regarding high-speed lines, the document sets the goal of completing a European high-speed railway network by 2050. High-speed railway, started developed in Europe in the late 1970s in France and Italy, and subsequently adopted in many other European countries [2]. The first high-speed line commissioned in Spain was in 1992 connecting the cities of Madrid and Seville. After that, many other lines have been deployed, converting Spain into the European country with the largest high-speed network. Figure 1.1 shows all the Spanish railway lines currently in operation.

Figure 1.1. Spanish high-speed railway lines.

According to the International Union of Railways, UIC, high-speed railway lines are defined as those dedicated lines where the trains can operate over 250km/h or conventional lines upgraded to 200km/h. Due to this particular characteristic, these lines require the use of special rolling stock, singular infrastructures and appropriate signaling systems that ensure a reliable, safety and efficient operation. Without doubt, the construction cost is one of the main drawbacks for the promotion an advancement of high-speed railway. High-speed lines are typically electrified by means of conventional transformer-based substations that must be connected to utility grids with high short circuit power capability because of their high energy consumption and their single-phase nature. This fact involves a significant increase in the cost of the installation that seriously limits their development.

In this context, new electrical power supply systems based on electronic power converters are being developed. One of the most promising one are the so-called advanced converter-based systems that are based on the combination of modern reversible and fully controllable converter-based traction substations with a continuous catenary scheme. These systems are not only capable of balancing the power in the utility grid, and thus reducing the short circuit power required, but also to perform an active power management of the whole grid. This latter characteristic represents a real qualitative leap that enables to align the evolution of railway electrification with the electrical power system transformation towards smart grids.

In order to analyze and evaluate the feasibility of advanced converter-based configurations, the development of simulation tools turns into a key factor. Railway simulation is a very challenging task even for conventional railway systems. On the first hand, electrical railway grids are multiphase networks that commonly includes asymmetrical elements, non-grounded connections and unbalanced loads. In addition, they can present both AC and DC electrification schemes. On the other hand, the loads of the system are spatiotemporally, modifying not only their consumption in time but also their location. Finally, the solving algorithm must be carefully analyzed. For example, the low X/R ratio presented in AC schemes makes traditional solving methods prone to fail.

The introduction of advanced converter-based systems has aggravated even more the simulation complexity previously described due to the necessity of including appropriate control strategies that guarantee the efficient and reliable operation of the railway grid. Many different control strategies for converter-based networks have been reported in literature but their applicability to the railway grids have been little explored. To the authors' knowledge there is not any railway simulation reported that includes any control approach for advanced converter-based systems beyond the simple constant voltage approach.

1.2 Objectives

The general objective of this thesis is to conduct a comprehensive analysis and comparison of the operation performance of advanced converter-based electrical railway power supply systems for high-speed lines. Such general and complex objective has been divided into more specific and measurable objectives that are briefly described in the following points:

- The analysis and comparison of the principal electrical railway power supply systems existing and proposed in literature. This study should provide a strong background in railway electrification in order to identify the main drawbacks of conventional configurations and to evaluate the feasibility and potential of the new proposals.

- The analysis and comparison of the principal simulation approaches for the study of the operation of electrical railway power supply systems. This analysis should provide a deep understanding of the principal limitations and benefits of the main models and solving algorithms for the simulation of conventional configurations in order to evaluate their potential and applicability to the advanced converter-based railway systems.

- The development of a simulation tool capable of determining the operation of conventional transformer-based and advanced AC and DC converter-based systems. Regarding the traffic system, the simulator must include a simple but a realistic traffic calculation that considers the topographic data, the kinematic limitations and the motor traction characteristic of the railway line considered. Regarding the electrical system, the tool must be able to calculate the voltage and current of the different conductors of the catenary, as well as the electrical power distributions among all traction substations. Furthermore, they must compute the power imbalance introduced into the grid when needed.

- The development of an operation control scheme for advanced AC and DC converter-based systems. This control schemes must be able to distribute the power efficiently between the traction converters substations according to the traffic conditions existing but being capable of adapting the power sharing under possible utility grid requirements. Finally, the control strategy must minimize the communication between traction substations in order to increase the reliability of the railway operation.

- The analysis and comparison of both conventional transformer-based and advanced AC and DC converter-based systems for a real simulation scenario. This analysis should provide a detail information of the principal mechanical and electrical variables in order to determine the potential and feasibility of advanced converter-based systems over conventional transformer-based systems.

1.3 Dissertation outline

The dissertation has been organized into six chapters. The first chapter introduces the context and motivation of the thesis, describes the main objectives defined and outlines the content of the chapters. Due to the wide variety of the topics covered in the dissertation, there is not a specific chapter devoted to the state of the art. It has been considered more enlightening to distribute the literature review according to the topic addressed on each chapter.

The second chapter provides a comprehensive revision of the principal electrical railway power supply systems existing and proposed in literature. This chapter has been divided into two main parts. The first part is focused on the transformer-based systems. It describes the principal elements found in the conventional configurations and the most important technological solutions reported to enhance their operation: balancing transformers and

converter compensators. The second part is devoted to the converter-based systems. As before, it starts with the description of the conventional configurations and subsequently it introduces the new developments found: advanced AC and DC systems.

The third chapter introduces the principal simulation approaches addressed in literature for the study of railway operation and it presents the simulation scheme followed in the thesis. This chapter has been also divided into two parts. The first part is focused on the traffic system simulation that addresses the movement and power calculation of the trains along the track. The second part is focused to the electrical system simulation that defines the power electrical power and voltage distributions of the elements of the system. Due to the importance of this latter part, it includes a comprehensive analysis of the principal electrical formulations and solving algorithms found in literature discussing their applicability to advanced converter-based systems. Finally, it describes the formulation and the algorithm used for each system in the thesis comprehensively.

The fourth chapter addresses the operation of the conventional transformer-based and advanced converter-based electrical railway power supply systems. It starts introducing the principal standards that regulate the electrical operation of railway systems. Then, it presents the problematic of the operation of advanced converter-based systems, discussing the different control approaches and analyzing their applicability to the advanced railway system. Finally, the chapter describes in depth the control approach proposed in the thesis, analyzing their effectiveness for a simple test case and comparing its performance with the conventional transformer-based operation.

The fifth chapter performs a comprehensive analysis and comparison of advanced and conventional system for a real electrical and traffic scenario. To this end, the Spanish high-speed line that connects the cities of Madrid and Valencia is used as benchmark. This line is conveniently transformed to obtain the corresponding AC and DC advanced configurations. According to the simulation model used, the chapter initially calculates the traffic system performance and concludes with the analysis and comparison of the electrical operation of the three electrical configurations. Finally, the sixth chapter outlines the main conclusions obtained, the original contributions of the thesis, and it provides possible future works to continue the research line initiated.

Chapter 2

Analysis of electrical railway power supply systems for high-speed lines

2.1 Introduction

Electrical railway power supply systems, ERPSS, are defined as the set of elements required to feed the trains with the necessary energy to ensure their proper operation. The type and configuration of these elements have changed significantly over the time driven by the technological developments available at each moment. Historically, the first railway electrifications date back to the late XIX century. They consisted of low voltage DC installations, typically 750-1500V, supplied from the utility grid by means of rotary converters or mercury arc rectifiers. The simplicity of the velocity control of DC motors made this type of systems very convenient at first, but their reduced maximum voltage capability motivated the development of AC electrification.

AC railway electrification arose in the beginning of the XX century with the development of the series-wound DC motors with pole commutator. Although these motors can use AC, they must have a low frequency to prevent sparks during commutations. The necessity of reduced frequency was solved by two different approaches. The first and earlier one was the creation of proprietary transmission systems with their own generation. This topology was adopted in Germany, Austria and Switzerland. The other approach was based on the utilization of rotary converters fed from the utility grid and it was implemented in Sweden and Norway. Both solutions used a nominal voltage of 15kV and a frequency of $16\frac{2}{3}$Hz. Meanwhile, DC electrification continued expanding in other countries like Spain or Italy with a higher voltage, 3kV.

The next milestone in railway electrification came with the inclusion of converters onboard after World War II. This fact made possible the use of high voltage levels at industrial frequency on the catenary, 25kV 25Hz, with DC traction motors on the train. The use of industrial frequency enables to connect the utility grid and the catenary by means of simple transformers and thus, reducing the cost of the traction substation significantly. As a result of this evolution process, there are five electrification schemes at the moment in Europe: 750V DC, 1500V DC, 3000V DC, 15kV 16⅔Hz and 25kV 50Hz [3]–[6].

Currently, most of the new ERPSS for medium and high power demanding applications such as high-speed lines are based on transformer-based configurations. Despite the aforementioned benefits, these systems present important power quality issues that are leading to the development of new technological solutions based on modern power converters. These new systems do not only involve a change in the electrical installation but also in the way that railway systems are operated. The next two sections describe the main conventional configurations and the principal developments found for the transformer-based and converter-based systems [7].

2.2 Transformer-based systems

2.2.1 Conventional configurations

ERPSS are typically divided into five main parts: the generation system, the transmission and distribution system, the traction substations, the catenary system and the electrical traction units. As it was explained before, the possibility of using transformers to feed the railway favored the utilization of the utility grid as generation system. Regarding the transmission and distribution lines, the proprietary and operator of the infrastructure has been changing instead. In some cases, the railway operator was in charge of building and maintaining the lines, while in other cases this role has been adopted by the utility grid operator. The current tendency is towards the latter approach.

The traction substations are the elements in charge of connecting the transmission or distribution system grid to the corresponding catenary system. For high power demanding applications, like high-speed rail, the traction substations must be connected directly to the transmission system. It is usually composed of two transformers in a single bus bar arrangement that provides a reasonable trade-off between flexibility and cost.

In order to reduce the power imbalance in the utility grid, each transformer is typically connected to different phases of the transmission system. This fact requires to divide the catenary into isolated electrical sections separated by neutral zones. Figure 2.1 shows the typical transformer-based arrangements. In the first case, the traction substation is directly connected to the utility grid, while in the second case; there is an intermediate proprietary railway transmission grid.

The catenary system is defined as the set of conductors in charge of transmitting the power to the trains from the traction substations. It is usually composed of many different conductors that are grouped regarding their voltage level. The positive conductors consist of the contact and messenger wires and additional positive feeders when needed. On the other hand, the neutral conductors are composed of the rails and, eventually, return lines. Finally, there is a third group for the negative conductors used in the bivoltage configurations.

The simplest catenary system is the direct feeding configuration. As shown in Figure 2.1, it uses a 25kV single-phase transformer that is connected between the positive lines and the rails. This scheme presents significant voltage drops due to the high resistance of the return path. In order to alleviate this issue, two principal schemes have been proposed. The first one is based on the utilization of an additional neutral conductor and a set of booster transformers whose primary and secondary windings are connected in series with the positive and neutral lines respectively. Finally, the neutral line is grounded between every two booster transformers in order to provide and additional path to the current to flow.

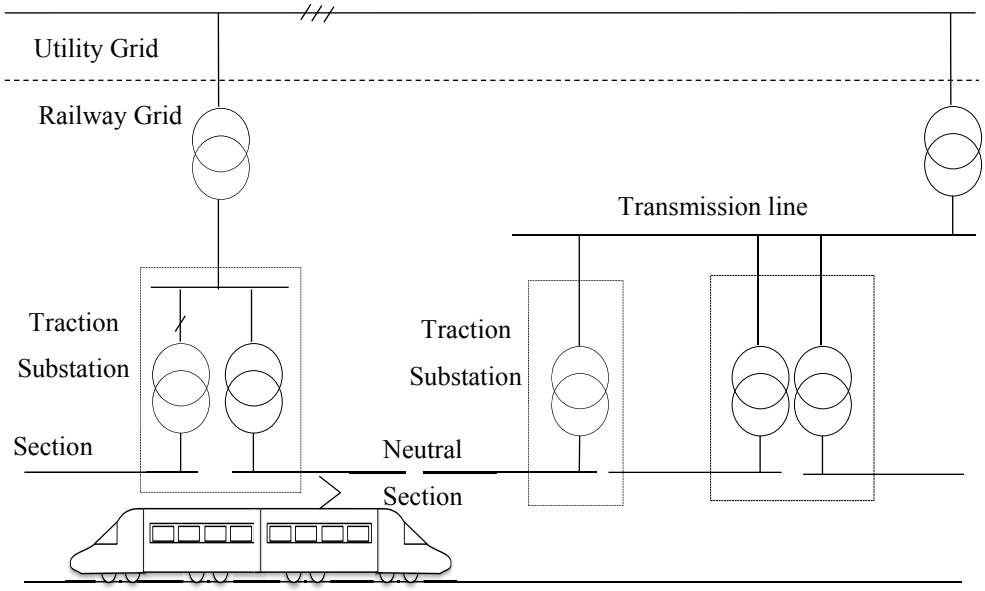

Figure 2.1. Conventional transformer-based configurations.

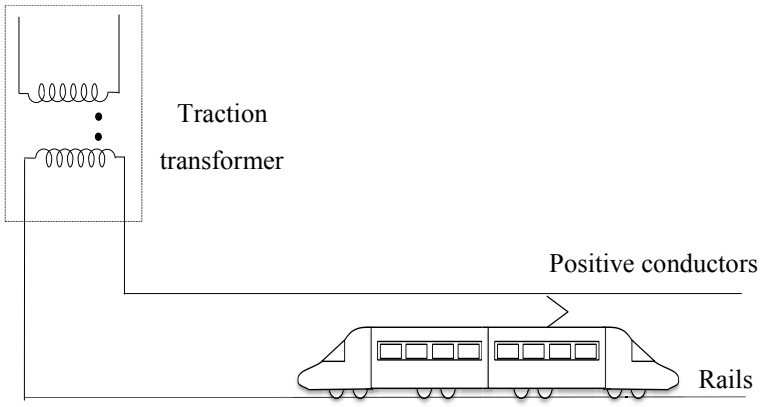

a)Monovoltage, direct feeding scheme.

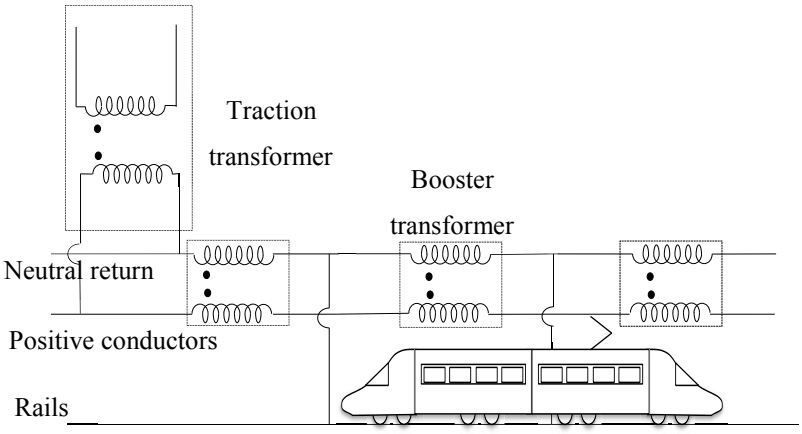

b)Monovoltage, booster feeding scheme.

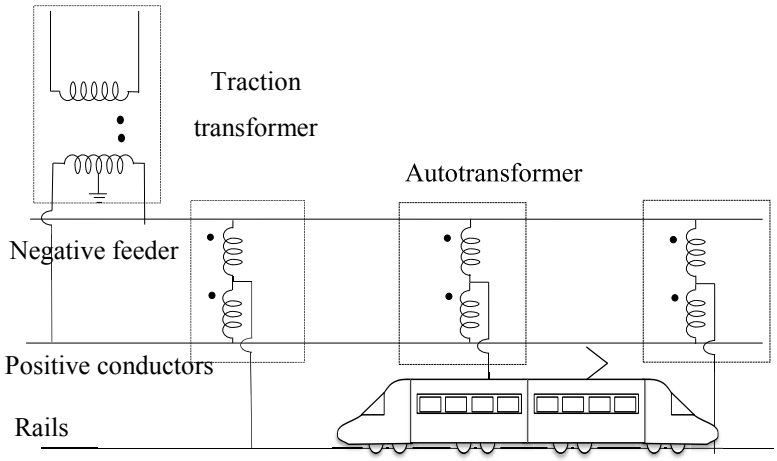

c)Bivoltage, autotransformer feeding scheme.

Figure 2.2. Catenary feeding schemes.

The second scheme is shown in Figure 2.2.c. This configuration uses a single-phase 50kV transformer with a secondary central tap grounded to feed the +25kV positive lines and the -25kV negative line. To reduce the transmission voltage from 50kV to 25kV, a set of autotransformers are placed along the catenary. Since this system uses two different voltage levels, it is also known as bivoltage in contrast to the two previous monovoltage configurations. It is important to highlight, the possibility of using non-symmetrical voltages on the catenary lines.

The electrical traction unit is the last element in the power supply scheme. It is in charge of proving electrical energy to the traction motors from the catenary. The type of these motors has changed significantly over the time. As commented before, the first motors used in railway electrification were DC and single-phase AC motors. Subsequently, with the development of power electronic converters, the use of three-phase AC asynchronous and synchronous motors has become the standard solution adopted due their lower cost and easier maintenance. Finally, it is important to highlight, that the power drawn from the catenary must also include the power of the auxiliary services such as the heating/cooling system or the lighting system.

Despite being the most common electrification scheme now, transformer-based configurations present important issues from the power quality point of view [8]. The power imbalance is perhaps the most important one although the harmonic pollution and the low power factor are also important issues to consider. As it is generally known, the connection of single-phase loads, like railway to three-phase utility grids produces a negative sequence current injection that distorts the voltage. This distortion can lead to a malfunctioning of the electrical equipment when it is not conveniently mitigated. To avoid it, transformer-based railway systems must be connected to utility grids with short circuit power enough to accept such imbalance [9], [10].

Besides the aforementioned power quality concerns, transformer-based configurations have a great obstacle to enhance the efficiency and reliability of the railway operation, i.e. the neutral zones. As commented before, the single-phase transformers of the traction substations are usually connected to different phases of the utility grid that makes necessary to divide the catenary into isolated electrical sections. As commented, it reduces the potential use of regeneration power and impede to feed the trains from different tractions substations at the same time.

2.2.2 Balancing transformers

Balancing transformers are specially connected power transformers capable of producing a balanced system of n phases from a balanced system of m phases. According to [11], this balanced transformation is based on two premises, the existence of a balanced set of electromotive forces in both sides of the transformer and a balanced set of magnetomotive forces on each limb of the transformer.

The four balancing connections most used in railway electrification are: Scott, Le-Blanc, Impedance matching and Woodbridge [12], [13]. As shown in Figure 2.3, these transformers present complex connections that usually require unequal number of turns on each limb to fulfill the two previous premises. These characteristics complicate enormously the manufacturing process and thus, their cost in comparison to conventional transformers.

The study of the voltage imbalance reduction by means of balancing transformers have been comprehensively studied in literature [14], [15]. Most of these works make use of simple formulae to calculate such impact. However, as [16] states, this latter approach can underestimate its real value because it neglects the interaction between the railway system and the electrical system.

In [17], the technical performance and cost comparison of different balancing and conventional transformers is accomplished. It concludes that although Balancing transformers have a higher initial cost, they require less power compensating capacity that results into a lower total investment. Furthermore, Balancing transformers can be an interesting option to reduce the harmonic pollution due to their special connections that can lead to a natural harmonic cancelation [18].

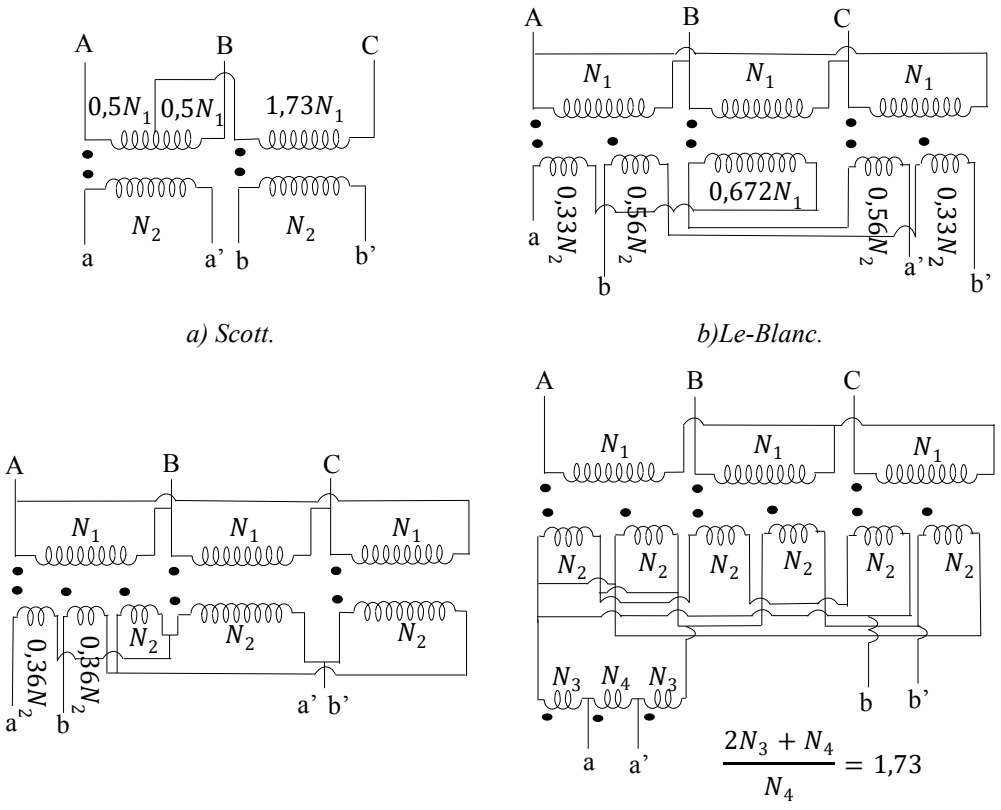

a) Scott. *b)Le-Blanc.*

c)Impedance matching. *c)Modified Woodbridge.*

Figure 2.3. Balancing transformers configurations.

2.2.3 Converter compensators

The outstanding development in power electronics has brought new possibilities to railway electrification. Power converter compensators are very powerful tools to solve the main power quality issues found in conventional transformer-based configurations. The next sections describe the most important power compensators found in literature.

a) SVC

The static VAR compensator (SVC) is an electronic device capable of providing variable impedance by means of their controllable switches, typically thyristors. SVC's can be classified as either thyristor controlled reactor (TCR) when the variable impedance is a reactance or thyristor switched capacitor (TSC) when it is a capacitor [19]. It is also common to add parallel constant impedance branches to cancel certain harmonics.

The most common application of these electronic devices is the voltage control. Rising the voltage level of the catenary makes possible to increase the power transmission capability of the line and thus the number of trains that can be fed in the same section. To this end, a single-phase TSC is placed at beginning or at the end of each section regulating the reactive power injected depending on the voltage of the catenary [20], [21]. The main drawback of this solution is that only provides discrete levels of reactive compensation.

Besides voltage control, SVC's can also be applied to balance the load. To this end, a three-phase SVC in delta arrangement is placed on the utility grid side of the traction substation [22]. As the Steinmetz circuit demonstrates, by simply controlling the reactive components connected to each phase, the system is able to transfer power between phases and so that to balance the load. It is important to take into account the possible resonances between the SVC and the system [23].

b) STATCOM

The advent of high power self-commutated switches such as GTO (gate turn-off thyristor), IGBT (insulated-gate bipolar transistor) or IGCTs (integrated gate-commutated thyristor) provided the development of voltage sources converters (VSCs) and all their potential applications. The static synchronous compensator (STATCOM) is one of them. It consists of a VSC that can provide variable continuous reactive power compensation without the use of large reactive energy storage elements by simply controlling the voltage magnitude. In [24] the utilization of the STACOM is presented to increase the catenary voltage during the railway operation.

As the SVC, the STATCOM can also provide load balancing on the three-phase utility grid [25]. The control technique can be based on the Steinmetz circuit principle but also on the direct power control. This latter approach relies on the statement that only balanced systems without current and voltage harmonics will produce constant instantaneous power. Accordingly, it can provide load balance and harmonic cancelation simultaneously.

c) Railway power conditioner

Another common power converter compensator is the so-called railway power conditioner. As shown in Figure 2.4, this solution consists of a two single-phase VSCs in back to back configuration whose AC sides are connected to different catenary sections by means of step-up transformers [26], [27]. The use of an appropriate coordination control between the converters can solve the problems of power imbalance, harmonic pollution and power factor correction at the same time.

The enhancement efforts of this compensator have been aimed to the simplification of the converter topology. For example, the work presented in [28] proposes the use of a half bridge converter configuration instead of the full bridge topology implemented in its conventional arrangement. This approach reduces the number of switches required by half. Other proposals [29], [30] advocate for replacing the two single-phase converters with a three-phase converter. In this case, the number of switches is reduced from eight to six. Finally, in order to eliminate the use of step-up transformers, there are two recent proposals based on the utilization on a hybrid converter [31] or a modular multilevel converter [32].

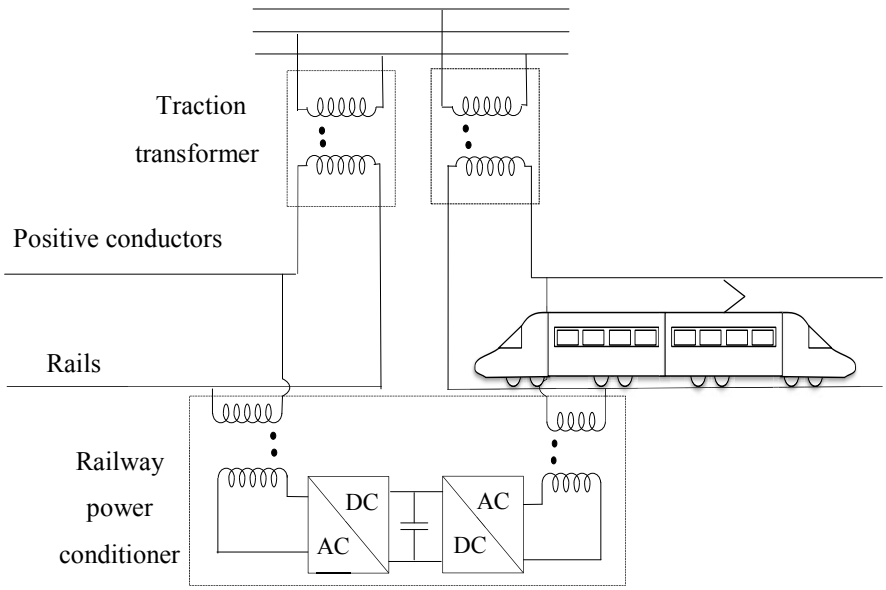

Figure 2.4. Railway power conditioner.

d) Co-phase power conditioner

The co-phase power conditioner [33], [34] can be seen as an evolution of the railway power conditioner that not only can solve the power quality concerns of the conventional transformer-based configurations but also reducing the number of neutral zones. As it is shown in Figure 2.5, it consists of two single-phase VSCs in back-to-back configuration connected in parallel to the traction transformer. Due to the converter possibility of controlling the voltage, the neutral zone at the front of each traction substation can be avoided. This solution can also be implemented using a balancing transformer [35].

There are three main operation modes regarding the element providing the energy. In the normal operation mode, the energy is supplied by both the transformer and the converter. The other two operation modes correspond to degraded conditions or in other words, situations where the traction transformer or the converter conditioner are not available. It is important to highlight, that in the latter situation the power imbalance is not corrected because the converter have a single-phase topology.

In order to reduce the compensation capacity of the converter and thus, its cost, some authors have proposed to combine the co-phase system with passive reactive elements connected in series with the step-up transformers [36], [37]. This approach is known as hybrid co-phase power conditioner and it is shown on the right side of the figure 2.5.

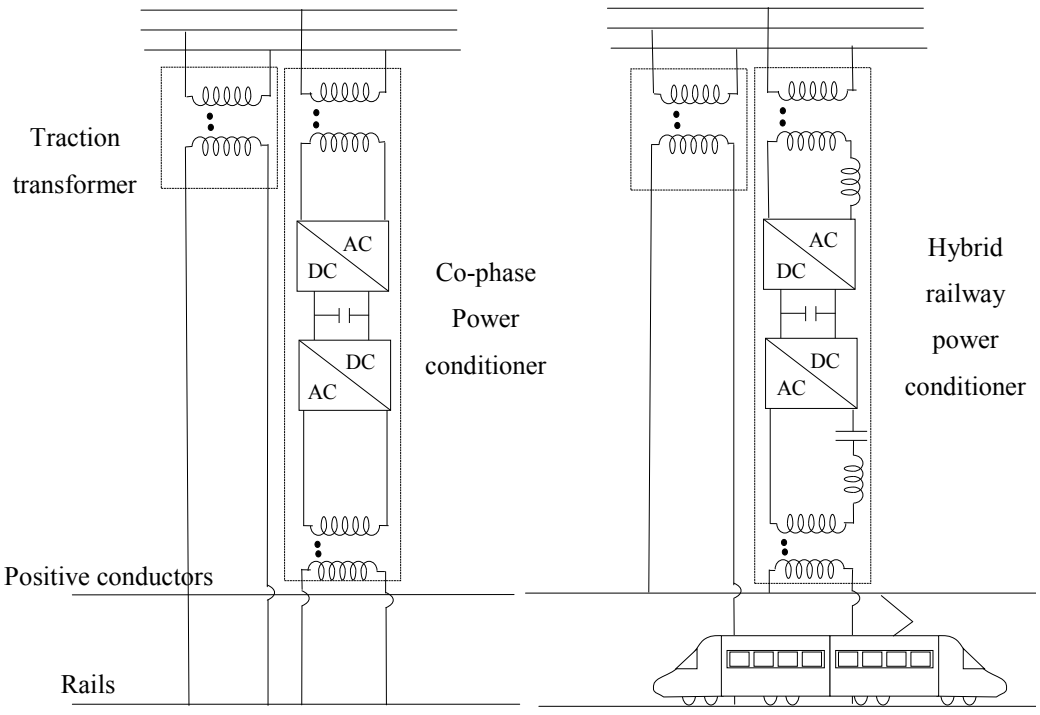

Figure 2.5. Co-phase power conditioner.

2.3 Converter-based systems

2.3.1 Conventional and advanced AC systems

As it was described in the introduction, the difficulties of using AC motors at industrial frequency at the beginning of railway electrification led to development of the AC low frequency railway systems. These systems can be implemented following two different approaches: centralized and decentralized. The centralized approach is based on the utilization on a proprietary transmission line that connects the catenary through a set of traction transformer substations. In this configuration, the electrical power is principally supplied by dedicated power plants, although it can also include some connections to the utility grid by means of traction converter substations when needed. On the contrary, the decentralized approach connects the catenary to the utility grid by means of traction converter substations. It is important to mention the possibility of building a parallel transmission grid to the catenary in order to increase the power transmission capability of the catenary. Figure 2.6 shows the two aforementioned approaches.

Regarding the traction converter substations, there are two possible configurations: rotary and static. Rotary converters were the first to appear and they consist of a three-phase motor connected to a single-phase generator linked together by a mechanical shaft. Depending on the motor type of the converter, the frequency conversion can be fixed or variable. If the motor is synchronous, the frequency conversion is fixed and equals to the ratio between the numbers of poles of the two electrical machines. On the other hand, if the motor is asynchronous, the frequency conversion can be regulated. As it will be discussed later, the type of converter used must be in accordance with the operation scheme adopted in the railway grid.

The high power losses along with the considerable maintenance cost of rotary converters have promoted the utilization of static ones. The first static converters were based on a direct power conversion approach by means of cycloconverters with thyristor valves. Later on, with the development of VSCs with self-commutated switches, the DC link converters have become the standard solution adopted. They consist of a three-phase to single-phase converters in back-to-back configuration. The topologies of these converters have changed significantly over the time. The first approaches were based on the series connection of two-level converters with high power switches. Subsequently, the different multilevel topologies with mature medium power switches [38] [39] [40] have been gaining ground. One of the most promising topology is the modular multilevel converter [41], [42] that can operate without the use of the final step-up transformer [43].

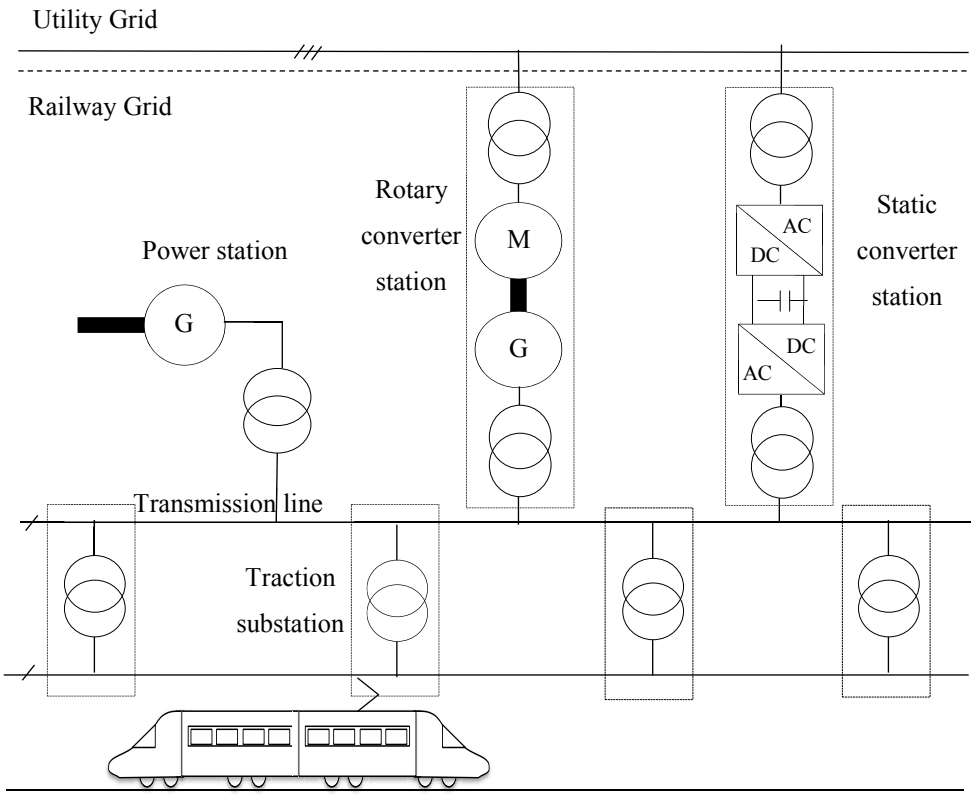

a)Centralized scheme.

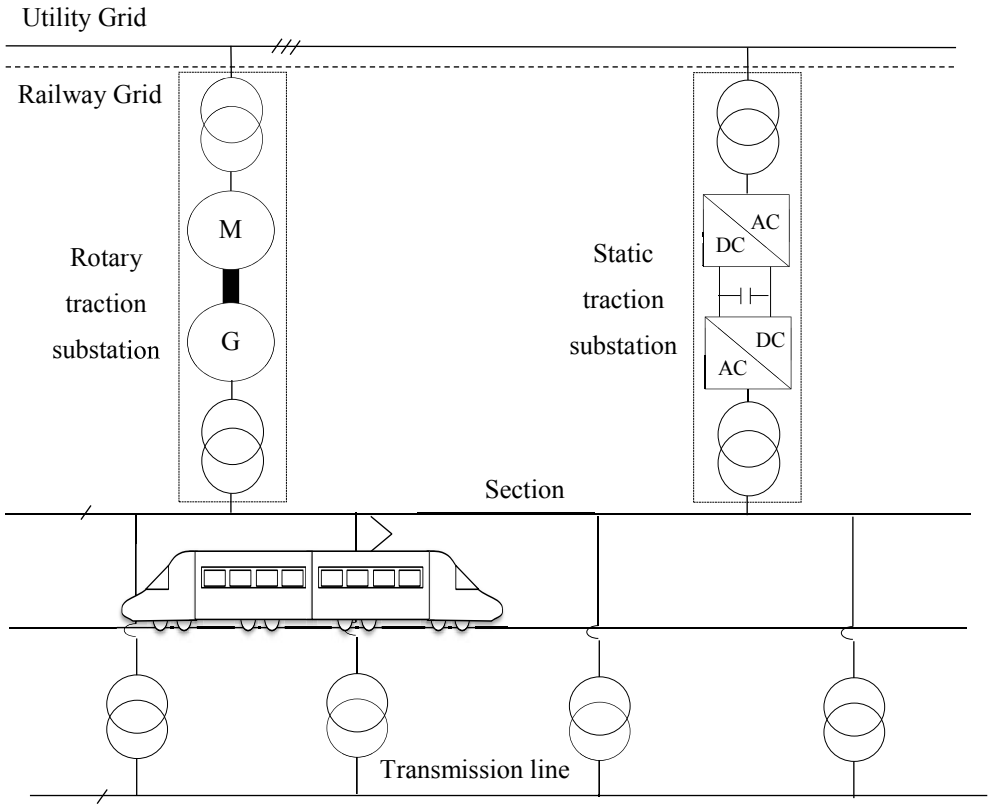

b)Decentralized scheme.

Figure 2.6. Conventional AC converter-based configurations.

In contrast to transformer-based configurations, AC converter-based systems present a non-sectioning catenary that enables to feed the trains from multiple traction substations simultaneously. The parallel connection of these substations requires having approximately the same phase in all of them under no load conditions. This issue is particularly important in case of decentralized systems with synchronous-synchronous rotary converters. As it was previously explained, they perform a fixed frequency conversion and thus, the angle set on the catenary at no load is directly proportional to the angle on the utility grid. In order to avoid possible circular currents, the voltage angle differences must be carefully studied and reduced when needed. Some of the most common measures undertaken to reduce it consist of the addition of series reactors or the utilization of tap changer transformers.

The operation of conventional AC converter-based systems depends on the configuration scheme adopted. In case of centralized schemes, the railway grid is operated asynchronously to the utility grid. It means that the railway operator is in charge of performing the frequency regulation and so that the active power control of the railway grid. In case of having rotary converters connected to the utility grid, they must have an asynchronous-synchronous configuration capable of accommodating the possible frequency variations between the two grids. Alternatively, decentralized schemes are operated synchronously to the utility grid. In this case, the frequency regulation is performed by the synchronous generators of the utility grid, but the active power control is reduced to the existence of static converter stations. This type of configuration requires the use of synchronous-synchronous rotary converters.

With the outstanding development in power electronic converters, the utilization of controllable static converter stations has become a very attractive option for the electrification of high-speed lines. On the first hand, they do not introduce any power imbalance into the utility grid and they can reduce the harmonic pollution and correct the power factor at the same time. On the other hand, they can perform an active power control strategy that can improve the reliability and efficiency of railway systems operation. In the light of these benefits, some authors have proposed the development of 25kV 50Hz advanced converter-based systems [44]–[46]. Despite being decentralized systems, they perform an asynchronous operation to the utility grid and thus, they combine the benefits of both configurations. It is noted, that this approach is aligned with the current evolution of the electrical power systems to smart grids [47].

2.3.2 Conventional and advanced DC systems

Conventional DC systems consist of a set of traction converter substations connected in parallel to a continuous catenary. As shown in Figure 2.7, these traction substations can be directly supplied from the utility grid or they can present an intermediate distribution line. In both cases, there are two main topologies for the traction substation. The first and simplest approach consists of a six-pulse non-controllable rectifier. The second and most extended one is based on the utilization of twelve-pulse non-controllable rectifier. In this later case, the traction substation requires the utilization of a three-phase transformer with two secondary windings in a wye and delta arrangement.

The use of diode rectifier substations is an important limitation that seriously impedes to reduce the cost of the installation and to enhance the railway operation. On the first hand, diode rectifiers cannot maintain the voltage fixed on the catenary, increasing the number of substations required. On the other hand, they do not allow a bidirectional power flow, reducing the potential of regenerative braking. In this context, railway engineers have proposed to replace the diodes with more advanced power switches. The thyristor rectifier converter is the most common approach encountered. In order to have a bidirectional power flow, the traction substations must include two three-phase thyristors rectifiers in antiparallel arrangement. More recently, VSC converters substations have been gaining ground. Their fully controllable power switches simplify the traction substation to a single power converter, but their high price is still a great barrier for most applications.

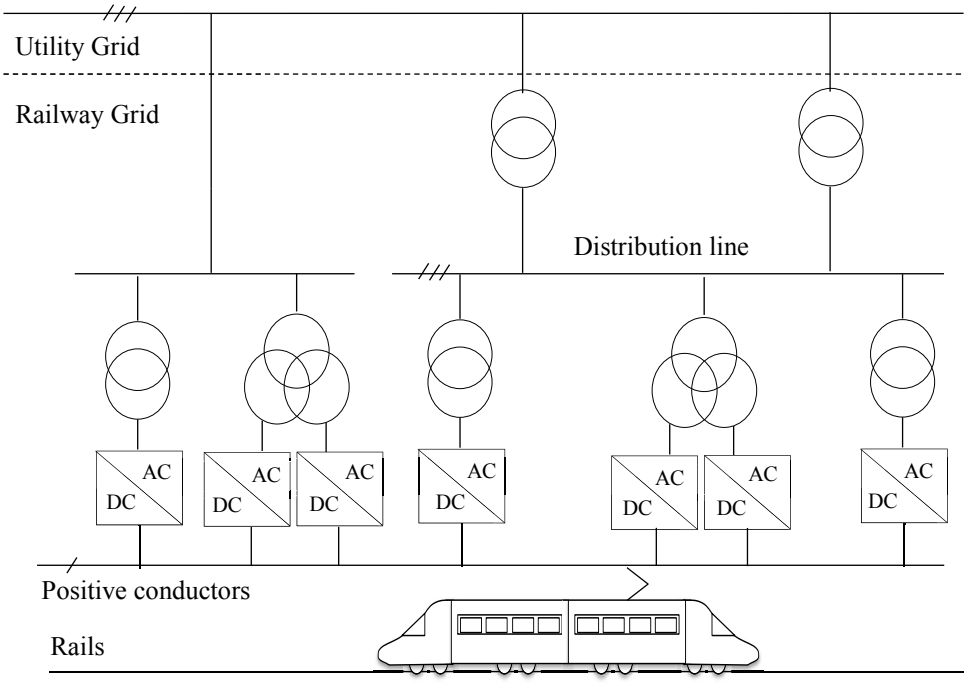

Figure 2.7. Conventional DC converter-based configurations.

Despite all the advantages brought by the new controllable traction substations, the low voltage magnitude accomplished so far reduces their application to low power demanding purposes. The idea of increasing the catenary voltage has been considered in many occasions in the past [48], but the cost and capabilities of the power electronics switches have always impeded it to thrive [49], [50]. It was only recently, with the outstanding developments achieved in high voltage direct current transmission grids when this idea has been gaining strength again.

In the work presented in [51], the authors propose a medium voltage DC converter-based system to feed a high-speed railway line. This approach is very similar to the advanced AC converter-based systems and so that, this will be named as advanced DC converter-based systems hereafter. These configurations have the same advantages presented in AC advanced systems, such as, active power control, load power balancing, harmonic pollution reduction or voltage support. However, the use of DC provides additional benefits and some drawbacks. The two most important advantages are the line losses reductions and the simplification of the control. On the downside, the fault clearance capacity is still an issue under research despite the great advances that have recently been made.

Finally, DC systems can also have the possibility of having bi-voltage catenary configuration for DC electrification schemes. In order to achieve it, the autotransformer stations used in AC must be replaced with equivalent autoconverter DC/DC ones that redistribute the current between the feeder lines. It also important the necessity of including a DC/DC converter at the front of each traction substations to guarantee a balanced DC voltage operation [52].

Chapter 3

Simulation of electrical railway power supply systems for high-speed lines

3.1 Introduction

Simulation methods are one of the most powerful tools in the study of the operation of electrical railway systems due to the low cost and great flexibility provided. For operation studies, the simulation of ERPSSs is typically divided into two main parts: the simulation of the traffic system, that defines the movement of the trains, and the simulation of the electrical system, that determines the power flow distribution. Both systems are naturally coupled, since the tractive force of the motor not only depends on the position and velocity of the train, but also on the voltage of the catenary and thus, the movement of the train cannot be calculated until the available power is defined. This coupling has also been aggravated due the restrictive operation controls imposed to the trains, such as the current limitation that sets a maximum power consumption depending on the voltage.

According to the previous information, the simulation of ERPSSs requires a co-simulation of the two systems where they are solved sequentially over the time considered. Figure 3.1.a. shows a general flowchart of the main parts included into a conventional simulator considering the traffic and electrical system coupling. The traffic system simulation is divided into three main parts. On the one hand, the mission driving curves calculation defines the driving characteristic for the trains of the railway line regarding the optimization objective desired. On the other hand, the Automatic Train Control, ATC is responsible for the calculation of the reference signals for the motor and for the brake. It

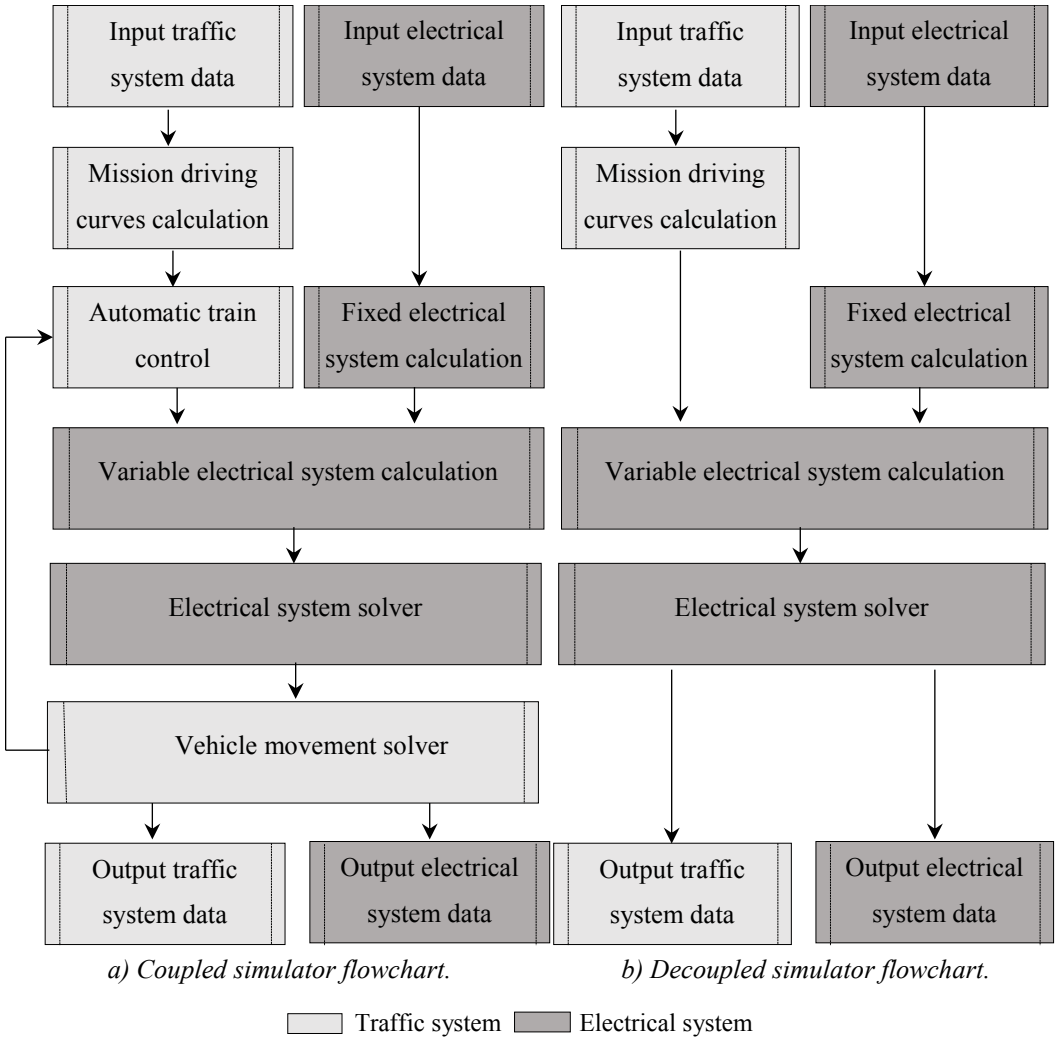

Figure 3.1. Simulator approaches.

can also include the possibility of incorporating external signals from the signaling system or from the driver [53]. Finally, the train movement calculation computes the new position and speed of the train according to the available power determined.

Regarding the electrical system simulation, there are three different approaches in literature depending on how the variable system topology is addressed. The first one and most evident is based on the recalculation of the system configuration. As shown in Figure 3.1.a, the electrical system is divided into fixed elements, which does not need to be updated and variable elements, which they do. This approach only includes the minimum number of elements, but it requires reformulating the system at every time step. The second approach is to discretize the catenary [54]. It does not change the number of nodes and their corresponding parameters during the simulation, but it requires to define a large number of nodes especially when high accuracy is required. The last approach make use of the graph theory, and it can be considered as an intermediate solution in the sense that it keeps the

topology of the system invariant but it includes more elements than needed for the formulation [55].

The previous simulation scheme can globally describe the structure of the principal commercial railway simulators such as OpenPowerNet/OpenTrack® [56] or Sytras Sidytrac®. The use of commercial simulators provides a friendly and reliable option but the low flexibility to include new elements and functionalities along with the high price represent a great barrier for academic purposes. In this context, researchers face the complicate challenge of development customized railway simulators according to their specific requirements.

Academic railways simulators have two main approaches depending on the relation between the traffic and electrical system adopted. The first one is in line with the coupled model previously described. Some examples are [57] or [58]. The second and most extended approach is based on a decoupled simulation scheme similar to Figure 3.1.b. It assumes that the traffic system is not affected by the electrical system state. Accordingly, the references generated by the ATC are always achieved, and so that, the real driving curves coincide with the mission driving ones. Some examples are [59], [60].

All simulators found in literature were able to determine the performance of conventional railway configurations with a greater or lesser level of detail, but none of them included any advanced scheme. Under such circumstances, the research was partially focused on the development of its own railway simulator capable of including both conventional and advanced systems. The next sections describe comprehensively the railway simulator created. It is based on a decoupled approach and the recalculation of the electrical system topology for the different traffic conditions. Its general configuration can be described by Figure 3.1.b.

3.2 Traffic system simulation

The traffic system simulation aims to determine the position and power consumption of the trains over the time. As mentioned before, the decoupled approach reduces the traffic simulation to the calculation of the mission driving curves of the trains. This task is typically divided into two parts. In the first part, the movement of a single train is studied. It must be carried out for each type of train and for each direction of the railway line. In the second part, the simulation results obtained are extrapolated to the different trains existing according to the traffic timetable. It is noted that this approach neglects the signaling system interaction.

3.2.1 Traffic system modeling

The most common train model is based on the point mass representation. Despite its simplicity, this model is adopted by many railway simulators because it has a good trade-off between accuracy and computational effort. According to this approach, the movement of a train of mass m, can be defined by means of the force balance presented in equation (3.1) and the definitions of the acceleration (a) and velocity (v) introduced by equations (3.2) and (3.3) respectively. F_t, F_b, F_r, F_g, F_c are correspondently the tractive, braking, running, gradient and curvature forces and t the time. The running, gradient and curvature efforts are usually grouped into one single term called resistive force.

$$F_t - F_b - F_r - F_g - F_c = m \cdot a \tag{3.1}$$

$$a = \frac{dv}{dt} \tag{3.2}$$

$$v = \frac{ds}{dt} \tag{3.3}$$

The tractive force is an active effort performed by the train in the same direction of the movement in order to increase or maintain the velocity, or to reduce a possible deceleration rate motivated by the resistive force. The maximum tractive force can be described by a piecewise function that depends on the train velocity. According to equation (3.4), for velocities lower than certain breaking velocity (v_0), the maximum tractive force is limited to the maximum tractive force of the motor, while for velocities values greater than the breaking velocity; the maximum tractive force is limited by the maximum power available. It is noted that the voltage influence has been neglected due to the low impact observed in high-speed lines.

$$0 \le F_t \le \begin{cases} F_{\max} & v \le v_0 \\ \dfrac{P_{\max}}{v} & v > v_0 \end{cases} \tag{3.4}$$

The braking force is an active effort performed by the train in the opposite direction of the movement in order to decrease or to maintain the velocity, or to decrease an acceleration rate motivated by the resistive force. There are three principal braking types: mechanical, pneumatic and electrical. The electrical brakes can be subdivided in turn into rheostatic and regenerative, depending on whether the braking energy produced is burnt into resistors or sent back to the catenary. This work will consider only electrical braking whose characteristic is defined by an equivalent expression to equation (3.4), where the maximum force and power values have negative values and are always less than or equal zero.

The running force, is an external passive effort that is opposed to the train movement. It is typically determined by means of the Davis formula, equation (3.5), where A, B and C are empirical coefficients that mainly depends on the train mass and the vehicle characteristics. The constant and linear terms of the equation describe the rolling and internal friction forces while the quadratic term the aerodynamic resistance that is more significant at high velocities.

$$F_r = A + B \cdot v + C \cdot v^2 \tag{3.5}$$

The gradient and curvature forces are external passive forces that can favor or disfavor the train motion depending on the topographic profile of the railway line. The gradient force is calculated using the equation (3.6) where g is the earth gravitational constant and α is the angle of the gradient slope. The curve force has been being neglected for this study because of the low values presented for high-speed lines. In case of being considered, it usually represented as an equivalent slope and thus, it can easily be calculated by and equivalent expression to equation (3.6).

$$F_g = m \cdot g \cdot \sin(\alpha) \tag{3.6}$$

3.2.2 Traffic system resolution

As it was explained before, the calculation of the train movement requires solving equations (3.1), (3.2) and (3.3). The analytical solution of these equations is very complex and only possible for very simple cases. Therefore, simulation techniques are usually adopted because they do not require any simplification and provide a good accuracy. Two main approaches are found depending on the integration variable selected: time (t) and position (s). Assuming the position as the integration variable and considering the acceleration constant during the integration step Δs, the values of the velocity and time for the next integration step can be calculated using equations (3.7) an (3.8) respectively.

$$v_2 = \sqrt{v_1 + 2 \cdot a \cdot \Delta s} \tag{3.7}$$

$$t_2 = t_1 + \Delta s \frac{2}{v_1 + v_2} \tag{3.8}$$

The value of the acceleration is obtained according to the force balance expressed in equation (3.1). It is noted that only one type of active force, tractive or braking, can be performed at the same time. The type of the active force depends on the driving mode and

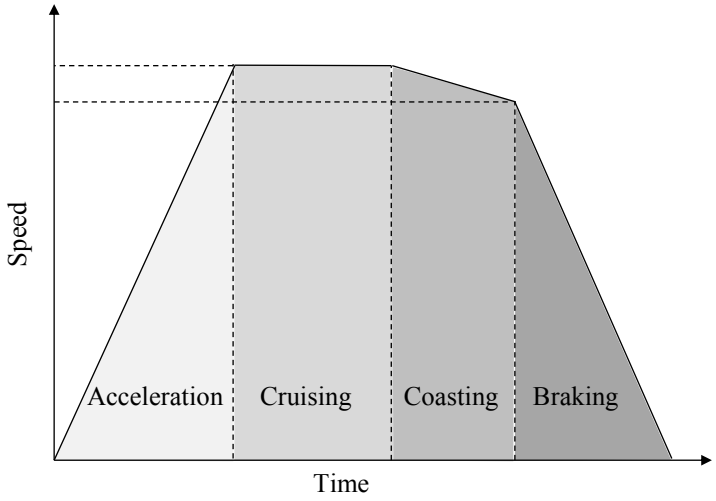

Figure 3.2. Train driving modes.

the value and sign of the resistive force encountered at each moment. As shown in Figure 5.3, there are four main train-driving modes: acceleration, cruising, coasting and braking.

During the acceleration mode, the train aims to increase its velocity and thus it is necessary to obtain a positive force balance on the train. To this end, there are two possible cases depending on the sign of the resistive force. When the sign is negative, the only possibility to increase the velocity is to perform a tractive force. However, according to the force balance described in (3.9), the acceleration can be positive or negative depending on the values of the tractive force performed and the resistive force encountered. In real situations the traction force available is normally sufficient to overcome the resistive force, but under simulation conditions may not.

$$a = \frac{F_t - F_r - F_g - F_c}{m} \tag{3.9}$$

In the second case, the resistive force has a negative value and hence the train movement is favored by the topographic profile. In this situation, the train can perform three different actions: a tractive effort when the acceleration rate is not sufficient, a null effort when the acceleration rate is enough or a braking effort when it is superior to the one desired. The braking mode is analogous to the acceleration mode, and thus a similar analysis can be accomplished.

The cruising model is used when the train has reached the maximum velocity and it is wanted to be maintained. In this case, the train must be performed a force equals to the resistive force and thus the acceleration is zero. It is noted, the active force can be both positive and negative depending on the value and sign of the resistive force. Finally, the coasting mode is often used to save energy. In this mode, the train does not consume any

power, decreasing or increasing their velocity according to the acceleration defined by the resistive force. In this latter case, the acceleration is given by the equation (3.10).

$$a = \frac{-F_r - F_g - F_c}{m} \tag{3.10}$$

Depending on the application of these four modes, different driving strategies can be defined. For this thesis, a minimum time trip strategy is selected that it represents the worst scenario possible. In practice, this mode is not used because it presents a high energy consumption. In this mode, the train will provide the maximum tractive and braking forces available at each velocity when accelerating and braking respectively as long as the maximum acceleration and decelerations limits are not exceeding. Once the trains reach the maximum velocity, the train will be driven in cruising mode.

One important issue is the definition of the instant to start braking in order to stop the train in the next station. To determine this point, this work uses the approach proposed in [61] and represented in Figure 3.3. The method calculates a forward curve that describes the velocity of the real course of the train, and the backward curve that follows the opposite course but with the acceleration constrains of the braking characteristic. The method finishes when the two curves are intersected.

Once the movement of the train is calculated for both directions, it is extended to the rest of the trains according to the traffic schedule provided. As it shown in Figure 3.4, the movement of the rest of the trains can be easily obtained by simply repeating the train profiles previously calculated according to the traffic timetable. In this case, the trains are assumed to have a constant headway and there is only one type of train circulating on the railway line.

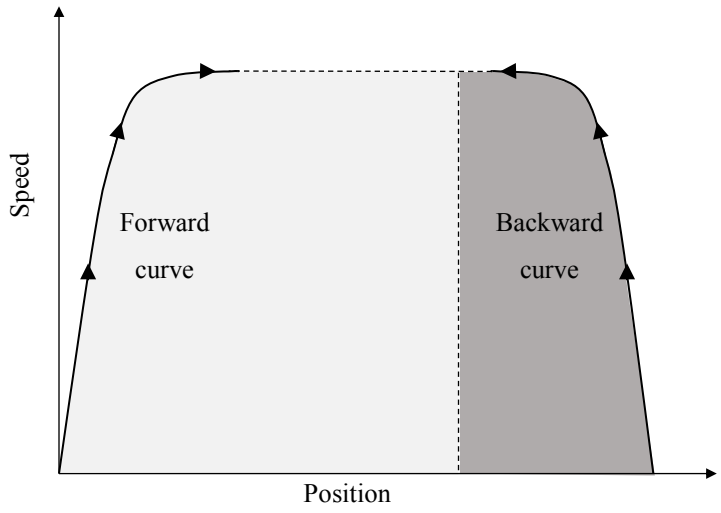

Figure 3.3. Braking point calculation.

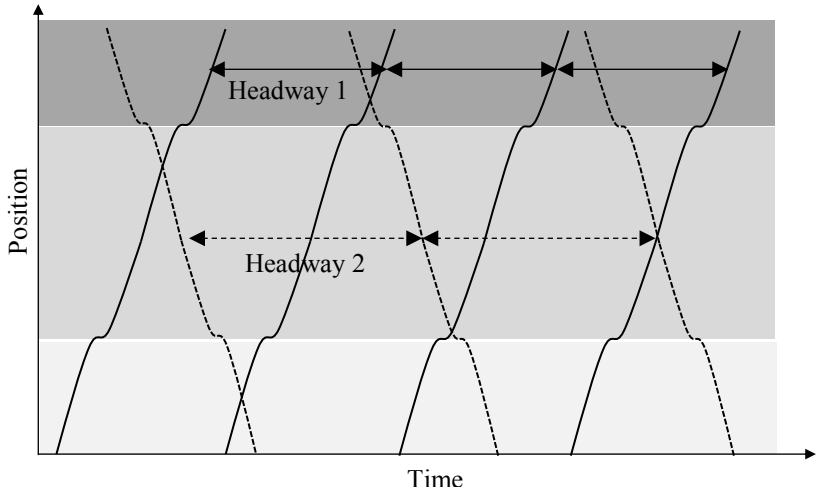

Figure 3.4. Traffic timetable calculation.

3.3 Electrical system simulation

The electrical system simulation aims to determine the electrical state of the power supply system according to the traffic condition existing. Since the train movement has a very slow dynamic when it is compared to the electromagnetic and electromechanical dynamics, the steady state modeling is the most suitable option for operation studies. Despite this apparent reduction in complexity, the steady state analysis of railway systems is still a very challenging task even for conventional configurations.

The steady state study of unbalanced electrical networks such as conventional transformer-based railway systems is traditionally performed by means of symmetrical components and formulated in terms of power balance equations and nodal constrains solved by full and decoupled Newton-Raphson algorithms. However, traditional power flow methods were developed for transmission grids that present very different characteristics to railway grids. On the one hand, the lack of symmetry of some of their components produce coupled sequence networks that eliminate the main advantage of this approach. On the other hand, the high R/X ratio of the lines, the radial or weakly mesh topologies of these grids and the significant power imbalances presented, make traditional power flow formulations and algorithms prone to fail.

To overcome all these difficulties many different power flows techniques have been addressed in the literature [62], [63]. Due to their similar characteristics, most of the work carried out in distribution grids can also be applicable to railway grids. These power flow techniques are principally defined in the phase frame [64] and they can be classified into derivative and non-derivative methods. Each of these methods can also be subdivided into

matrix-based and non-matrix-based methods depending on the requirement of the formulation of a network matrix or not.

The Gauss-Seidel algorithms are the most widespread approach among non-derivative matrix-based methods and they basically consist of the iterative solution of the Ohm's law. In contrast to traditional Gauss-Seidel algorithms where the Ohm's law is formulated in terms of the admittance matrix; in distribution systems, the impedance version is preferred due to the better and faster convergence properties of this matrix [65]. The simplicity of the formulation of Gauss-Seidel methods has converted them into a very common option for distribution power flow solvers [66], [67] and AC electrical railway power supply simulators [54], [68]. However, they present some limitations with the introduction of PV nodes [69] and with the number of iteration required for large electrical power systems.

The backward/forward sweep (BFS) algorithm is a very common non-derivative non-matrix-based method in distribution power flow studies. Taking advantage of the radial topology of these grids, the algorithm does not require the formulation of the network matrix. It consists of a two-step procedure in which the branch currents are first calculated (backward sweep) by means of the nodal currents, and then, the nodal voltages are updated (forward step). It is a very straightforward and powerful tool for radial grids, but they need modifications when the grid is meshed [70] and PV nodes added [71]. Likewise Gauss-Seidel algorithms, BFS algorithm has been successfully applied to distribution grids solvers [72] and railway grids [73], [74].

Among derivative matrix-based power flow methods, Newton-Raphson algorithms are the most extended approach. As it was explained before, these algorithms present convergence difficulties when traditional power flow formulations are applied to distribution grids. This issue has been solved with the development of the current-injection method (CIM) [75] that performs a nodal current balance instead of a nodal power balance. This method requires less iterations than BFS for heavily loaded systems, it is more robust for meshed grids and more reliable with PV nodes [76]. One example of the application of this method to an AC railway grid can be found in [77].

The latter three methodologies are good candidates for the solution of conventional transformer-based systems, but their application to the study of advanced converter-based systems presents important limitations. As it will be discussed in chapter four, some of the controls typically performed on the converters do not enable to represent them as conventional PQ or PV nodes [78],[79]. Furthermore, these converters can include non-

grounded connections that prevent or complicate enormously the use of conventional nodal power flow methods.

The multiphase power flow is a general formulation initially developed for the study of harmonics power flows [80] and subsequently applied to the steady-state initialization of electromagnetic transient simulations [81]. In contrast to conventional power flow techniques, where the active elements are represented as nodal constrains, multiphase nodal power flow uses a modified nodal analysis where the active elements can be defined as branch constrains. This approach is capable of reproducing any network topology and any control device law straightforwardly, and thus, this method has been selected for the formulation of the electrical railway system in the thesis.

Although multiphase power flow has been traditionally applied to AC electrical systems, there is not any reason that impede its use for DC systems as well. The analysis of AC/DC systems has been addressed in literature by two principal methods. The first approach is based on a sequential methodology, where the AC grid and the DC grid are solved sequentially until the linked variables converge [82]. The second approach is called unified and it solves of the equations at the same time [83]. One of the main disadvantages of these two latter approaches is that they define different equations for AC and DC grids increasing the difficulty and the computational burden unnecessarily. To avoid it, this thesis proposes a general unified formulation where the same equations can be applied to AC and DC elements.

3.3.1 Electrical system modeling

The electrical system can be described as a set of individual electrical elements interconnected. In general, an electrical element E_i (Figure 3.5.a) can be modeled by means of a passive network P^{Ei}, composed of n passive components, and an active network A^{Ei}, composed of m active components. In conventional nodal analysis, the passive network is typically represented by means of a node admittance matrix $\underline{Y}^{Ei}$ and the active network as node constrains expressed in terms of the node voltages. However, multiphase power flow uses a modified nodal analysis [84] where the active components are defined by their corresponding currents and represented as branch constrains.

According to this element representation, the electrical system (Figure 3.5.b) can be modeled by means of the combination of a general passive network, P that contains all the passive components of the elements of the system, and a general active network A that includes all the active components. This component disaggregation simplifies the

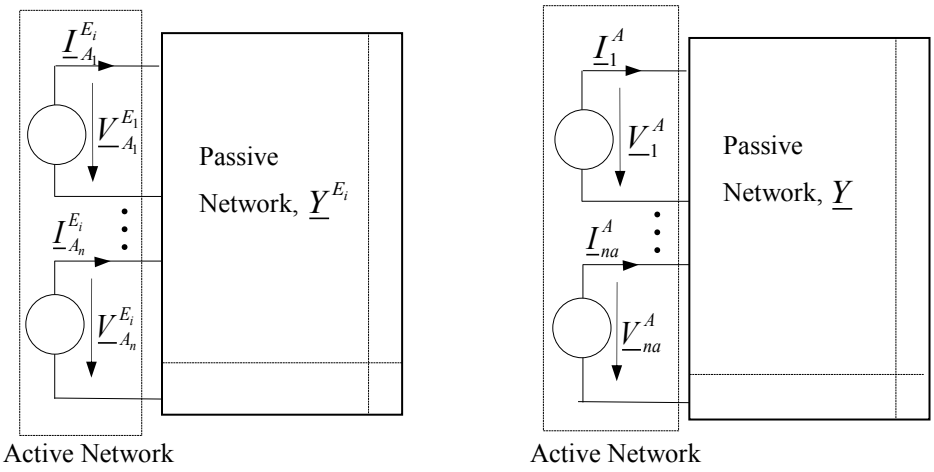

a) Element representation. *b) System representation.*

Figure 3.5. Electrical system representation.

formulation of the system equations because it enables to define general control equations for all the elements and it avoids distinguishing between phases and between elements.

According to this information, the electrical system can be formulated by means of the current balance equations (3.11) and (3.12), where V and δ represents the magnitude and the angle of the voltages of the nodes $\underline{V}$, Y and θ are the magnitude and angle of the elements of the system node admittance matrix $\underline{Y}$, I and ψ denote the magnitude and the angle of the current of the active components $\underline{I}$ and Γ^A the incidence matrix of the active components.

$$-\sum_{j\in N} Y_{ij}V_j\cos(\theta_{ij}+\delta_j)+\sum_{k\in A}\Gamma^A_{ki}I^A_k\cos(\psi^A_k)=0 \tag{3.11}$$

$$-\sum_{j\in N_{AC}} Y_{ij}V_j\sin(\theta_{ij}+\delta_j)+\sum_{k\in A_{AC}}\Gamma^A_{ki}I^A_k\sin(\psi^A_k)=0 \tag{3.12}$$

The incidence matrix of the active components defines the connections of the active components of the electrical system, and thus it must have as many rows and columns as active components and nodes are in the system. In order to complete this matrix, the connection of each active component must be analyzed; so that, for a given a given active component *k,* connected between nodes *i* and *j*, the columns, *i* and *j* of the row *k* of the matrix will be filled with 1 and -1 respectively. The rest of the elements of the row *k* are defined with 0.

The system node admittance matrix defines the admittances distribution of the electrical system and it can be obtained by means of the admittance matrix of the elements according equation (3.13). It is noted that, all these matrices must have the same dimension and hence they must be referred to the total number of nodes of the system.

$$\underline{Y} = \sum_{i \in E} \underline{Y}^{E_i} \tag{3.13}$$

As it was previously explained, AC/DC power flows uses different equations for AC and DC systems. However, DC equations can be seen as a simplification of the AC ones, where one of the two components of the AC variables remain constant. Since a polar representation is used in this thesis, the angle of the DC variables would be constant, and it should be calculated a priori. In contrast to the magnitude, the angle of the DC variables can be determined easily, and it can only have two values 0 or π. According to this information, the current balance equation presented in equation (3.11) is valid for both AC and DC nodes, while the equation (3.12) is only applied for AC nodes.

a) Catenary representation

For power flow studies, the catenary is usually represented as a multidimensional equivalent lumped π passive network (Figure 3.6), where the inductive and resistive effects of the conductors are considered in the series branch, and the capacitive effects equally distributed between the two parallel branches. These branches can conveniently be described by means of a series impedance primitive matrix ($\underline{Z}_s^{Ln_i}$) and a parallel admittance primitive matrix ($\underline{Y}_p^{Ln_i}$) whose elements can be calculated using the modified Carson's equations and the potential coefficients respectively [85]. Finally, the primitive matrix of catenary line ($\underline{Y}_{pri}^{Ln_i}$) is performed by means of equation (3.14). This matrix defines the relation between the voltage and the currents of the components of the passive network.

Although the primitive representation provides a full description of the catenary, all this information is rarely needed. In most of the configurations, the conductors of the same phase and same voltage level (positive, negative and neutral) are interconnected along the track, enabling to combine them into equivalent conductors using Kron reduction. According to this information, the primitive admittance matrix for monovoltage and bivoltage catenary configurations can be reduced to an equivalent primitive matrix of 2×2 (positive and neutral) and 3×3 (positive, negative and neutral) respectively. Furthermore, it is also common to eliminate the neutral from the representation reducing one extra dimension. In this case, the model is known as implicit neutral.

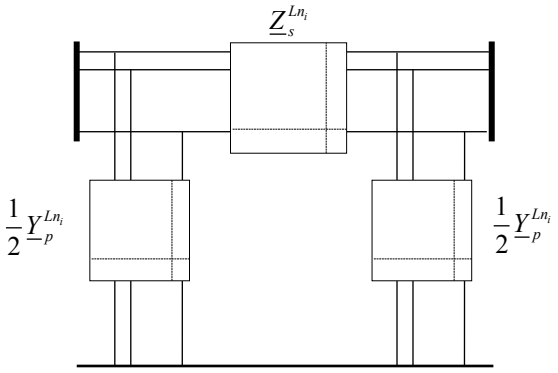

Figure 3.6. Catenary representation.

$$\underline{Y}_{pri}^{Ln_i} = \begin{bmatrix} \left(\underline{Z}_s^{Ln_i}\right)^{-1} & 0 & 0 \\ 0 & \frac{1}{2}\underline{Y}_p^{Ln_i} & 0 \\ 0 & 0 & \frac{1}{2}\underline{Y}_p^{Ln_i} \end{bmatrix} \tag{3.14}$$

Finally, it is necessary to express the element equations in terms of the voltage and current nodes. In non-coupling systems, the node admittance matrix can be easily obtained by simple rules, but for cases where there some passive components are coupling, the use of the incidence matrix is very advantageous. The passive incidence matrix of the element Γ^{P,Ln_i} is created following the same rules used for the active network; so that for a given passive component *k*, connected between nodes *i* and *j*, the columns, *i* and *j* of the row *k* will be filled with 1 and -1 respectively. The rest of the elements of the row are defined with 0. Equation (3.15) defines the relation between the node admittance matrix *i* ($\underline{Y}^{Ln_i}$) and the primitive admittance matrix of the line *i*.

$$\underline{Y}^{Ln_i} = \left(\Gamma^{P,Ln_i}\right)^t \left(\underline{Y}_{pri}^{Ln_i}\right)\left(\Gamma^{P,Ln_i}\right) \tag{3.15}$$

b) Transformers representation

A single-phase transformer can be represented as an equivalent lumped T passive network where the leakage and cooper losses are considered in the series branches, and the iron and the magnetizing losses concentrated in the parallel branch. For power flow studies, the parallel branch is usually neglected, simplifying the model to a single series impedance as shown in Figure 3.7. This equivalent circuit can be formulated by means of primitive admittance matrix described in Equation (3.16), where $\underline{y}'_{sc}$ is the short circuit admittance referred to the primary side and (N_1/N_2) the transformer turn ratio.

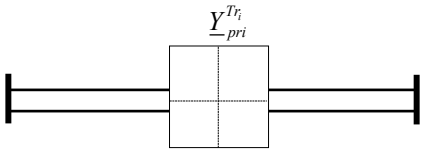

Figure 3.7. Single-phase transformer representation.

$$\underline{Y}_{pri}^{Tr_i} = \begin{bmatrix} \underline{y}'_{sc} & -\frac{N_1}{N_2}\underline{y}'_{sc} \\ -\frac{N_1}{N_2}\underline{y}'_{sc} & \left(\frac{N_1}{N_2}\right)^2 \underline{y}'_{sc} \end{bmatrix} \tag{3.16}$$

This primitive admittance matrix relates the voltages and the currents of the windings of the transformer. In order to express them in terms of the voltages of the nodes, it is necessary the utilization of the incidence matrix again. With the incidence matrix, any transformer arrangement can be performed. The autotransformers can be represented by this method as well by simply recalling that they have the primary negative terminal and secondary positive terminal connected in series. Once the incidence matrix is calculated, the node admittance matrix is calculated using and analogous expression to Equation (3.15)

The single-phase transformer with a secondary center tap grounded has been modeled by means of a single-phase three windings transformer whose equivalent circuit is shown in Figure 3.8. In order to determine its primitive matrix, it is necessary to perform three short circuit tests, obtaining three different short circuit admittances $\underline{y}'_{sc,1-2}$, $\underline{y}'_{sc,1-3}$ and $\underline{y}'_{sc,2-3}$. The impedances of the standard equivalent circuit are obtained by means of the equations (3.17), (3.18) and (3.19) where the previous impedances have been referred to the primary side.

$$\underline{y}'_1 = \frac{1}{2}(\underline{y}'_{sc,1-2} + \underline{y}'_{sc,1-3} - \underline{y}'_{sc,2-3}) \tag{3.17}$$

$$\underline{y}'_2 = \frac{1}{2}(\underline{y}'_{sc,1-2} + \underline{y}'_{sc,2-3} - \underline{y}'_{sc,1-3}) \tag{3.18}$$

$$\underline{y}'_3 = \frac{1}{2}(\underline{y}'_{sc,2-3} + \underline{y}'_{sc,1-3} - \underline{y}'_{sc,1-2}) \tag{3.19}$$

With these values, the primitive matrix of the equivalent circuit can be computed using equation (3.20) where (N_1/N_2) and (N_1/N_3) are the transformer turn ratio between the primary and secondary and primary and tertiary respectively. It is noted that the internal node of the equivalent circuit has been eliminated using the Kron reduction.

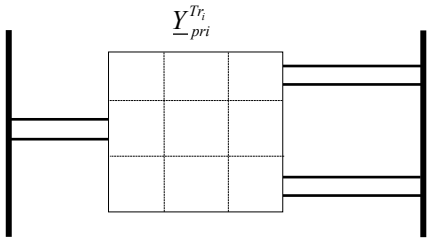

Figure 3.8. Single-phase three windings transformer representation.

$$\underline{Y}_{pri}^{Tr_i} = \frac{1}{\underline{y}'_1+\underline{y}'_2+\underline{y}'_3}\begin{bmatrix} \underline{y}'_1-(\underline{y}'_1)^2 & -\left(\frac{N_1}{N_2}\right)\cdot\underline{y}'_1\cdot\underline{y}'_2 & -\left(\frac{N_1}{N_3}\right)\cdot\underline{y}'_1\cdot\underline{y}'_3 \\ -\left(\frac{N_1}{N_2}\right)\cdot\underline{y}'_1\cdot\underline{y}'_2 & \left(\frac{N_1}{N_2}\right)^2\cdot(\underline{y}'_2-(\underline{y}'_2)^2) & -\left(\frac{N_1}{N_2}\right)\left(\frac{N_1}{N_3}\right)\cdot\underline{y}'_2\cdot\underline{y}'_3 \\ -\left(\frac{N_1}{N_3}\right)\cdot\underline{y}'_1\cdot\underline{y}'_3 & -\left(\frac{N_1}{N_2}\right)\left(\frac{N_1}{N_3}\right)\cdot\underline{y}'_2\cdot\underline{y}'_3 & \left(\frac{N_1}{N_3}\right)^2\cdot(\underline{y}'_3-(\underline{y}'_3)^2) \end{bmatrix} \quad (3.20)$$

The modeling of three-phase transformers in distribution systems is usually performed by means of single-phase transformer units. This is a simplification because it does not consider the coupling between the phases, but it has been proved to be a good approximation for most power flow studies. A more detailed models can be found in [86], where the symmetrical components are used. The primitive matrix of the three-phase transformer can be simply obtained assembling three single-phase transformer primitive matrices in a diagonal matrix as equation (3.21) describes, where the submatrices are calculated by equation (3.16). Subsequently, depending on the transformer connection arrangement, the incidence matrix is computed, and the node admittance matrix calculated.

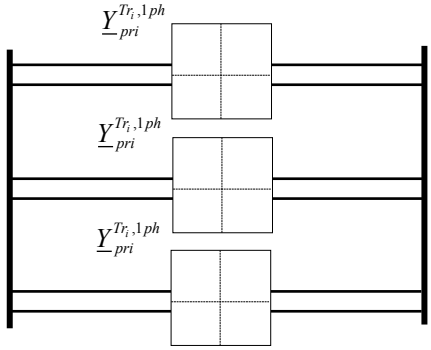

Figure 3.9. Three phase transformer representation.

$$\underline{Y}_{pri}^{Tr_i} = \begin{bmatrix} \underline{Y}_{pri}^{Tr_i,1ph} & 0 & 0 \\ 0 & \underline{Y}_{pri}^{Tr_i,1ph} & 0 \\ 0 & 0 & \underline{Y}_{pri}^{Tr_i,1ph} \end{bmatrix} \quad (3.21)$$

It is important to highlight that the three-phase transformer for advanced converter-based systems can have any connection scheme but the delta connection on the secondary side is usually preferred to reduce the harmonics injections. Transformer configurations including delta arrangement produce singularities issues in resolution methods that requires of inverse calculation. This problem can be avoided by connecting a high enough fictitious reactance from the delta terminals to the ground [87].

c) Train representation

The representation of the train in power flow studies has been extensively discussed in literature. In the beginning, trains were modelled as constant impedance or current source components. These two representations are especially convenient for short circuit studies, but they are not very realistic for power flow purposes. The use of modern VSC onboard enables to adjust the electrical power to the voltage condition existing on the catenary. Thus, the most common representation now is as a single-phase power source, *i* defined by the equations (3.22) and (3.23).

$$\sum_{j\in N} \Gamma_{ij}^{A} V_j I_i^{A} \cos(\delta_j - \psi_i^{A}) = P_{0,i}^{A} \tag{3.22}$$

$$\sum_{j\in N_{AC}} \Gamma_{ij}^{A} V_j I_i^{A} \sin(\delta_j - \psi^{A}) = Q_{0,i}^{A} \tag{3.23}$$

On the left side of each equation, it is represented respectively the active and reactive power calculated in terms of the node voltages and the current of the active component. On the right side of the equation, there are the active and reactive power ($P_{0,i}^{A}$ $Q_{0,i}^{A}$) demanded by the train. The active power has been calculating according to the traffic simulation previously defined. This power must include the auxiliary services consumption and consider the efficiency of the traction unit components. Alternately, the reactive power has been set to 0.95 in order to fulfill the standard recommendation. It is noted that the active equation is valid for both AC and DC railway electrification schemes. For this latter case, the second equation does not apply.

Although this model is the most common, there are other more complex representations of the train that includes the squeeze control and the overcurrent protection [73]. These control strategies aim to improve the reliability of the railway grid by reducing the power demanded and injected by the train when the catenary voltage is out of certain limits. These limitations are common for low voltage DC networks such as metros trams railway lines, but for high-speed railway lines rarely affects.

d) Utility grid representation

As it shown in Figure 3.10, the utility grid has been represented as a combination of a three-phase voltage source and a three-phase impedance. The three-phase voltage source is described by means of a magnitude and an angle balance that must be performed for each phase of the element. Equation (3.24) and Equation (3.25) show respectively the magnitude and the angle balance for one of the phases. On the left hand side of the equations, it is calculated the voltage magnitude and angle of the active element *i,* in terms of the node voltages using the active incidence matrix. On the left side of the equations, there are correspondently the voltage magnitude $V_{0,i}^{A}$ and the voltage angle $\delta_{0,i}^{A}$ references. Since the utility grid is assumed symmetrical, the voltage magnitude references defined for the other two active elements must be equal, while their angles must be 120 degrees apart.

$$\left(\sum_{j\in N}\Gamma_{i,j}^{A}V_j\cos(\delta_j)\right)^2+\left(\sum_{j\in N}\Gamma_{i,j}^{A}V_j\sin(\delta_j)\right)^2=\left(V_{0,i}^{A}\right)^2 \tag{3.24}$$

$$\arctan\left(\frac{\sum_{j\in N}\Gamma_{ij}^{A}V_j\sin(\delta_j)}{\sum_{j\in N}\Gamma_{ij}^{A}V_j\cos(\delta_j)}\right)=\delta_{0,i}^{A} \tag{3.25}$$

The strength of the grid is typically defined by its short circuit power and thus, the series impedance must be determined according to this value. Assuming a symmetrical line, the positive-sequence impedance $\underline{Z}_1$ can be easily obtained by simply dividing the square of the voltage rate over the short circuit power. Finally, considering the zero-sequence impedance $\underline{Z}_0$ three times the positive one and the negative $\underline{Z}_2$ equals to the positive, the admittance matrix of the element can be easily obtained by equation (3.24).

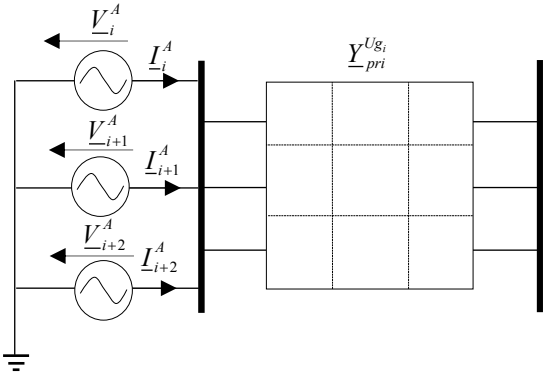

Figure 3.10. Utility grid representation.

$$\underline{Y}_{pri}^{Ug_i}=3\begin{bmatrix}\underline{Z}_0+2\underline{Z}_1 & \underline{Z}_0-\underline{Z}_1 & \underline{Z}_0-\underline{Z}_1\\ \underline{Z}_0-\underline{Z}_1 & \underline{Z}_0+2\underline{Z}_1 & \underline{Z}_0-\underline{Z}_1\\ \underline{Z}_0-\underline{Z}_1 & \underline{Z}_0-\underline{Z}_1 & \underline{Z}_0+2\underline{Z}_1\end{bmatrix}^{-1} \tag{3.26}$$

e) Converters representation

The representation of VSCs in power flow studies is typically reduced to a controllable AC voltage source behind a complex impedance. The voltage source defines the voltage level according to the control strategy implemented while the impedance represents the phase reactor and the filter typically included to enhance the converter operation [84] [85]. When the DC part is involved, the previous model has to be extended by adding a DC voltage source linked to the AC voltage source by an active power balance. This VSC representation can be easily adapted to model any other converter arrangement based on the combination of VSCs. For example, neglecting the converter impedance, two VSCs in back to back configuration can be represented as two interdependent AC voltage sources [90] or two VSCs in front to front configuration as two interdependent DC voltage sources.

According to this information, the AC/AC traction substation of advanced AC converter-based systems can be represented as a three-phase AC voltage source linked to a single-phase AC voltage source. As it is shown in Figure 3.11, the three phases of the VSC converter on the utility grid side correspond to the active elements *i*, *i+1* and *i+2*, while the phase of the VSC on the railway grid to the active element *i+3*. It is noted, that the neutral of the sources on the utility grid side will coincide with the neutral of the railway grid on the railway side.

The operation of the sources is defined by the control strategy adopted. As it will be comprehensively described in chapter four, the active power of the AC/AC converter station will be controlled by the VSC on the railway grid by means of a droop control strategy whose behavior is defined in equations (3.27) and (3.28). On the left side of the equations, it is calculated respectively the active and reactive power injected by the VSC converter on the railway grid side in terms of the node voltages and the current of the active component. On the right side of the equations, there are the droop characteristics that defines correspondently the active and reactive power delivered according to the angle and

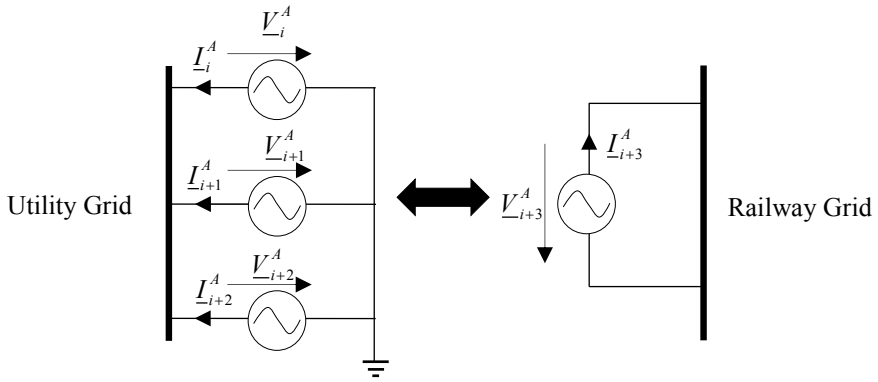

Figure 3.11. AC/AC traction susbation representation.

voltage variations. As it is noted, both the active and reactive power depends on the angle and voltage variations due to the existing power coupling. This coupling is defined by the X/R ratio of the catenary line. Thus, for a pure inductive grid, the active power only depends on the angle difference and the reactive power on the voltage magnitude difference; while for pure resistive grids, the active power only depends on the voltage magnitude difference and the reactive power on the angle magnitude difference. Finally, the terms $k^A_{\delta,i}$ and $k^A_{v,i}$ correspond to the angle and voltage droop parameters defined.

$$\sum_{j\in N}\Gamma^A_{i+3,j}V_jI^A_{i+3}\cos(\delta_j-\psi^A_{i+3})=-\frac{X}{Z}\cdot k^A_{\delta,i+3}\cdot(\arctan\left(\frac{\sum_{j\in N}\Gamma^A_{i+3,j}V_j\sin(\delta_j)}{\sum_{j\in N}\Gamma^A_{i+3,j}V_j\cos(\delta_j)}\right)-\delta^A_{0,i+3})- \\ -\frac{R}{Z}\cdot k^A_{v,i+3}\left(\sqrt{\left(\sum_{j\in N}\Gamma^A_{i+3,j}V_j\cos(\delta_j)\right)^2+\left(\sum_{j\in N}\Gamma^A_{i+3,j}V_j\sin(\delta_j)\right)^2}-\left(V^A_{0,i+3}\right)\right) \tag{3.27}$$

$$\sum_{j\in N_{AC}}\Gamma^A_{i+3,j}V_jI^A_{i+3}\sin(\delta_j-\psi^A_{i+3})=\frac{R}{Z}\cdot k^A_{\delta,i}\cdot(\arctan\left(\frac{\sum_{j\in N}\Gamma^A_{i+3,j}V_j\sin(\delta_j)}{\sum_{j\in N}\Gamma^A_{i+3,j}V_j\cos(\delta_j)}\right)-\delta^A_{0,i+3})- \\ -\frac{X}{Z}\cdot k^A_{v,i}\left(\sqrt{\left(\sum_{j\in N}\Gamma^A_{i+3,j}V_j\cos(\delta_j)\right)^2+\left(\sum_{j\in N}\Gamma^A_{i+3,j}V_j\sin(\delta_j)\right)^2}-\left(V^A_{0,i+3}\right)\right) \tag{3.28}$$

The VSC on the utility grid side is controlled to keep the voltage of the DC link constant. To this end, the converter must maintain an active power balance so that the active power delivered by the converter on the utility grid side must be equal and opposite to the active power drawn from the utility grid converter. This power balance is expressed in Equation (3.29). On the left side of the equation, it is calculated the active power of one phase of the VSC in terms of the node voltages and the current of the active component. On the right side, it is calculated the active power balance of the rest of the active elements of the system.

$$\sum_{j\in N}\Gamma^A_{ij}V_jI^A_i\cos(\delta_j-\psi^A_i)=-\sum_{k\in A}\sum_{j\in N}\Delta^A_{ik}\Gamma^A_{kj}V_jI^A_k\cos(\delta_j-\psi^A_k) \tag{3.29}$$

It is noted that a new matrix called Δ is introduced. This matrix includes the information of the dependency of the active elements of the systems. Accordingly, when there is a dependency between two active components, *i* and *j*, the element *Δ(i,j)* is filled with one divided by the total number of sources that depend on the active element *j*. Finally, when there is not any relation between two components the element is filled with 0. By means of this matrix, the active power of the active component considered is only linked to the active power of the active components that depends on.

In this active power balance, it is also common to add a losses term. There are many different models to estimate these losses [91]. The most extended approach is based on a quadratic polynomial expression that includes the commutation and conduction losses. This expression is thought for a single VSC, and its extension to other combination of VSCs is not straightforward. In this situation, this thesis has opted not to include the converter losses in the formulation. Finally, besides to the operation control laws defined before, the VSC must operate within the certain operation limits. There are three main limits to consider the maximum current flowing through the power electronics switches, the ratio between the DC voltage and the AC voltage and the power capability limits.

Besides the active power regulation, VSCs can also provide reactive power due to the additional degree of freedom of the power switches. This fact can be used to provide voltage regulation to the grid, by simply injecting a fixed amount of reactive power or keeping the voltage magnitude constant. In this thesis, the reactive power on the utility grid is maintained to zero, and thus the equation (3.23) can be used.

The AC/DC converter representation can be seen as a simplification of the previous model, where the AC source on the railway grid is substituted by a DC source. As in the previous elements representation, the formulation used in this thesis enables to use the same equation for AC and DC. Accordingly, the voltage source on the railway grid will be modelled using equation (3.27). As generally known, the inductance part of the electrical line in DC systems does not affect the steady state operation, and the left side of the equation coincides with the conventional droop approach for DC systems, where the active power is controlled according to the voltage magnitude difference.

Finally, the DC/DC converters have been modeled as two DC interdependent power sources assuming they are composed of two single phase VSCs in front to front configuration. In this case, the control performed has been defined to mimic the autotransformer behavior. In this sense, one of the voltage sources is controlled to maintain the same voltage of the other source. This behavior can be described by equation (3.30). On the other hand, the other voltage source will be controlled to maintain the power balance and thus, the Equation (3.29) can be used. To the author' knowledge there is not any model reported so far for the implementation of DC/DC autoconverters.

$$\sum_{j \in N_{DC}} \Gamma^{C}_{i,j} V_j \cos(\delta_j) = -\sum_{k \in C_{DC}} \sum_{j \in N_{DC}} \Delta^{C}_{i,k} \Gamma^{C}_{i,j} V_j \cos(\delta_j) \tag{3.30}$$

3.3.2 Electrical system resolution

a) Formulation

Multiphase power flow uses a conventional Newton-Raphson algorithm to solve the system equations. In order to facilitate the implementation of the method, it is firstly necessary to define a systematic procedure to assemble all the equations in a simple and efficient way. As it was previously explained, the electrical system is defined by means of the voltage of the nodes and the currents of the active components. These variables have complex values when the system is AC and real values when the system is DC. Accordingly, the total number of equations needed to solve is equal to the double of the summation of the number of AC nodes and the number of AC active components minus the summation of the number DC nodes and the number of DC active components.

The nodes equations were presented in (3.11) and (3.12) and repeated in equations (3.31) and (3.32). They represent the real and imaginary current balance in the nodes of the system. It is worth noticing again that the equation (3.31) is applied for both AC and DC nodes, and thus, f_1 will be a function vector with a number of rows equals to the total number of nodes. On the contrary, the equation (3.32) is only applied to AC nodes and thus, f_2 will be a function vector with a number of rows equals to the number of AC nodes.

$$f_{1,i\in N} = -\sum_{j\in N} Y_{ij}V_j \cos(\theta_{ij}+\delta_j) + \sum_{k\in A} \Gamma^A_{ki} I^A_k \cos(\psi^A_k) \tag{3.31}$$

$$f_{2,i\in N_{AC}} = -\sum_{j\in N_{AC}} Y_{ij}V_j \sin(\theta_{ij}+\delta_j) + \sum_{k\in A_{AC}} \Gamma^A_{ki} I^A_k \sin(\psi^A_k) \tag{3.32}$$

The active element equations were presented in (3.22), (3.23), (3.24), (3.25), (3.27), (3.28), (3.29) and (3.30). Accordingly, there are eight different types of control laws, specifically: active power (A_1), reactive power (A_2), voltage magnitude (A_3), voltage angle (A_4), active droop control (A_5), reactive droop control (A_6), active power balance (A_7), and voltage magnitude balance (A_8). Grouping the active elements according to the type of control performed is very advantageous since it reduces the total number of different equations needed and allows to incorporate new control laws straightforwardly. According to this information, the new set of vectors are defined in equations (3.33), (3.34), (3.35), (3.36), (3.37), (3.38), (3.39) and (3.40) , whose dimensions are equal to the number of active components with the corresponding control law implemented.

$$f_{3,i\in A_1} = \sum_{j\in N} \Gamma_{ij}^A V_j I^A \cos(\delta_j - \psi_i^A) - P_{0,i}^A \tag{3.33}$$

$$f_{4,i\in A_2} = \sum_{j\in N_{AC}} \Gamma_{ij}^A V_j I^A \sin(\delta_j - \psi_i^A) - Q_{0,i}^A \tag{3.34}$$

$$f_{5,i\in A_3} = \left(\sum_{j\in N} \Gamma_{ij}^A V_j \cos(\delta_j)\right)^2 + \left(\sum_{j\in N} \Gamma_{ij}^A V_j \sin(\delta_j)\right)^2 - \left(V_{0,i}^A\right)^2 \tag{3.35}$$

$$f_{6,i\in A_4} = \arctan\left(\frac{\sum_{j\in N} \Gamma_{ij}^A V_j \sin(\delta_j)}{\sum_{j\in N} \Gamma_{ij}^A V_j \cos(\delta_j)}\right) - \delta_{0,i}^A \tag{3.36}$$

$$\begin{aligned} f_{7,i\in A_5} = {} & \sum_{j\in N} \Gamma_{ij}^A V_j I_i^A \cos(\delta_j - \psi_i^A) + \frac{X}{Z}\cdot k_{\delta,i}^A \cdot \left(\arctan\left(\frac{\sum_{j\in N} \Gamma_{ij}^A V_j \sin(\delta_j)}{\sum_{j\in N} \Gamma_{ij}^A V_j \cos(\delta_j)}\right) - \delta_{0,i}^A\right) + \\ & + \frac{R}{Z}\cdot k_{v,i}^A \left(\sqrt{\left(\sum_{j\in N} \Gamma_{ij}^A V_j \cos(\delta_j)\right)^2 + \left(\sum_{j\in N} \Gamma_{ij}^A V_j \sin(\delta_j)\right)^2} - \left(V_{0,i}^A\right)\right) \end{aligned} \tag{3.37}$$

$$\begin{aligned} f_{8,i\in A_6} = {} & \sum_{j\in N} \Gamma_{ij}^A V_j I_i^A \sin(\delta_j - \psi_i^A) - \frac{R}{Z}\cdot k_{\delta,i}^A \cdot \left(\arctan\left(\frac{\sum_{j\in N} \Gamma_{ij}^A V_j \sin(\delta_j)}{\sum_{j\in N} \Gamma_{ij}^A V_j \cos(\delta_j)}\right) - \delta_{0,i}^A\right) + \\ & + \frac{X}{Z}\cdot k_{v,i}^A \left(\sqrt{\left(\sum_{j\in N_{AC}} \Gamma_{ij}^A V_j \cos(\delta_j)\right)^2 + \left(\sum_{j\in N_{AC}} \Gamma_{ij}^A V_j \sin(\delta_j)\right)^2} - \left(V_{0,i}^A\right)\right) \end{aligned} \tag{3.38}$$

$$f_{9,i\in A_7} = \sum_{j\in N} \Gamma_{ij}^A V_j I_i^A \cos(\delta_j - \psi_i^A) + \sum_{k\in A}\sum_{j\in N} \Delta_{ik}^A \Gamma_{kj}^A V_j I_k^A \cos(\delta_j - \psi_k^A) \tag{3.39}$$

$$f_{10,i\in A_8} = \sum_{j\in N_{DC}} \Gamma_{ij}^A V_j \cos(\delta_j) - \sum_{k\in A}\sum_{j\in N_{DC}} \Delta_{ik}^A \Gamma_{kj}^A V_j \cos(\delta_j) \tag{3.40}$$

b) Initialization

The Newton-Rapson method requires an initial point to start to iterate. In contrast to conventional power flow formulations, the use of an initial flat point leads to non-convergence issues for all the cases studied. In order to avoid this problem, a new initialization method has been developed.

The method proposed consists of obtaining an equivalent linear representation of the active components of the system. To this end, it is necessary to substitute the active components with any of these four options: ideal voltage source *VS*, ideal current source

CS, and dependent voltage source *DVS* and dependent current source *DCS*. The key aspect is to define the equivalences between the non-linear constrains and the linear ones.

For the active components with an implemented power control law (A_1, and A_2), they are replaced by a current source whose values is calculated according to the power set and the best voltage prediction available. For the active components with an implemented voltage control law (A_3, and A_4), they are obviously replaced by a voltage source whose value is set according the control values defined. For the active components controlled in droop mode (A_5 and A_6) they are replaced with a voltage source whose value is set to the nominal values defined in the droop laws (V_0^A and δ_0^A). For the active components with a power dependent control (A_7), they are replaced with a current source whose values is calculated according to the power of their corresponding dependent components and the best voltage prediction obtained. Finally, the active components controlled in voltage dependent mode (A_8), are obviously replaced with a voltage depend power source. For the DC case, the same rules apply but the second control law is not implemented.

According to the previous component equivalences, it is possible to define the system of equations (3.41), where the *Id* represents the identity matrix whose size is determined according to the number of elements of the corresponding type. It describes in the first row the current balance in the nodes of the system, including the contributions of the branches and the corresponding currents of the active components. The second, third, fourth and fifth rows represents the constitutive equation of a voltage source, a current source, a voltage dependent source and a current dependent source.

$$\begin{bmatrix} \underline{V} \\ \underline{I}^{VS} \\ \underline{I}^{CS} \\ \underline{I}^{VDS} \\ \underline{I}^{CDS} \end{bmatrix} = \begin{bmatrix} \underline{Y} & \Gamma'^{VS} & \Gamma'^{CS} & \Gamma'^{VDS} & \Gamma'^{CDS} \\ 0 & 0 & Id & 0 & 0 \\ \Gamma^{CS} & 0 & 0 & 0 & 0 \\ \Delta^{VDS} - Id^{VDS} & 0 & 0 & 0 & 0 \\ 0 & 0 & 0 & 0 & \Delta^{CDS} - Id^{CDS} \end{bmatrix}^{-1} \begin{bmatrix} 0 \\ \underline{V}_0^{VS} \\ \underline{I}_0^{CS} \\ 0 \\ 0 \end{bmatrix} \tag{3.41}$$

In this case, since the power of the dependent elements are not known a priori, it is necessary to solve the system twice assuming in the first time a power value of zero. In this second iteration, the voltage of the droop control active components is corrected according to the droop characteristics.

c) Resolution

The Newton-Raphson method is based on the approximation of the system equations by the tangent hyperplane at the different iteration points. This plane is represented by means of the Jacobian matrix *J*, defined by equation (3.42). The Jacobian matrix is a square matrix that is composed of the derivatives of the system equations ($f_1, f_2 ... f_{10}$). with respect to system variables: the voltage magnitude of the nodes (V), the voltage angle of the AC nodes (δ_{AC}), the current magnitude of the active elements (I^A) and the current angle of the active AC elements (ψ^A_{AC}).

$$J = \begin{bmatrix} \frac{\partial f_1}{\partial V} & \frac{\partial f_1}{\partial \delta_{AC}} & \frac{\partial f_1}{\partial I^A} & \frac{\partial f_1}{\partial \psi^A_{AC}} \\ \frac{\partial f_2}{\partial V} & \frac{\partial f_2}{\partial \delta_{AC}} & \frac{\partial f_2}{\partial I^A} & \frac{\partial f_2}{\partial \psi^A_{AC}} \\ \vdots & \vdots & \vdots & \vdots \\ \frac{\partial f_{10}}{\partial V} & \frac{\partial f_{10}}{\partial \delta_{AC}} & \frac{\partial f_{10}}{\partial I^A} & \frac{\partial f_{10}}{\partial \psi^A_{AC}} \end{bmatrix} \tag{3.42}$$

In conventional transmission analysis, the Jacobian matrix calculation can be simplified due to the decoupling existing between the active and the reactive power flow. Unfortunately, railway grids are more similar to distribution grids, and the method requires the use of a full version of the matrix. It is noted, that some terms of the matrix are zero, alleviating the computing burden. The derivative terms can be easily obtained according to the derivation rules and their expressions will be not included in the thesis. Finally, once the Jacobian matrix is obtained, the new values of the system variables can be calculated by means of equation (3.43) These operations are repeated until the difference between the variables for the iteration *n* and *n+1* is lower than a tolerance value defined.

$$\begin{bmatrix} V \\ \delta_{AC} \\ I^A \\ \psi^A_{AC} \end{bmatrix}^{n+1} = \begin{bmatrix} V \\ \delta_{AC} \\ I^A \\ \psi^A_{AC} \end{bmatrix}^{n} - \begin{bmatrix} \frac{\partial f_1}{\partial V} & \frac{\partial f_1}{\partial \delta_{AC}} & \frac{\partial f_1}{\partial I^A} & \frac{\partial f_1}{\partial \psi^A_{AC}} \\ \frac{\partial f_2}{\partial V} & \frac{\partial f_2}{\partial \delta_{AC}} & \frac{\partial f_2}{\partial I^A} & \frac{\partial f_2}{\partial \psi^A_{AC}} \\ \vdots & \vdots & \vdots & \vdots \\ \frac{\partial f_{10}}{\partial V} & \frac{\partial f_{10}}{\partial \delta_{AC}} & \frac{\partial f_{10}}{\partial I^A} & \frac{\partial f_{10}}{\partial \psi^A_{AC}} \end{bmatrix}^{-1} \begin{bmatrix} f_1 \\ f_2 \\ \vdots \\ f_{10} \end{bmatrix} \tag{3.43}$$

Chapter 4

Operation of advanced converter-based electrical railway power supply systems

4.1 Introduction

The operation of any electrical power supply system is defined as the set of actions required to ensure the continuity and security of the electrical supply under adequate conditions of quality and cost. So far, the operation of conventional transformer-based systems has been considered as a passive activity whose only challenge was the design of an electrical installation capable of fulfilling the operation standards for the worst-case scenario.

Probably, one of the most important standards to ensure a reliable railway operation is the EN50163:2004 [92]. This standard defines the admissible voltage levels for the principal railway electrification schemes. As shown in Table 4.1, it sets a lower and a higher permanent and non-permanent voltage limits for every standard voltage level existing now. In this way, the catenary voltage should lie within the range between the lowest permanent and the highest permanent voltages in normal conditions. The permitted duration of voltage conditions between the permanent and non-permanent voltage limits shall not exceed two minutes for lowest values and five minutes for the highest ones.

In order to maintain the catenary voltage within admissible ranges, the trains must include a control system that limits the maximum current drawn depending on the voltage level on the catenary. According to the European standard EN50388:2005 [93], this maximum current must be linearly reduced from the maximum current demanded by the train at nominal voltage (I_{max}) to the current consumed by the auxiliary services (I_{aux}). As

Table 4.1. Nominal voltages and their permissible limits [92]

Electrification system	*Lowest non-permanent voltage* $U_{min2}(V)$	*Lowest permanent voltage* $U_{min1}(V)$	*Nominal Voltage* U_n *(V)*	*Highest permanent voltage* $U_{max1}(V)$	*Highest non-permanent voltage* $U_{max2}(V)$
D.C. (mean values)	*500*	*500*	*750*	*900*	*1000*
	1000	*1000*	*1500*	*1800*	*3600*
	2000	*2000*	*3000*	*3600*	*3900*
AC (r.m.s values)	*11000*	*12000*	*15000*	*17250*	*18000*
	17500	*19000*	*25000*	*27500*	*29000*

shown in Figure 4.1, the limitation starts when the voltage on the catenary is lower than the nominal one multiplied by a reduction factor (a) that depends on the electrification system. Finally, when the voltage on the catenary is lower than the non-permanent one, the train cannot consume any power to traction. Finally, the current should also be limited when the train is regenerating. In this case, the standard only mentions that the current injected should not produce voltage conditions out of the cases included in the standard EN50163:2004.

Another important aspect to guarantee an efficient operation is the power factor of the train. According to the standard EN50388:2005 the power factor can be adapted to control the voltage line using a capacitive behavior when the train is on a traction mode and an inductive behavior when the train on regenerative mode. This standard defines in the annex E the desirable power factor behavior shown in Figure 4.2. As it can be seen, it distinguishes two forbidden areas colored in dark grey and two non-desired areas colored in light grey. Accordingly, the standard encourages the trains to work with power factor values between 0.95 inductive and 0.95 capacitive.

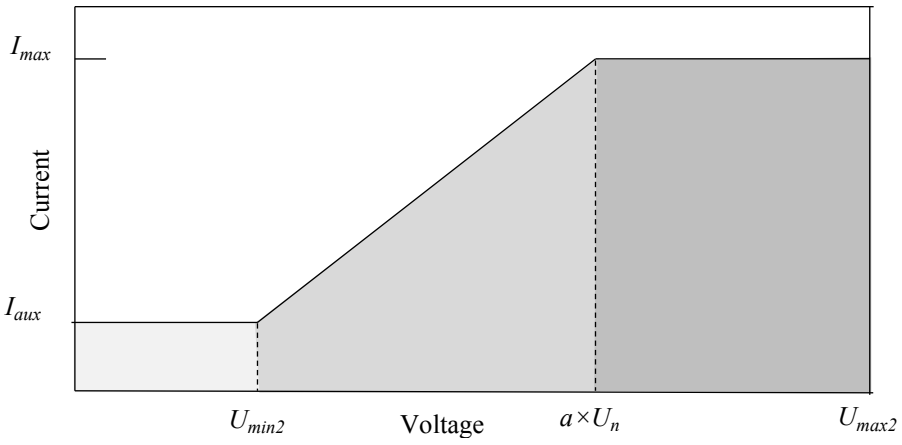

Figure 4.1. Train current limitation.

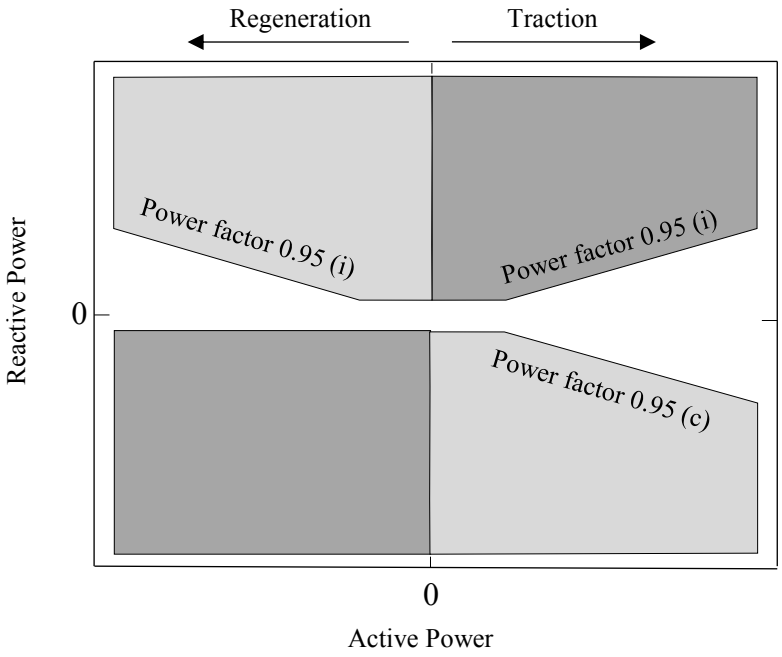

Figure 4.2.Train power factor recommendation.

Besides the previous constrains and recommendations, the railway operation must also guarantee that the currents flowing through the conductors of the catenary are below the maximum levels defined by the manufacturer, and the maximum power imbalance introduced into the utility grid does not exceed the admissible rate defined by the transmission system operator. For the Spanish case, Red Eléctrica de España (REE), the operator of the Spanish transmission system, sets a maximum phase imbalance of 2% for time periods lower than 1 minute and 1% for longer periods. This power imbalance is calculated as the ratio between the negative and the positive sequence values of the voltage.

As noticed, the only active actions taken so far are related to the operation control of the trains, which are the only elements in the system with the ability of adapting their performance to enhance the railway operation. However, the introduction of advanced converter-based systems can change this situation radically. Their controllable traction substations are very powerful elements to improve the system efficiency and reliability. The next section proposes a control system for the operation of advanced AC and DC converter-based configurations that distributes the power according to the distance between the trains and the substations but capable of increasing or decreasing the degree of cooperation between the substations depending on the conditions of the network without the need for communication between their elements. Finally, the performance of this control is analyzed for a simple test case for two catenary configurations and compare with the conventional transformer-based solution.

4.2 Hierarchical control system for advanced converter-based systems

The operation of advanced converter-based ERPSSs is essentially determined by the control system implemented. In general, there are two opposite control schemes in literature: centralized and decentralized [94]. The centralized approach is based on a central controller that defines the control references of the different distributed resources according to the operation objective defined. On the contrary, decentralized approaches perform the operation of the system by means of local controllers located at each distributed resource. These controllers always have the information of their corresponding energy resource, but they can also include information of some others. In this latter case, the control scheme is also known as distributed control [95].

The implementation of a fully centralized scheme or a fully decentralized scheme is often avoided. On the first hand, fully centralized control requires the use of fast communication channels and powerful computational resources that makes its implementation very costly for extended geographic areas such as railway systems. Furthermore, the operation of the whole system relies on the performance of a single controller reducing the reliability significantly. On the other hand, fully decentralized control provides lower cost and higher reliability, but it complicates enormously the achievement of global objectives since the information available is limited to the local environment. Taking into account all these considerations, researchers have opted for the development of hierarchical control systems [96].

Hierarchical control divides the operation of the grid into different levels with different time scales. In this sense, the higher levels have greater time scales and provides supervisory control over the lower levels. This disaggregation is very advantageous since the different control actions require very different time responses. The number and actions of these levels differs in literature, but in general, they all include two broad levels. The lower level is in charge on maintaining the power balance in the grid while performing the power sharing defined by the higher level. On the other hand, the higher level is in charge of defining the power sharing and maintain the power quality of the grid. Figure 4.3 shows the application of this scheme to an advanced converter-based ERPSS, where the higher level has been implemented using a centralized control configuration and the lower level a decentralized control scheme.

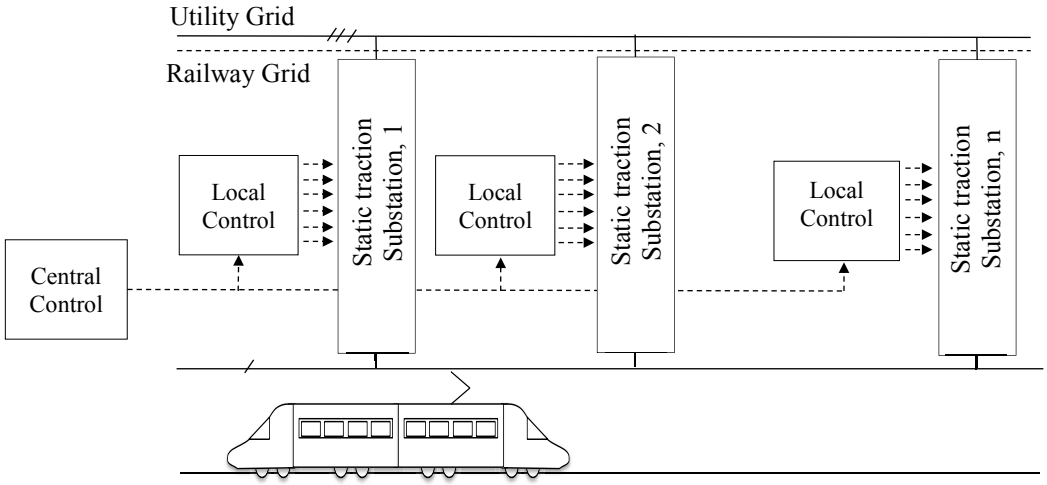

Figure 4.3. Hierarchical control scheme for advanced converter-based ERPSS.

Under a scenario where the availably and the price of the energy are the same for all traction substations, it is reasonable to share the power demanded by the trains according to their distance to each traction substation. Thus, the traction substations closer to the train will provide more power than the farther ones and vice versa. In order to achieve this power sharing, the central controller must provide the right control references to the local controllers. According to [97], there are three main local control modes: grid feeding, grid forming and grid supporting. In the grid-forming mode, the converters behave as an ideal voltage source that fixes the magnitude and the angle of the voltage regardless of the power delivered. Alternatively, in the grid–feeding mode, the converters behave as an ideal source that injects a specific amount of the power irrespective of the voltage level. Finally, the grid supporting mode can be seen as an intermediate option were the converters regulate their voltage and frequency or angle according to the power delivered.

Depending on the combination of the local control modes previously described, three principal control schemes can be defined in order to guarantee the power balance and the power sharing between converters. The first and simplest one is the master-slave approach where one converter, called master is controlled in grid forming mode, while the rest of the converters, called slaves are controlled in grid feeding mode. The application of this scheme to advanced railway grids is not very convenient. On the first hand, the power balance is performed by a single converter, reducing the reliability and requiring the connection of the master unit to strong grids. On the other hand, the power sharing depends on the central controller performance that must update the power references of the slave converters for the different traffic conditions. Accordingly, this scheme needs a fast communication channel that increases the cost significantly.

The second approach is the direct voltage control [98] where all converters have implemented a grid-forming mode. By simply setting the same voltage in all the traction substations, the power demanding by the trains will be distributed among the power converters according to the corresponding distance between the trains and the substations. Although it seems a very simple and efficient solution, it presents important drawbacks. The first and most reported one is the possibility of existing circulating currents. Since the voltage is imposed externally, small errors in the magnitude definition or in the synchronization of the angle of the converters can lead to undesirable power flow distribution. Another important disadvantage is the complexity to define cooperation strategies between substations in order to alleviate a possible contingency in the electrical grid. In this case, the new voltage sets should be calculated by means of an optimal power flow that must be run every time the traffic condition varies.

The third and last approach is the well-known droop control. This control is based on the operation scheme followed by conventional synchronous generators. As it is generally known, synchronous generators naturally increase or decrease their velocity and so that the electrical frequency depending on the power balance in the grid. Due to the inexistence of mobile parts, the droop equations for voltage source converters are based on the power transmission fundamentals instead. In order to understand these relations, the simple circuit shown in Figure 4.4 is used. It represents two single phase inverters that are feeding a load through two electrical lines defined by the impedances $\underline{Z}_1$ and $\underline{Z}_2$. The converters are represented as two ideal voltage sources of voltages $\underline{V}_1$ and $\underline{V}_2$; and the load as a current source whose voltage is defined as $\underline{V}_3$. Solving the circuit, the active and reactive power (P_i and Q_i) delivered by the converter i, are given by equations (4.1) and (4.2) respectively.

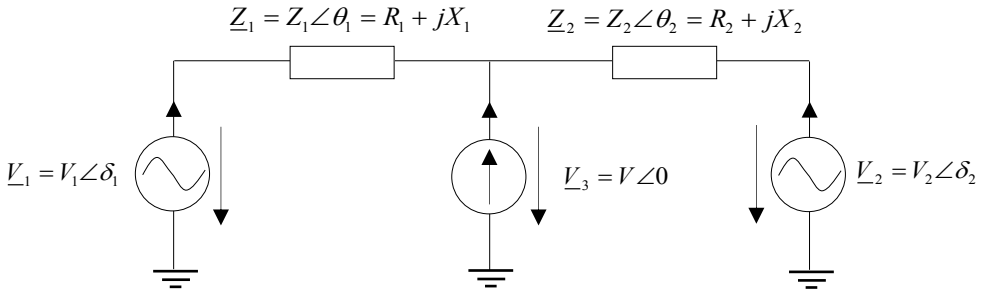

Figure 4.4. Power tranmsision fundamentals analysis.

$$P_i = \frac{V_i}{R_i^2 + X_i^2}\left[R_i\left(V_i - V\cos(\theta_i)\right) + X_i V\sin(\delta_i)\right] \tag{4.1}$$

$$Q_i = \frac{V_i}{R_i^2 + X_i^2}\left[-R_i V\sin(\delta_i) + X_i\left(V_i - V\cos(\theta_i)\right)\right] \tag{4.2}$$

For high and medium voltage lines, the inductance part is significantly higher than the resistance one and thus, this latter term can be neglected. Furthermore, the power angle, δ is relatively small and so that the sine can be represented by the de angle and the cosine by 1. Therefore, the equations (4.1) and (4.2) can be simplified into equations (4.3) and (4.4) respectively.

$$P_i \approx \frac{V_i V \delta_i}{X_i} \tag{4.3}$$

$$Q_i \approx \frac{V_i (V_i - V)}{X_i} \tag{4.4}$$

According to equations (4.3) and (4.4), the active power mainly depends on the angle difference while the reactive power on the voltage magnitude difference. With this information, researches have proposed the control equations (4.5) and (4.6), where $k_{w,i}$ and $k_{v,i}$ are the frequency and voltage droop parameters, and w_0 and V_0, the frequency and voltage references. As observed in Figure 4.5.a, when the frequency of the grid is greater than the frequency reference, the power converter absorbs power and when the frequency of the grid is lower than the reference, the converter injects power. A similar analysis can be done for the reactive power, but this time with the voltage magnitude (Figure 4.5.b). The values of the droop parameters are calculated as the rate between the maximum active and reactive power for the maximum frequency and voltage variations permitted.

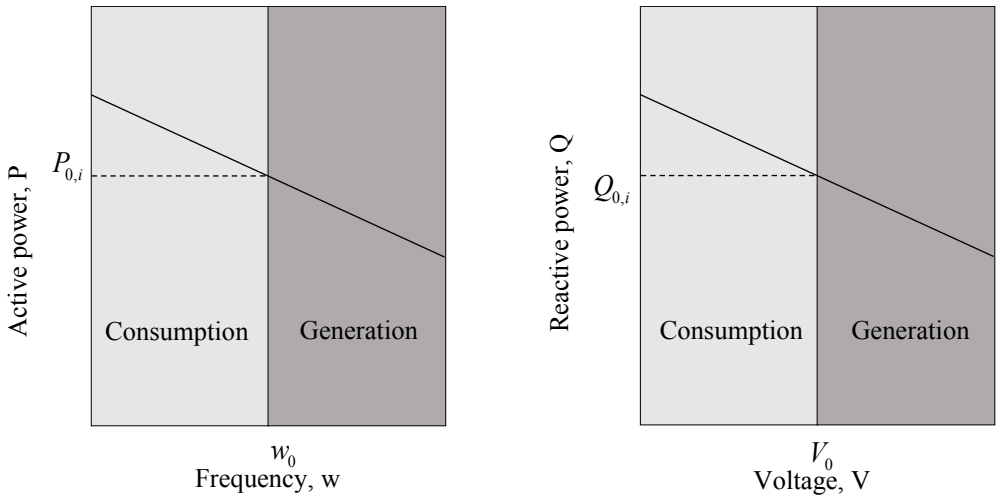

a) Active power. *b) Reactive power.*

Figure 4.5. Droop characteristics.

$$P_i = P_{0,i} - k_{w,i}(w - w_{0,i}) \tag{4.5}$$

$$Q_i = Q_{0,i} - k_{v,i}(V_i - V_{0,i}) \tag{4.6}$$

In contrast to the master-slave and the direct voltage control approaches, the active and reactive power in the droop control strategy is self-regulated by means of the frequency and the voltage of the grid without the necessity of communications. Ideally, the active power and reactive power will be distributed according to the droop coefficients previously defined. Thus, in order to distribute the power according to the distance between the traction substations the droop coefficients must be adapted regarding the traffic conditions. Once again, the power sharing will depend on the performance of the central controller.

In order to alleviate this issue, it is necessary to incorporate the traffic conditions to the droop characteristics. The definition of cost droop functions is really difficult for this application due to the high variability of the traffic conditions. Therefore, this work proposes to take advantage of the impedance influence on the power sharing. The impedance represents a natural indicator of the train position since it increases its value when the train is far and decreases when the train is near. Unfortunately, the frequency is a global variable that does not provide any information about the traffic. In order to solve this fact, this thesis suggests using the angle instead.

The angle droop control was firstly introduced in [99] in order to eliminate the frequency variations in rural networks. In contrast to frequency droop control, it requires a common timing reference that synchronize the angle of the converter stations. The global positioning system (GPS) is the most extended solution adopted. This approach is widely used for phasor measurements units in power systems, although the application to smaller systems have been gaining ground. It is important to highlight that this solution does not need any information of the rest of the converters. According to this information, the new control law for the active power is given by equation (4.7).

$$P_i = P_{0,i} - k_{\delta,i}(\delta_i - \delta_{0,i}) \tag{4.7}$$

As it was previously explained, angle droop control is affected by the line impedance and hence it can provide a natural traffic system indicator. In order to analyze this effect, the simple test case shown in Figure 4.6 is used. This case is composed of two traction substations controlled according to the strategy previously proposed that are feeding a single train. Assuming the line purely inductive, the impedances seen from each traction substation are *(1-a)·X_T and a·*X_T; where X_T represents the total impedance of the section and *a,* the relative position of the train. The variable *a* has a value of one when the train is at the traction substation number one, and a value of zero when it is at the second traction substation.

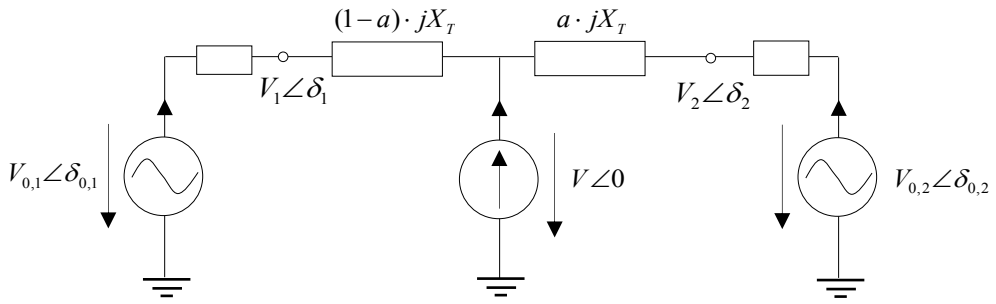

Figure 4.6. Impedance influence on the power sharing.

In order to analyze the power sharing ratio, the voltage drop on the train is divided into two parts. The first part is a virtual voltage drop due to the droop control and the second part corresponds to the voltage drop due to the line impedance. When the droop coefficients are enough low, the first part can be neglected, and the active and reactive power can be easily calculated by means of equations (4.1) and (4.2) respectively. According to equations (4.8) and (4.9), the active and reactive power are shared according to the line impedance, that is modified with the train positions. This means that the closer the train is to a traction substation, the higher the power provided by this substation.

$$\frac{P_1}{P_2} \approx \frac{\frac{V_1 V \delta_1}{X_1}}{\frac{V_2 V \delta_2}{X_2}} \approx \frac{aX_T}{(1-a)X_T} = \frac{a}{(1-a)} \tag{4.8}$$

$$\frac{Q_1}{Q_2} \approx \frac{\frac{V_1 (V_1 - V)}{X_1}}{\frac{V_2 (V_2 - V)}{X_2}} \approx \frac{aX_T}{(1-a)X_T} = \frac{a}{(1-a)} \tag{4.9}$$

On the other hand, when the droop coefficients are high enough, the second part of the voltage drop can be neglected and the active and reactive powers are given by equations (4.7) and (4.6) respectively. In this situation the power sharing is given by equations (4.10) and (4.11). These equations show how the power sharing is governed by the ratio between the droop coefficients regardless of the train position. It is noted that for high droop values the angles of the converters tends to be equal and the voltage magnitudes tend to zero.

$$\frac{P_1}{P_2} \approx \frac{-k_{\delta,1}(\delta_1 - \delta_{0,1})}{-k_{\delta,2}(\delta_2 - \delta_{0,2})} \approx \frac{k_{\delta,1}}{k_{\delta,2}} \tag{4.10}$$

$$\frac{Q_1}{Q_2} \approx \frac{-k_{v,1}(V_1 - V_{0,1})}{-k_{v,2}(V_2 - V_{0,2})} \approx \frac{k_{v,1}}{k_{v,2}} \tag{4.11}$$

Finally, when both factors are significant, the determination of an analytical formula turns into a very difficult task even for this straightforward example. However, as it will be demonstrated in the simulation results, it presents an intermediate behavior, where the hyperbolic power sharing ratio is gradually transformed into a horizontal line. Figure 4.7 shows the active power sharing performance for the three aforementioned situations. Finally, an analogous study can be performed for the reactive power.

All the previous analyses were based on the assumption of purely inductive grids, but railway grids usually present significant resistance values that make the previous approach inefficient. For the general case, the active and the reactive power are coupled and so that a variation in the voltage magnitude or in the voltage angle leads to active and reactive power variations. In order to improve the transient response and enhancing the power sharing, engineers have proposed two main methods. The first and most extended is the introduction of a virtual impedance. The implementation of this strategy is very challenging for railway systems since the train movement modifies the impedance values of the lines complicating the task dramatically.

The second one is the definition of a rotational fictitious power whose active and reactive parts only depend on the angle and the voltage values. It is important to highlight that it is a fictitious power and the real power is still coupled. However, this approach enables to enhance the power sharing significantly. The calculation of this rotational active and reactive power is given by equations (4.12) and (4.13). As it observed, this expression incorporates cross terms that defines with better accuracy the electrical power transmission fundamental previously explained.

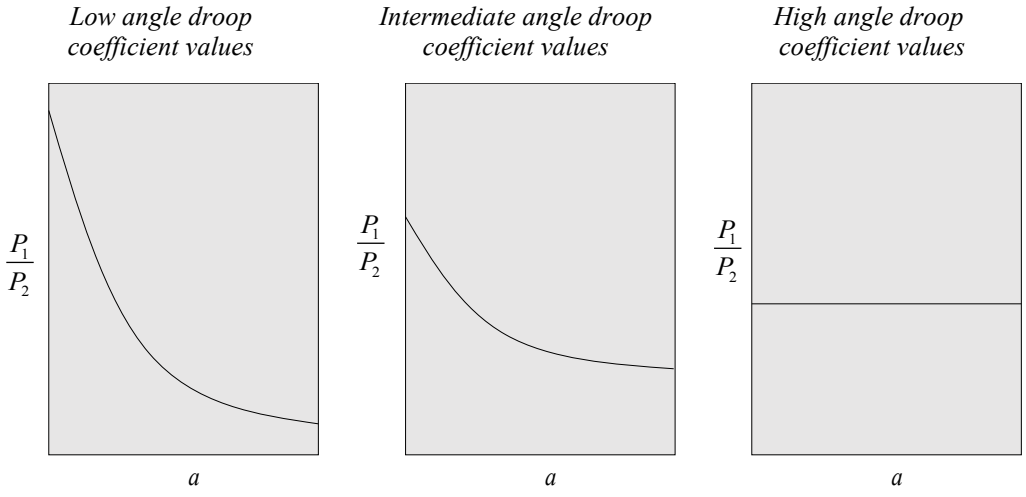

Figure 4.7. Active power sharing analysis.

$$P_i = P_{0,i} - \frac{X_i}{Z_i} k_{\delta,i}(\delta_i - \delta_{0,i}) - \frac{R_i}{Z_i} k_{v,i}(V_i - V_{0,i}) \tag{4.12}$$

$$Q_i = Q_{0,i} + \frac{R_i}{Z_i} k_{\delta,i}(\delta_i - \delta_{0,i}) - \frac{X_i}{Z_i} k_{v,i}(V_i - V_{0,i}) \tag{4.13}$$

An additional and very important advantage of the use of this rotational power is that the same equations used for AC can be applied for DC. In DC grids, the reactive part does not affect in the steady state operation and thus the equation (4.12) can be simplified into (4.14). As expected, the active power in DC grids is controlled by the voltage magnitude.

$$P_i = P_{0,i} - k_{v,i}(V_i - V_{0,i}) \tag{4.14}$$

According to all these results, the operation of the advanced converter-based system can be performed by means of simply adapting the droop coefficients according to the utility grid conditions. In normal operation conditions, the operation of the system will aim to distribute the power efficiently and thus, the droop coefficients should be defined as highest as possible. However, under a possible contingency in the utility grid, a possible decrease in the power consumption in some traction substations can contribute to a better stability of the grid. In this case, the central controller of the system shown in Figure 4.8 will decrease the droop coefficients, thus rising the power cooperation between the substations.

In the next section the operation of conventional and advanced converter-based systems is comprehensively studied for a simple electrical configuration. Although its simplicity they illustrate very well the performance of the system and facilitate the understanding of more complicate cases such as the one analyzed in chapter five.

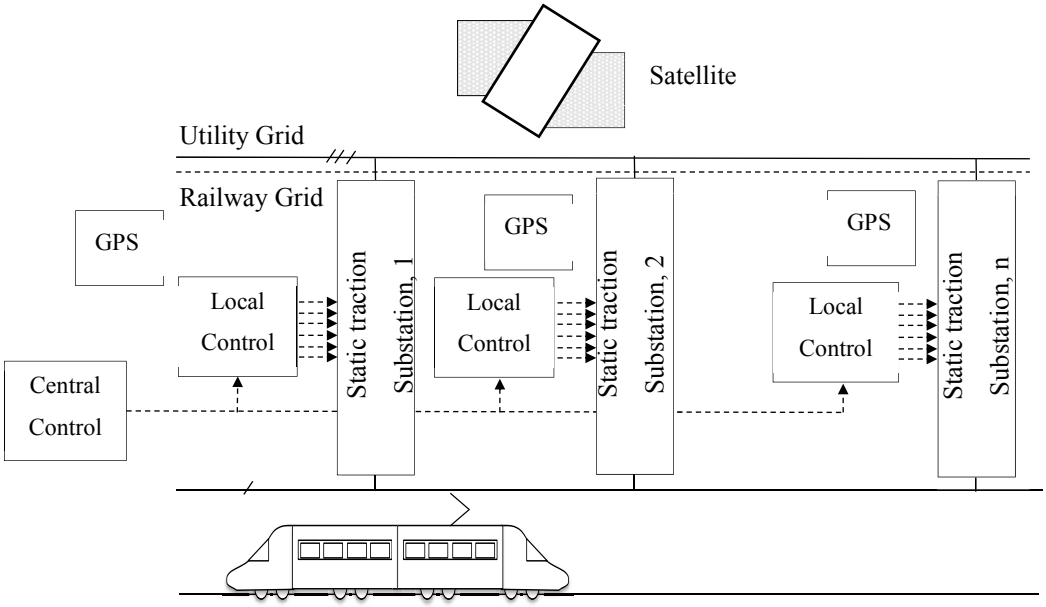

Figure 4.8. Hierarchical control scheme proposed for advanced AC converter-based systems.

4.4 Operation analysis of conventional transformer-based systems

This section analyses the operation of conventional transformer-based electrical railway power supply systems by means of a simple electrical scheme composed of two sections for two catenary configurations. In the first case, Figure 4.9.a, the catenary has a direct monovoltage configuration and the length of each section has a value of 15km. The second case, Figure 4.9.b, has a bivoltage autotransformer catenary configuration, and the length of each section has been consequently increased to 30km. Hereafter, the first and second cases will be referred as monovoltage and bivoltage cases respectively.

The catenary conductor data are listed in Table 4.2. Both catenary systems have the same conductor properties and arrangement except for the negative feeder. As it was explained in chapter three, a full representation of the catenary is rarely used in power flow studies. Accordingly, the monovoltage catenary arrangement has been reduced to an equivalent positive feeder while the bivoltage to a positive and negative equivalent conductor whose corresponding primitive reduced matrices are shown in Figure 4.10 and Figure 4.11 correspondently. It is noted that the neutral conductors (return and rails) have been implicitly included into these equivalent matrices.

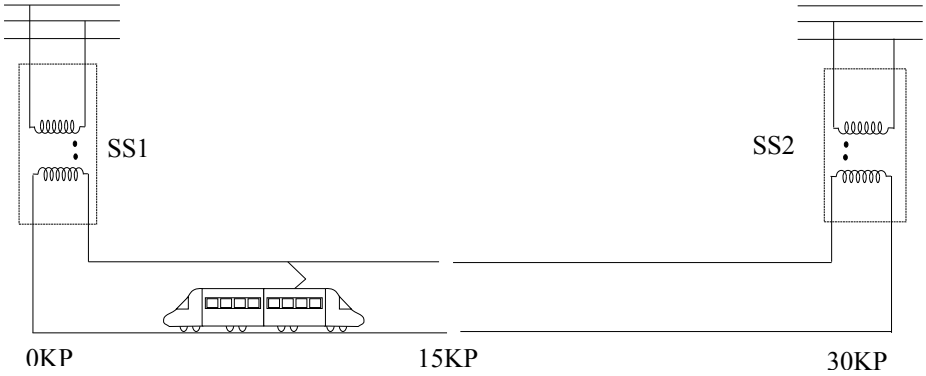

a)Monovoltage configuration.

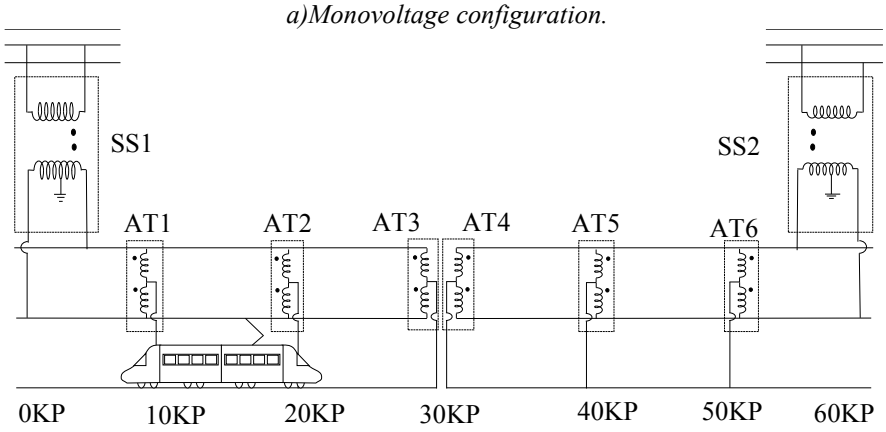

b)Bivoltage configuration.

Figure 4.9. Conventional transformer-based test cases definition.

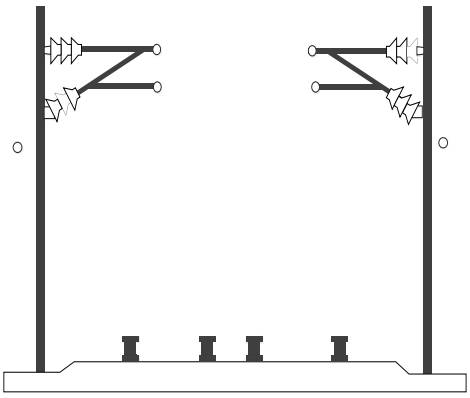

$$Z = 1e-4(1.1+2,83j) \quad \Omega/m$$

Figure 4.10. Monovoltage catenary arragement.

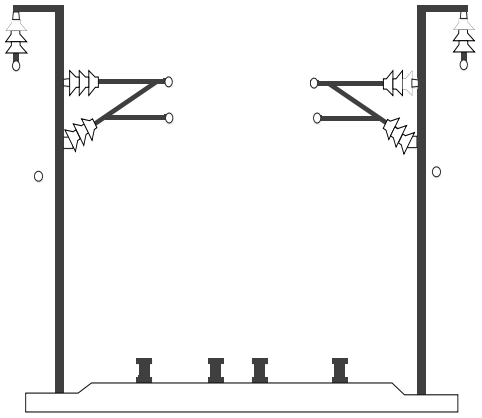

$$Z = 1e-4\begin{bmatrix} 1.1+2.8j & 0.7+1.22j \\ 0.7+1.2j & 1.3+3.1j \end{bmatrix} \quad \Omega/m$$

Figure 4.11. Bivoltage catenary arragement.

Table 4.2. Catenary conductor data. Conventional transformer-based analysis.

Name	*Horizontal Position (m)*	*Vertical Position (m)*	*Section* (m^2)	*Resistance* $(\Omega \cdot m^{-1})$	*Type*
Contact 1	*-2,35*	*5,3*	*6.91e-3*	*1.39e-4*	*Cu-Mg*
Contact 2	*2,35*	*5,3*	*6.91e-3*	*1.39e-4*	*Cu-Mg*
Sustainer 1	*-2,35*	*6,3*	*5.50e-3*	*1.87e-4*	*Cu*
Sustainer 1	*2,35*	*6,3*	*5.50e-3*	*1.87e-4*	*Cu*
Negative feeder 1	*-6,65*	*6,85*	*9.46e-3*	*1.19e-4*	*LA-280*
Negative feeder 2	*6,65*	*6,85*	*9.46e-3*	*1.19e-4*	*LA-280*
Return 1	*-5,75*	*5,4*	*6.08e-3*	*3.07e-4*	*LA-110*
Return 2	*5,75*	*5,4*	*6.08e-3*	*3.07e-4*	*LA-110*
Rail 1	*-3,1*	*0*	*1.08e-1*	*4.64e-6*	*UIC-60*
Rail 1	*-1,53*	*0*	*1.08e-1*	*4.64e-4*	*UIC-60*
Rail 2	*1,53*	*0*	*1.08e-1*	*4.64e-4*	*UIC-60*
Rail 2	*3,1*	*0*	*1.08e-1*	*4.64e-4*	*UIC-60*

The transformer data are listed in Table 4.3. As shown in Figure 4.9.a and in Figure 4.9.b, the monovoltage catenary configuration uses a single-phase traction transformer while the bivoltage a single-phase traction transformer with a secondary center tap grounded. All traction substations are assumed to be fed form from a 220kV utility grid with a short circuit power of 10GW purely inductive. Finally, the traffic is reduced a single train that consumes an active power of 10MW with a load factor of 0.95 inductive.

Table 4.3. Transformer parameters. Conventional transformer-based analysis.

Parameter	*Traction substation Monovoltage*	*Traction substation Bivoltage*	*Autotransformer substation*
Voltage Ratio	*220/25*	*220/25/25*	*25/25*
Nominal Power (MVA)	*60*	*60*	*10*
Short circuit impedance (pu)	*0.1j*	*0.1j/0.1j/0.05j*	*0.05j*

4.4.1 Monovoltage case analysis

Figure 4.12 describes the geometrical locus of the voltage and the current between the maximum and the minimum values obtained for the equivalent positive conductor over its length. In order to illustrate how these distributions are calculated, three different instants corresponding to the train position of seven, ten and thirteen kilometers are studied.

According to Figure 4.12.a, the voltage on the equivalent positive conductor decreases linearly from the traction substation to the train position and it remains constant from this point to the end of the section. As it can be observed, it presents an initial voltage drop due to the utility grid and transformer impedances. Finally, the voltage on the non-loaded section have a constant and equal value to nominal voltage of 25kV. According to all this information, the minimum catenary voltage will be reached when the train is placed at the end of the section and the maximum when the section is non-loaded. The same analysis can be performed when the train is on the second section.

According to Figure 4.12.b, the current flowing through the equivalent positive conductor has a constant value from the traction substation to the train position, and it remains zero from this point to the end of the section. The current on the non-loaded section is zero. As it is noted, the value of the current demanded by the train increases with the distance between the tractions substation and the train. Accordingly, the maximum current will be reached when the train is placed at the end of the section and the minimum when the section is non-loaded. The same analysis is valid when the train is on the second section.

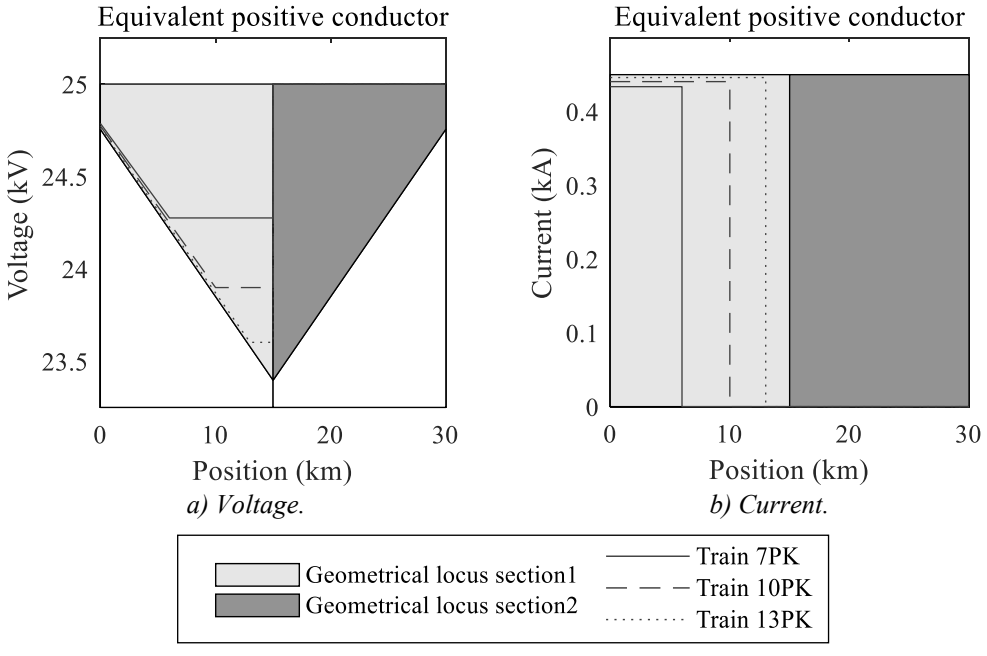

Figure 4.12. Voltage and current analysis. Transformer-based monovoltage system.

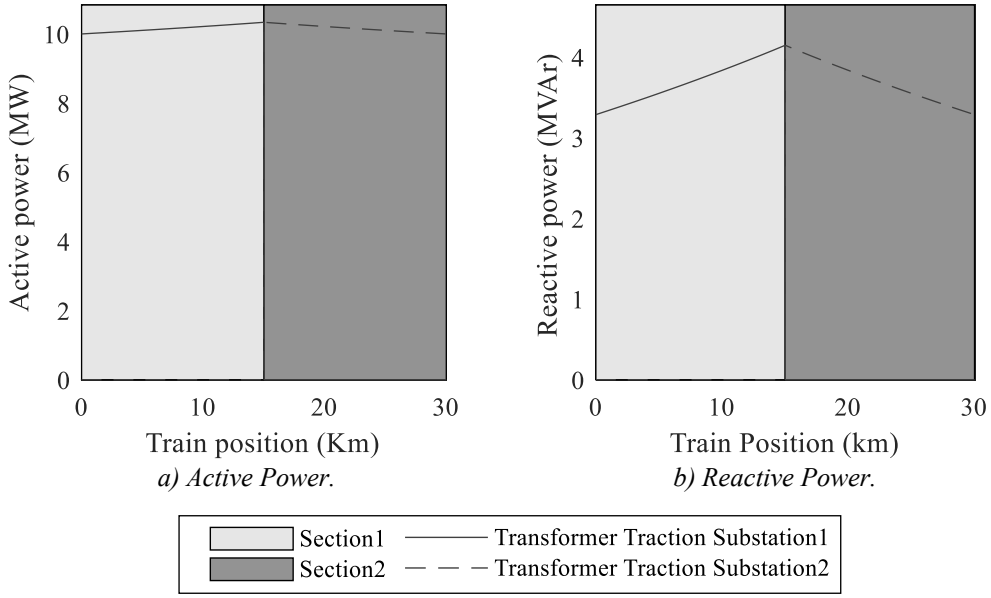

Figure 4.13. Power analysis. Transformer-based monovoltage system.

Figure 4.13.a and Figure 4.13.b describes respectively the active and reactive power provided by each traction substation for all the train positions. As it can be observed, the active and reactive power delivered by the traction substation of the loaded section increases as the distance to the train rises, while the active and reactive power of the traction substation of the non-loaded section remains constant and equal to zero.

4.4.2 Bivoltage case analysis

Figure 4.14 describes the geometrical locus of the voltage and the current between the maximum and the minimum values obtained for the equivalent positive and negative conductors over their length. Following the same approach used in the monovoltage case analysis, four different instants corresponding to the train positions of twenty-three, twenty-five, twenty-seven and twenty-nine kilometers are included in order to illustrate how these distributions are obtained.

For the equivalent positive conductor, the voltage decreases from the traction substation to the train, and it increases from the train to the end of the section. It is noted, that the voltage drop rate is increased at the autotransformers positions. Finally, the voltage on the non-loaded sections remains constant and equals to the nominal value of 25kV. It is especially interesting the voltage behavior between the autotransformers adjacent to the train. As it is observed in Figure 4.14.a, the minimum voltage describes a parabolic curve, so that the voltage drop rate stars decreasing as the train approaches the next autotransformer, reaching a minimum value after which the voltage starts to rise again. Accordingly, the minimum voltage will describe a parabolic curve between every two autotransformers and the maximum value will be constant and equal to the nominal one.

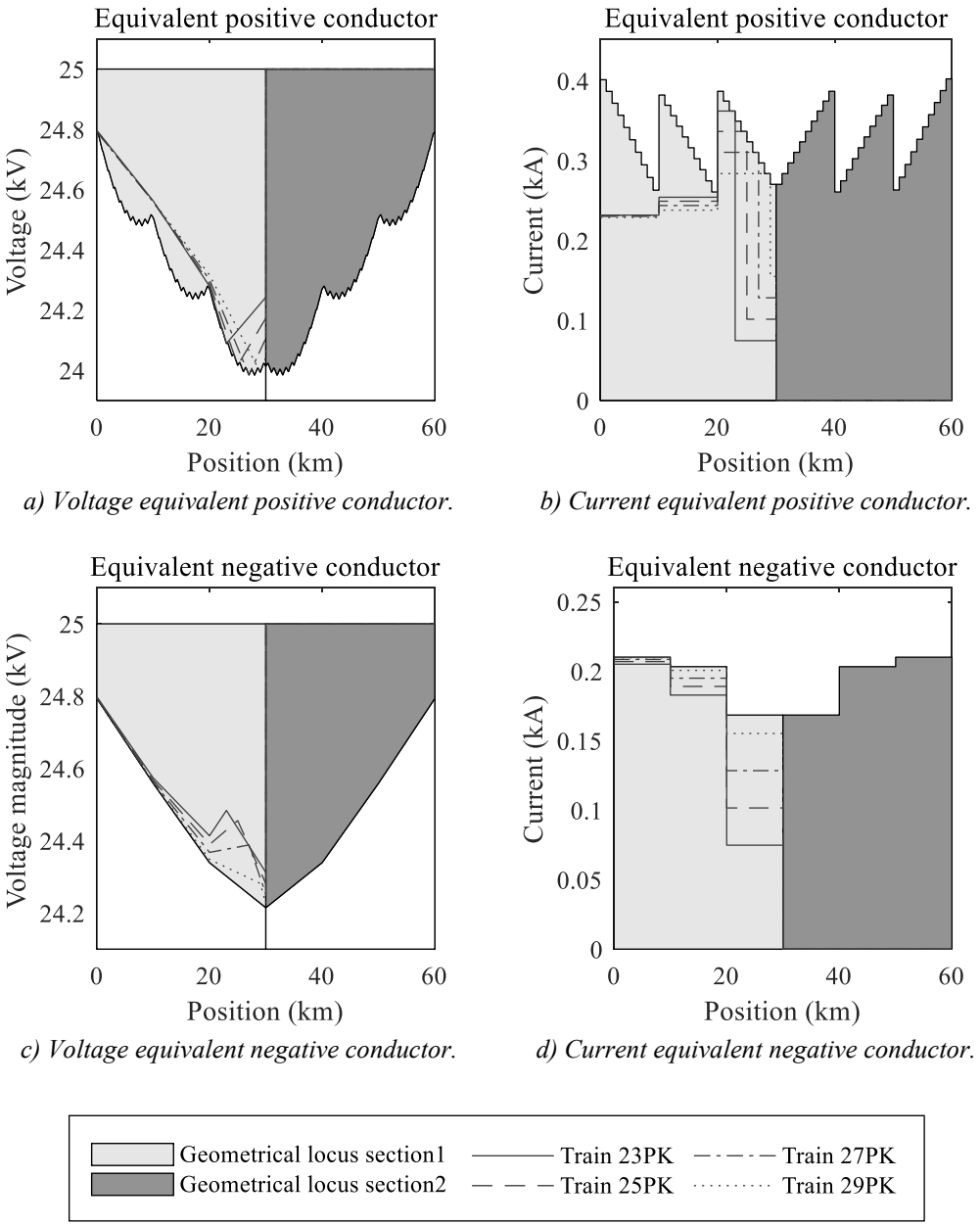

a) Voltage equivalent positive conductor.

b) Current equivalent positive conductor.

c) Voltage equivalent negative conductor.

d) Current equivalent negative conductor.

Figure 4.14 Voltage and current analysis. Transformer-based bivoltage system.

The current distribution is also very different to the monovoltage case. As shown in Figure 4.14.b the current drawn by the train is supplied from both side of the conductor. The first part will come from the positive conductor and second part from the negative feeder. As it is observed, the current magnitude is reduced at each autotransformer due to the current balance performed. It is also important to highlight the influence of the train position in the maximum currents value presented in the conductor. According to the results obtained, the maximum current is reduced as the train approaches to the new autotransformer, reaching the minimum values at the autotransformer positions.

The voltage on the negative feeder decreases from the traction substation to the last autotransformer placed in between. From this point, the voltage starts to increase reaching a maximum, from which it starts to drop again. This current behavior can be easily explained by the analysis of the current distribution on the positive feeder. As it was previously explained, the current on the positive conductor has two different directions that induces voltage drops with different signs on the negative feeder. As the train moves to the next autotransformer, the current is reduced, and so does, the voltage induced on the negative feeder. According to this information, the minimum voltage will be reached when the train is placed at the end of the sections and the maximum when the section is non-loaded.

Figure 4.14.d shows the current flow distribution on the negative feeder. It presents a constant value between every two autotransformers which value is increased as we approach to the traction substation due to the balancing performance of the autotransformers. Accordingly, the maximum values will be reached when the train is placed at the end of the section and the minimum when the train is not on the section.

Figure 4.15 shows the active and reactive power provided by each traction substation for all the train positions. In contrast to the monovoltage case, they describe a parabolic tendency that is repeated every two autotransformers due to the current distribution previously explained. Finally, the active and reactive power remains zero when the section is unloaded.

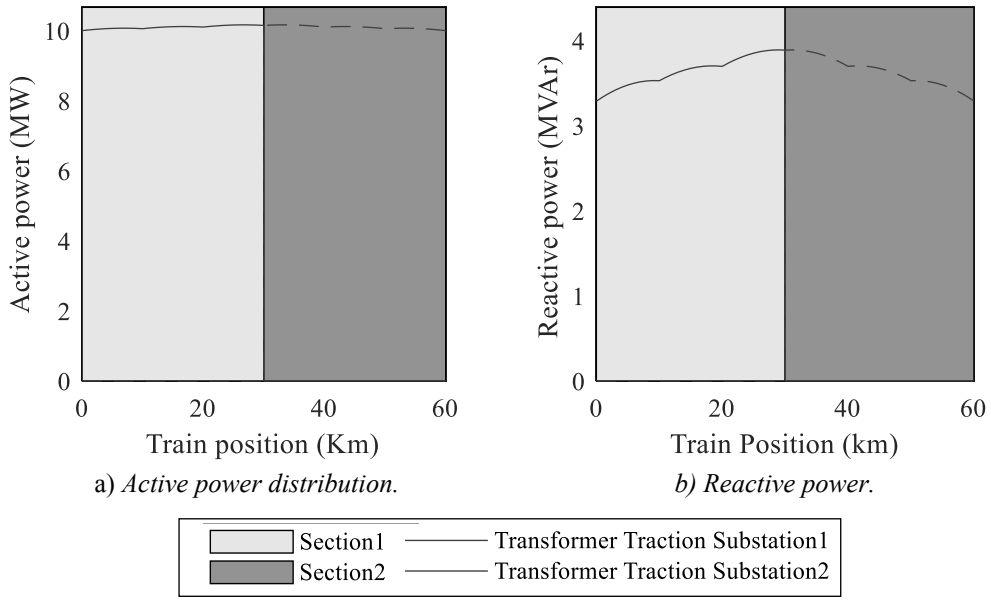

a) *Active power distribution.* *b) Reactive power.*

Figure 4.15. Power analysis. Transformer-based bivoltage system.

4.4.3 Imbalance analysis

Figure 4.16 and Figure 4.18 show the root squared mean of the active and reactive power provided by each phase of the utility grid for the bivoltage catenary case. The monovoltage case have a similar behavior and it is not included. As expected, only two phases of the utility grid are loaded because of the single-phase nature of the railway traction transformer. According to the results obtained, the traction transformer of the substation one, SS1 is connected to phases A and B while in the traction substations number two, SS2 it is connected between phases B and C. Accordingly, only these phases present power consumption. It is interesting to notice that the power is also distributed differently between these two phases. Finally, since the train consumption is maintained constant for all the train positions the RMS values are the same for the two traction substations.

As it was explained in the introduction of this chapter, the voltage imbalance produced by the railway system must be lower than the 1% for time periods of one minute. Figure 4.17 shows the imbalance factor calculated for every position of the train for four different short circuit power values of the utility grid: 1GVA, 2.5GVA, 5GVA and 10GVA. As expected, the imbalance factor increases with the distance because of the higher power consumed and it is reduced as the short circuit power of the utility grid is increased. According to these results, the minimum short circuit power should be higher than 5GVA in order to fulfill the grid code of the Spanish utility grid operator.

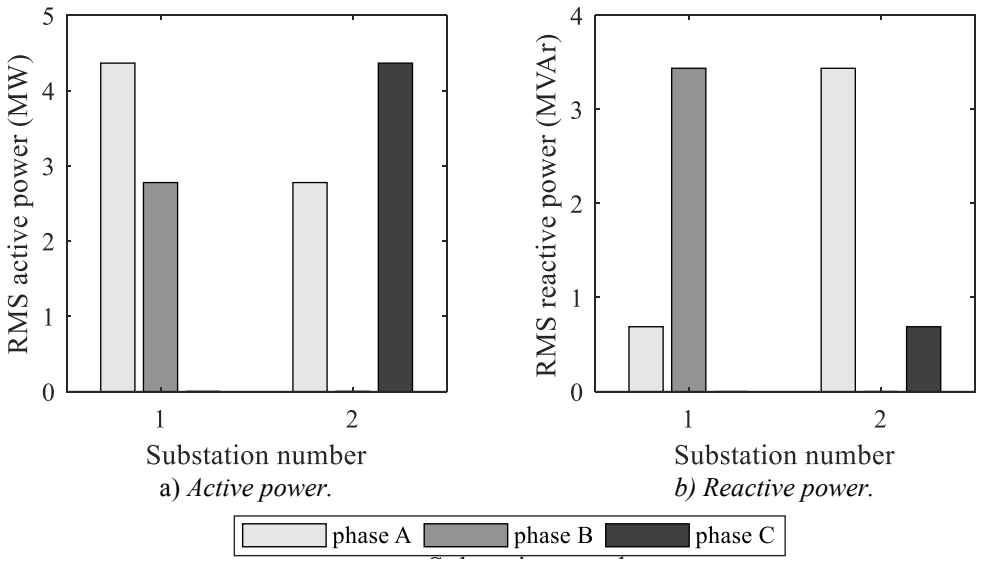

Figure 4.16. Imbalance abnalysis. Conventional transformer-based systems.

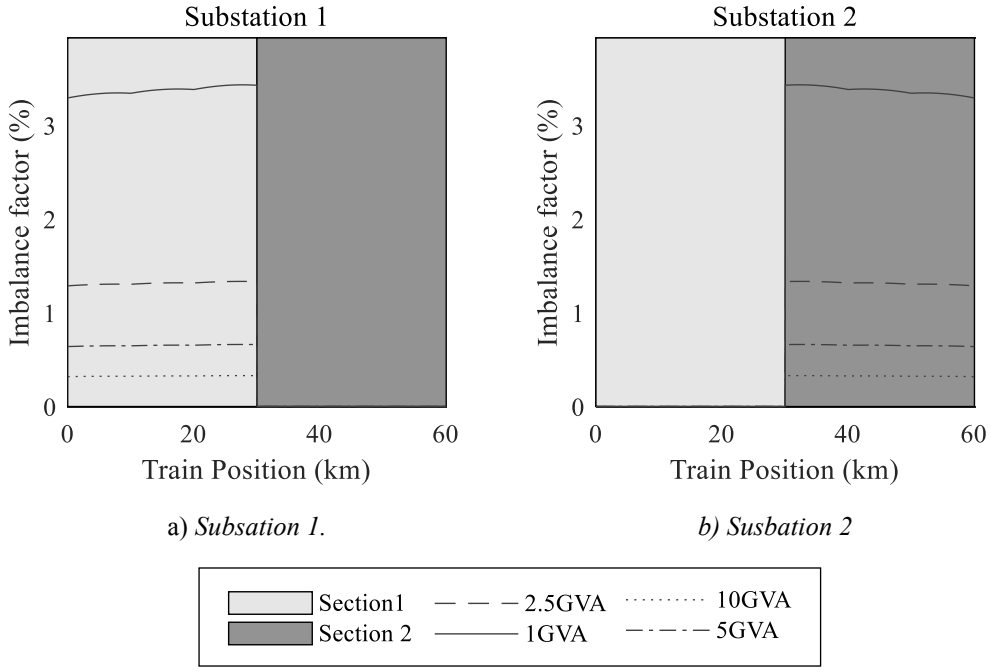

a) *Subsation 1.* *b) Susbation 2*

Figure 4.17. Power imbalance factor. Conventional transformer-based systems.

4.5 Operation analysis of advanced AC converter-based systems

This section analyses the operation of advanced AC converter-based systems using the control strategy proposed. To this end, the two previous test cases used for the study of the operation of conventional transformer-based configurations have been adapted to obtain the corresponding advanced schemes.

For the monovoltage case, Figure 4.18.a, the traction substations have been replaced with converter ones consisted of a single-phase VSC and a three phase VSC in back-to-back configuration. For the bivoltage case, Figure 4.18.b the traction substation has the same configuration used for the monovoltage case but with a double nominal DC voltage. Furthermore, two additional autotransformers have been added at the front of each traction substations in order to balance the load of the positive and negative equivalent conductors. In addition, for both configurations the two sections have joined.

Both cases are fed from the same utility grid used for the base test case whose voltage is adapted to the converter operation level by means of a three-phase transformer. For the monovoltage case, the transformer has winding connection of Ynd with a voltage ratio of 220/55 and a nominal power of 60MVA. For the bivoltage configuration, the transformer has a Ynd configuration with a voltage rate of 220/110 and nominal power of 60MVA. Both transformers have a short circuit impedance of 0.1jpu.

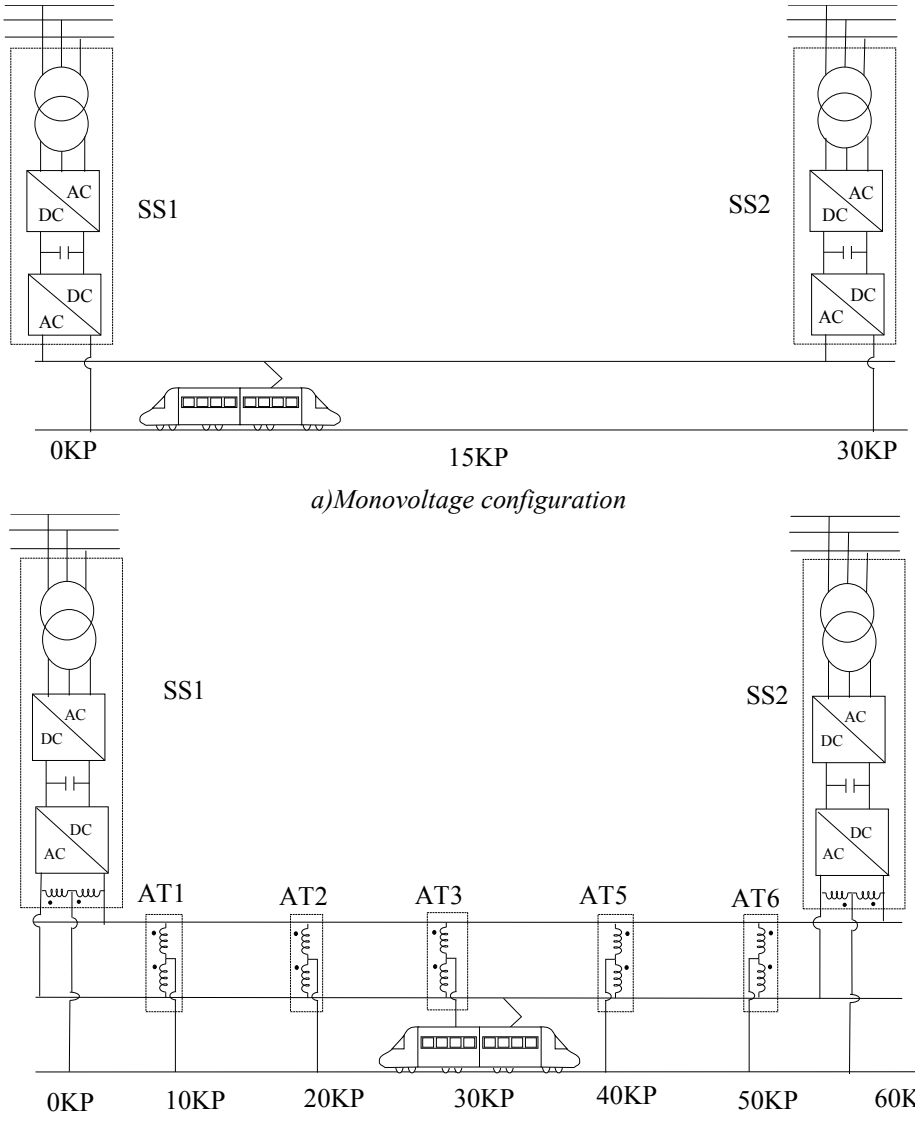

a)Monovoltage configuration

b)Bivoltage configuration

Figure 4.18. Advanced AC converter-based test cases definition.

The converter on the utility grid side is set to maintain the DC voltage constant and to inject zero reactive power. The converter on the railway side has implemented the control proposed with an angle droop parameter of 60/0.1 MW/rad and a voltage droop parameter of 60/3000Mvar/V.

4.5.1 Monovoltage case analysis

Figure 4.19 describes the geometrical locus of the voltage and the current between the maximum and the minimum values obtained for the equivalent positive conductor over its length. In order to explain these distributions, three different instants corresponding to the train positions seven, ten and thirteen kilometers have been included.

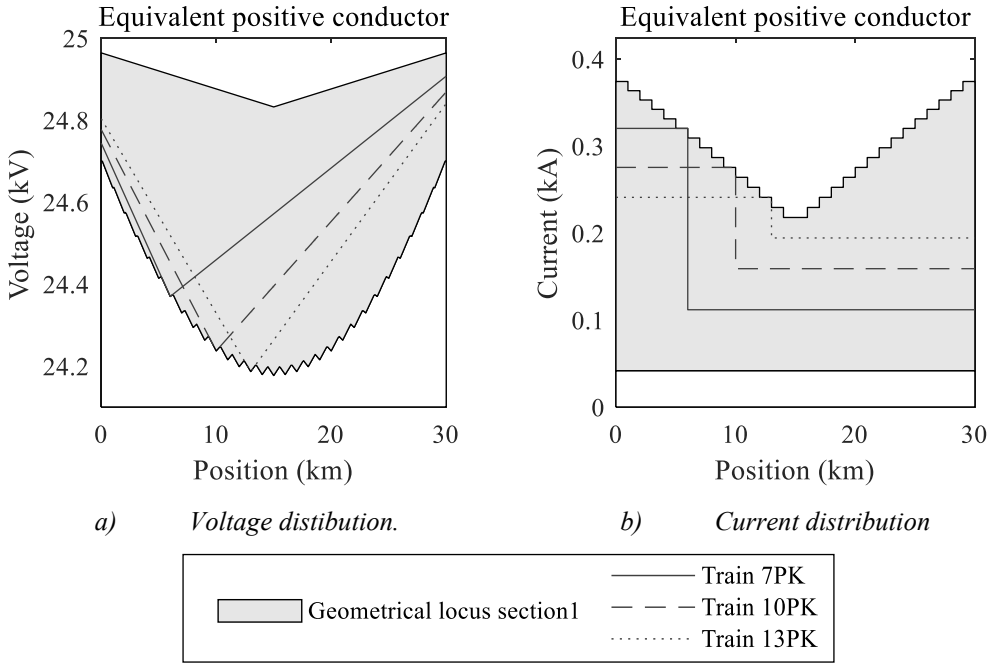

Figure 4.19.Voltage and current distribution.
Advanced AC converter-based monovoltage system.

As shown in Figure 4.19.a, the voltage on the equivalent positive conductor decreases from both traction substation to the train position. This voltage drop is driven by two different effects, the lines losses that increases with the distance between the traction substation and the train, and the droop control that increases in the opposite direction. As it is observed, as the train approaches the central part of the section, the conductor points closer to the traction substation present voltage values higher than when the train is located near to the traction substation. According to this information, the minimum voltage values for a conductor point is always reached when train is located at this point.

On the other hand, the maximum voltage of the first half of the section will be reached when the train is located at the second substations and the minimum voltage values of the second half of the section when the train is located at the first substation. It is noted that the minimum voltage values are always below 25kV because the droop control require a voltage drop to provide power.

As shown in Figure 4.19.b, the current flowing through the equivalent positive conductor has a constant value from each traction substation to the train position. The value of these currents depends on the distance between the train and the corresponding substation, so that, it decreases as the distance increases and it increases as the distance decreases. Accordingly, the maximum values for the equivalent positive decreases from the traction substations to the middle of the section. On the other hand, the minimum current value never reaches zero because both substations are always loaded. This minimum value occurs when the train is located at the substations.

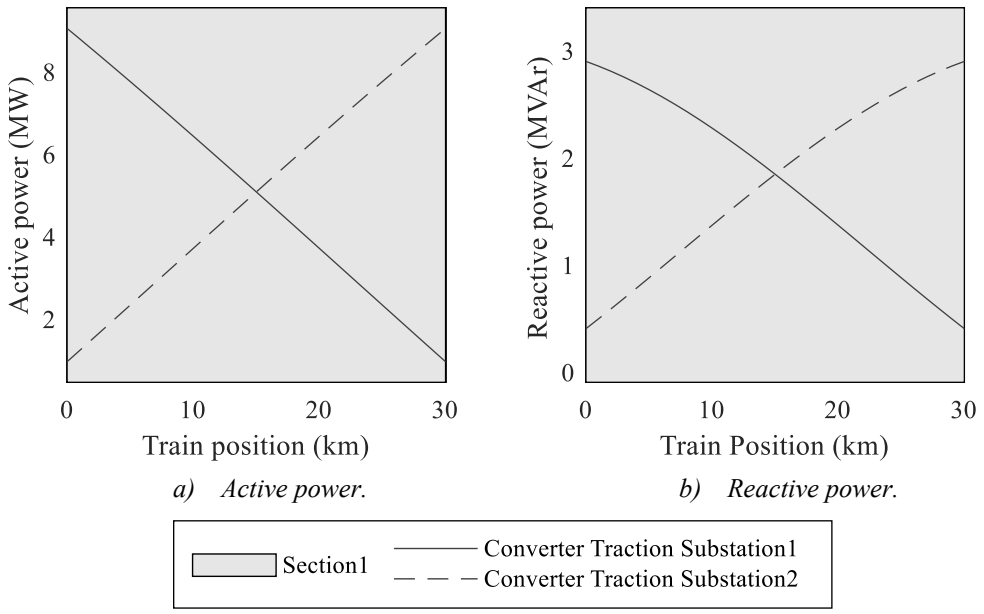

a) Active power. *b) Reactive power.*

Figure 4.20. Power distribution. Advanced AC converter-based monovoltage system case.

Figure 4.20.a and Figure 4.20.b show the active and reactive power sharing between the two traction substations. As expected, the active and reactive power provided by each substation decreases as the train moves away from their corresponding traction substation. It is interesting that the curves evidence a non-linear tendency because of the non–linear relation between the losses of the line and the distance.

4.5.2 Bivoltage case analysis

Figure 4.20 represents the voltage and current geometrical locus between the maximum and minimum values obtained for the equivalent positive and negative conductor over their length for all the train positions. This chart also includes four different instants corresponding to the train positions of twenty-three, twenty-five, twenty-seven and twenty-nine kilometers.

As shown in Figure 4.21.a, the voltage on the equivalent positive conductor decreases from the traction substations to the train position, accentuating the voltage droop rate every autotransformer. The voltage behavior between the two adjacent autotransformers is similar to the one obtained for the conventional transformer-based system. Thus, the minimum voltage will describe a parabolic curve that is repeated between every two autotransformers. On the other hand, the maximum value of the voltage of first half of the section will be reached when the train is located at the second substations and the minimum voltage values of the second half of the section when the train is located at the first substation.

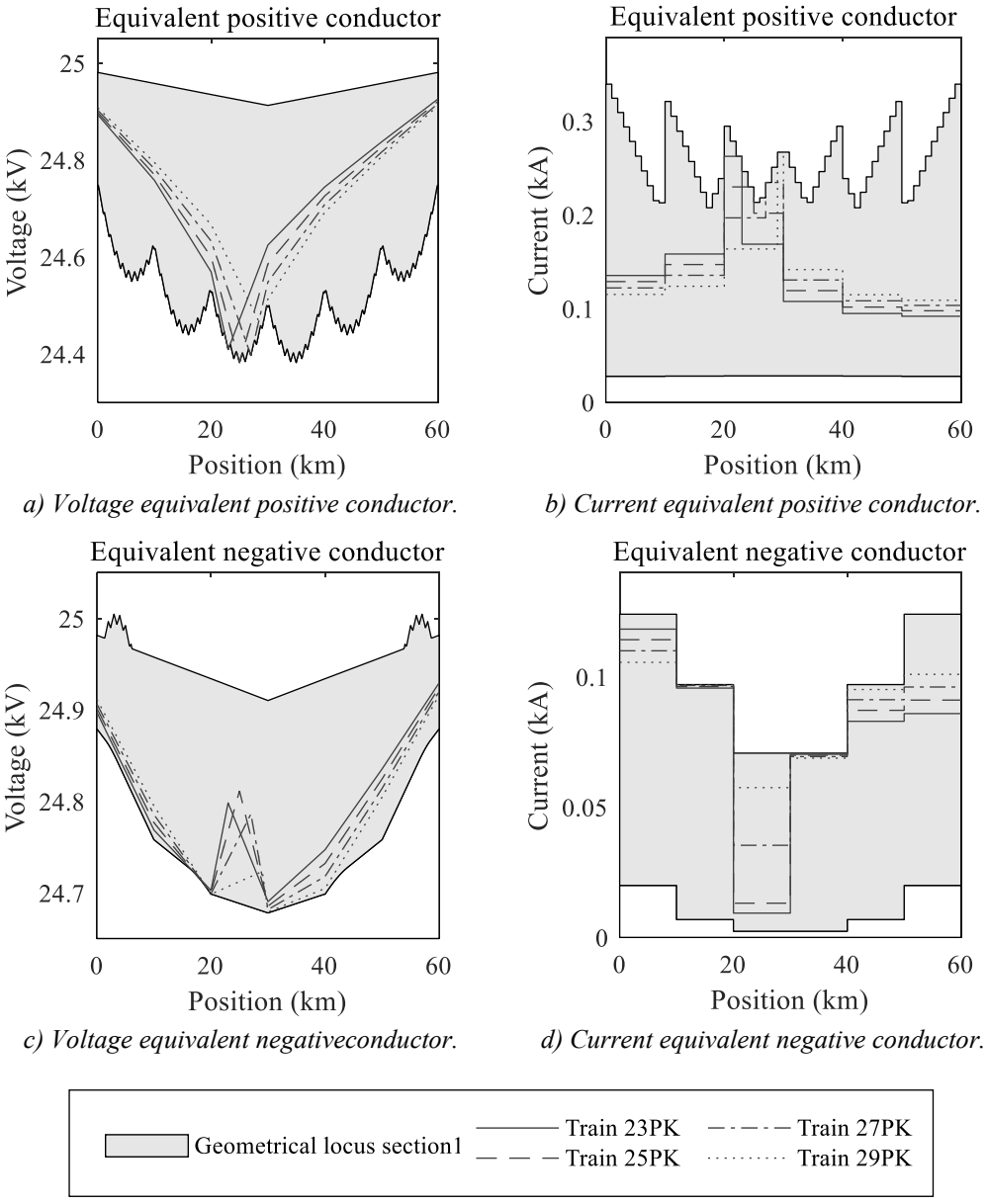

a) Voltage equivalent positive conductor. *b) Current equivalent positive conductor.*

c) Voltage equivalent negativeconductor. *d) Current equivalent negative conductor.*

Figure 4.21.Voltage and current distribution.Advanced AC converter-based bivoltage system.

The current flowing through the equivalent positive conductor is the result of the current distribution performed by the autotransformers. According to Figure 4.21.b, the current is divided at every train position, and it reduces its value between every autotransformer until reaching the corresponding tractions substation. In contrast to the current distribution obtained for the conventional transformer-based systems, where the maximum current always decreases between every two autotransformers, the possibility of feeding the traction from the other substations simultaneously alters this behavior. As it is noted, the maximum current can present and initial decreasing tendency until reaching a minimum from which it stat to increase again. Finally, the minimum current of the equivalent positive conductor is never zero and whose value is obtained when the train is located at the other traction substations.

The voltage on the equivalent negative conductor decreases from the traction substation to the last autotransformer placed between the traction substation and the train. From this point to the train position, the voltage increases due to the coupling existing between the positive and the negative conductors. Finally, the voltage starts to decrease again. It is interesting to note how the voltage rise can produce voltage magnitudes superior to the nominal voltage. According to these results, the minimum values occur when the train is placed at the autotransformer positions and the maximum values when the train is located at the traction substations.

The current flowing through the equivalent negative feeder is constant every two autotransformers and its value increases as the distance to the traction substation is reduced due to the balancing effect of the autotransformers. As it is observed in Figure 4.21.d, the current behavior within the two autotransformers adjacent to the train is the opposite, increasing its value as the distance increases.

Finally, the active and reactive power distributions obtained are depicted in Figure 4.22. According to the results obtained, the active and reactive power provided by each traction substation decreases as the distance with the train increases. This power reduction shows a quadratic behavior that is repeated between every two autotransformers. Although this effect is more significant in the reactive power, it is also presented in the active power.

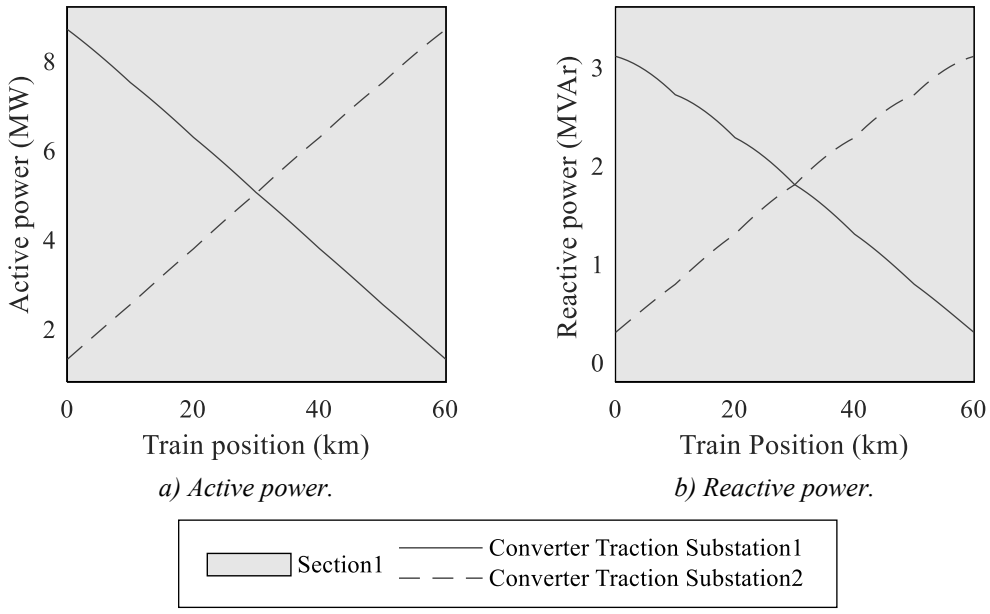

a) Active power. *b) Reactive power.*

Figure 4.22 Power distribution. Advanced AC converter-based bivoltage system.

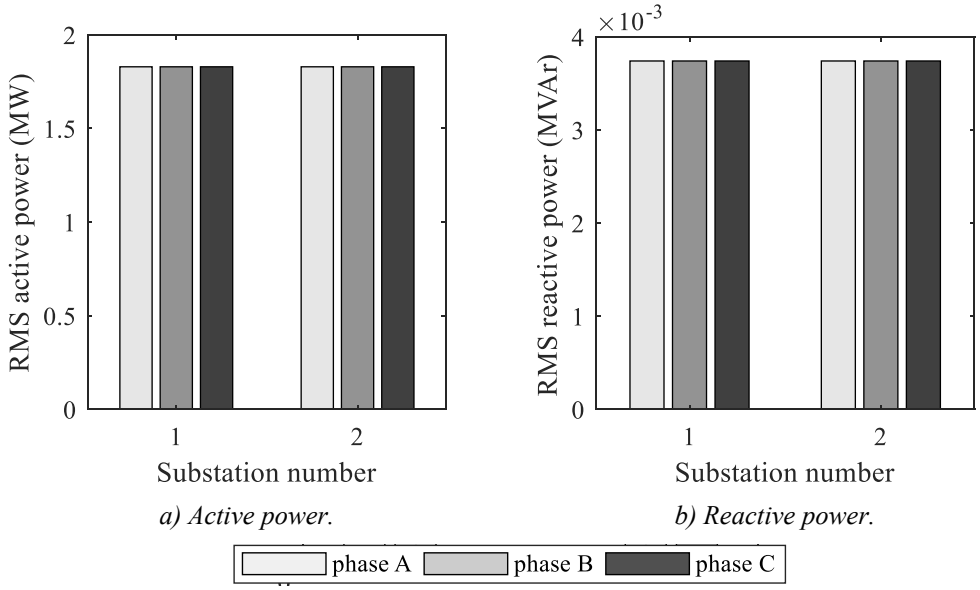

Figure 4.23. Power imbalance. AC advance converter-based bivoltage systems.

4.5.3 Imbalance analysis

Figure 4.23 shows the root square mean of the active and reactive power provided by each phase of the utility grid for the bivoltage catenary case. The monovoltage case has a similar behavior and it is not included. According to the results obtained, the active power demanded by each traction substation is distributed equally among the utility grid phases. Furthermore, the reactive power consumption has been reduced to the line losses.

4.5.4 Power sharing analysis

This section analyzes the effectiveness of the control strategy proposed to increase the power cooperation between traction substations for advanced AC converter-based systems. As it was previously explained, the active power sharing between traction substations can be increased by simply decreasing the value of the angle droop parameters of the traction substations. These parameters are defined equally for all traction substations in order to preserve the positive influence of the line impedance on the power distribution. The conclusions obtained are the same for the monovoltage and bivoltage catenary configurations, and thus, only the bivoltage case is presented.

Figure 4.24.a describes the active power supplied by the traction substation one for the different positions of the train and for four different angle droop parameters: 60/0.1MW/rad, 60/0.3, 60/0.6MW/rad and 90/0.9MW/rad. As it is observed, the active power supplied by the traction substation one decreases as the distance between the traction substation and the train increases. On the other hand, the increment of the value of the angle droop parameter evidences a rise in the cooperation between the traction substations.

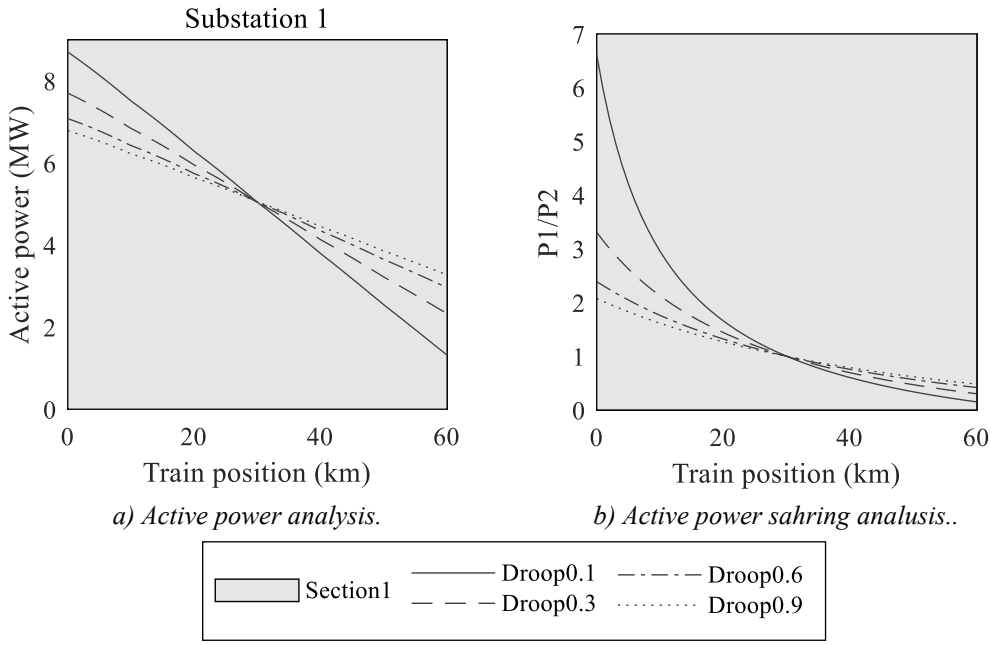

a) Active power analysis. *b) Active power sahring analusis..*

Figure 4.24. Active power sharing analysis. Advanced AC converter-based bivoltage system.

According to Figure 4.24.b, the maximum power ratio ranges from six and a half to almost two for the two extreme angle droop parameters. As it is noted, all the curves intersect at the middle of the section. In this case, the line impedance is the same for both converters and so that the active power sharing is equal to one.

However, the variation of the angle droop parameter also modifies the reactive power sharing because of the power coupling presented. Figure 4.25.a. shows the reactive power supplied by the traction substation one for the different position of the trains and for the four angle droop parameters considered. In this case, the increment of the angle droop parameter reduces the reactive power cooperation. As it is observed in Figure 4.25.a, the reactive power provided by the traction substation even presents negative values when the angle droop parameter is reduced significantly

This situation has been reported in the Norway and Sweden railway power supply systems [100]. As it was explained before, these systems consist of a set of rotary converter stations that operates synchronously with the utility grid. Accordingly, the angle is defined by the utility grid, but the generator has the ability of controlling the voltage. In these systems, the voltage regulation is typically controlled to maintain the voltage magnitude of the railway grid constant but under high loading conditions, due to the power coupling existing, the angle difference can produce an inversion of the reactive power provided. To avoid this problem, they normally reduce the voltage depending on the active power consumed.

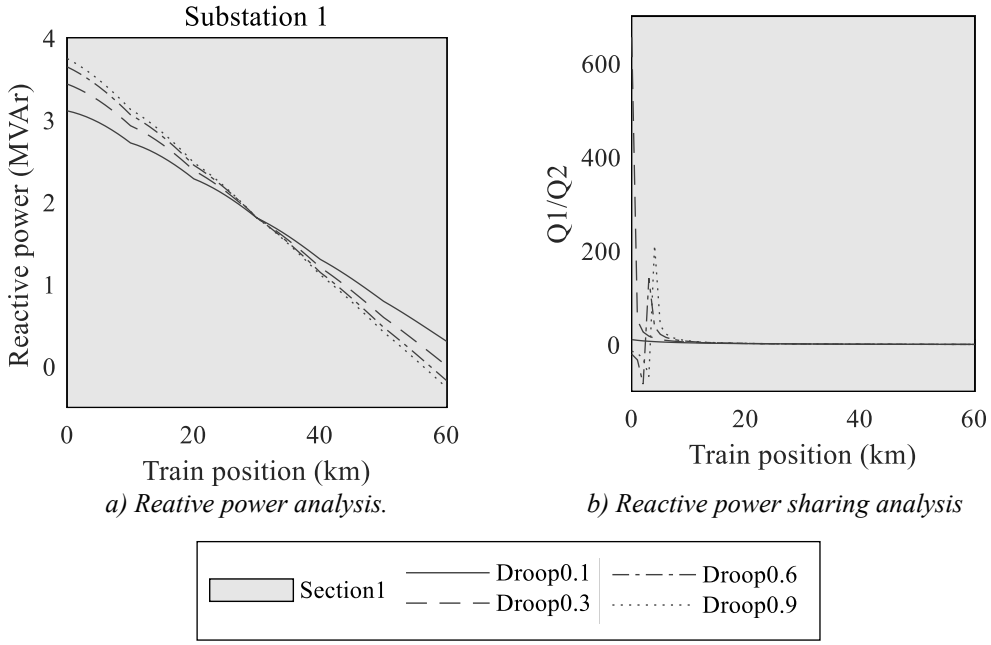

a) Reative power analysis. *b) Reactive power sharing analysis*

Figure 4.25. Reactive power sharing analysis. Advanced AC converter-based bivoltage system.

Following the same approach explained before, the voltage droop coefficient is increased to 60/10000 MW/V in order to enable a higher voltage variation. Figure 4.26 describes the active and reactive power sharing ratios obtained for the four angle droop parameters for the new voltage droop parameter. As it is observed, the active power sharing has been slightly modified but it preserves the sane behavior previously discussed. On the other hand, the reactive power sharing is always positive and thus, the traction substation never consumes reactive power.

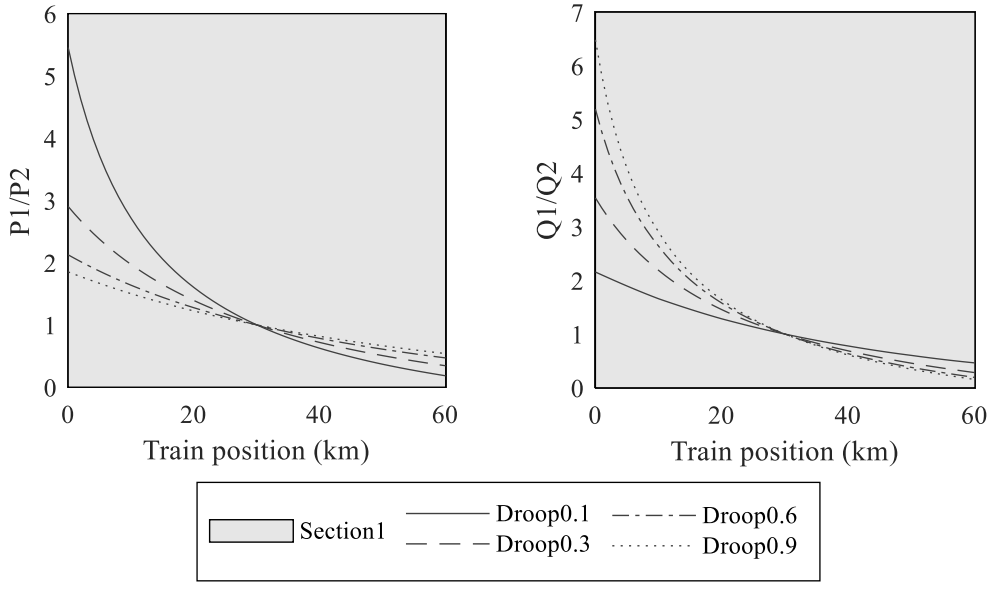

Figure 4.26. Reactive power sahring correction. Advanced AC converter-based bivoltage system.

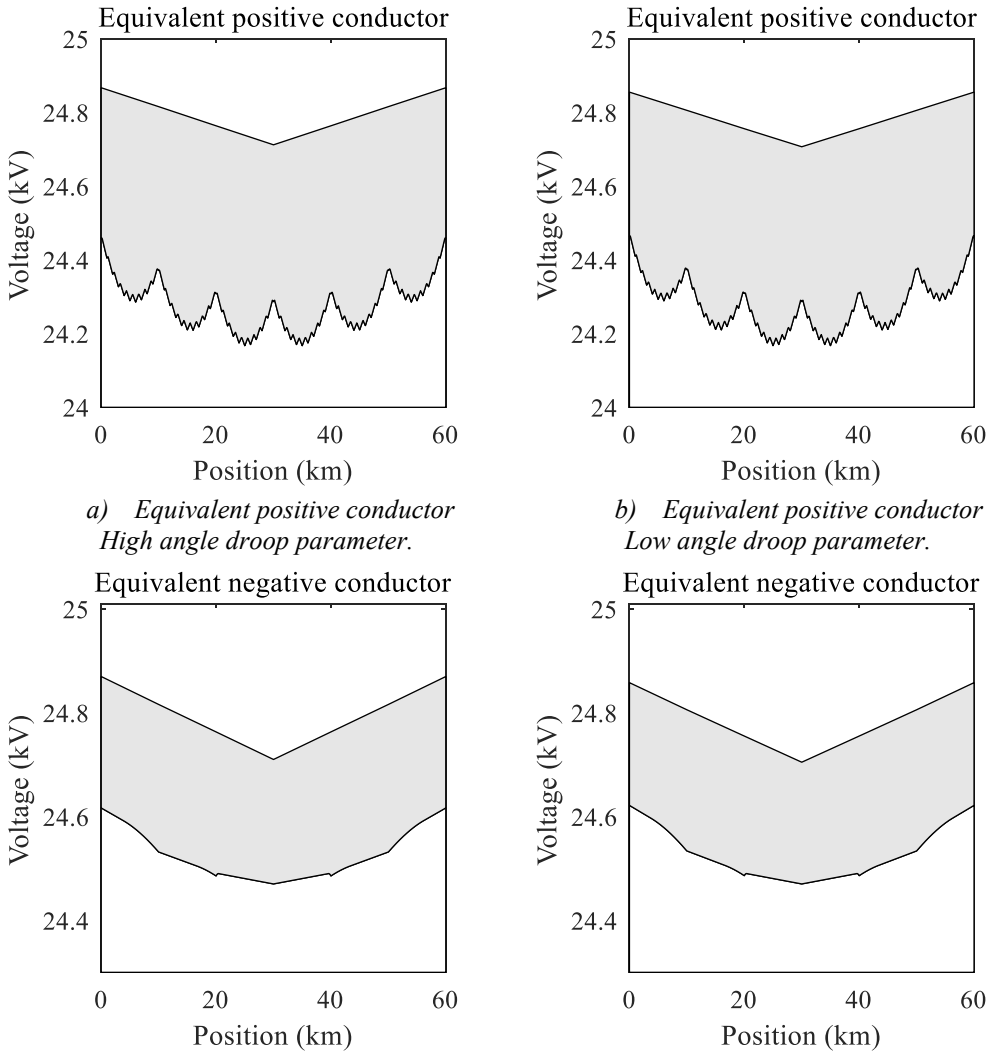

a) Equivalent positive conductor High angle droop parameter.

b) Equivalent positive conductor Low angle droop parameter.

c) Equivalent negative conductor High angle droop parameter.

d) Equivalent negative conductor Low angle droop parameter.

Figure 4.27. Voltage distribution. Power sharing analysis. Advanced AC converter-based bivoltage system.

Finally, in order to validate the operation strategy, it is necessary to verify that the voltage levels are within the admissible levels defined by the standard. To this end, the Figure 4.27 has been included. This figure describes the voltage magnitude for the equivalent positive and negative conductor over their length for the two extreme angle droop parameters previously studied. According to these results, the variation of the angle droop parameters hardly modifies the voltage distribution obtained, and thus the voltage magnitudes are within the admissible levels.

4.6 Operation analysis of advanced DC converter-based systems

This section analyzes the operation performance of the of advanced DC converter-based systems using the control strategy proposed. Following the same methodology conducted for advanced AC converter-based systems, the conventional transformer-based test case described in section 4.4, is transformed into an advanced DC converter-based one for both catenary configurations.

For the monovoltage case, Figure 4.28.a, the traction transformers have been replaced with converter stations consisting of a three phase VSC. For the bivoltage case, Figure 4.28.b the traction substation has the same configuration used for the monovoltage case, but they include an additional DC/DC autoconverter to balance the load of the positive and negative equivalent conductors. In addition, all autotransformers have been replaced with DC/DC equivalent autoconverters.

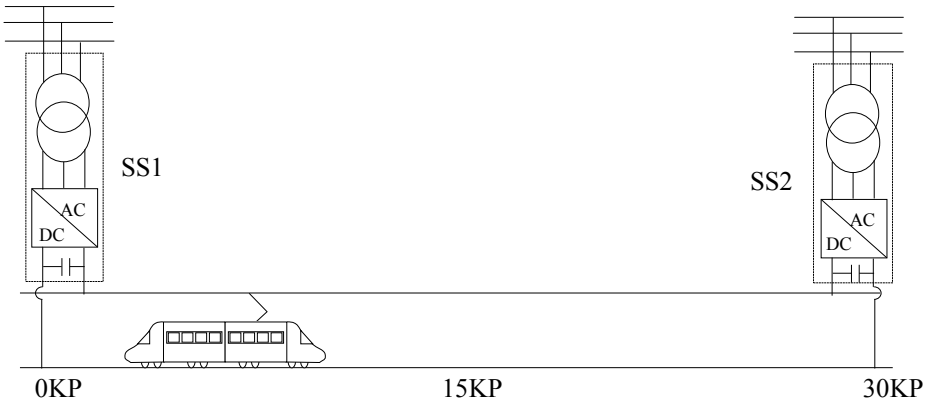

a)Monovoltage configuration

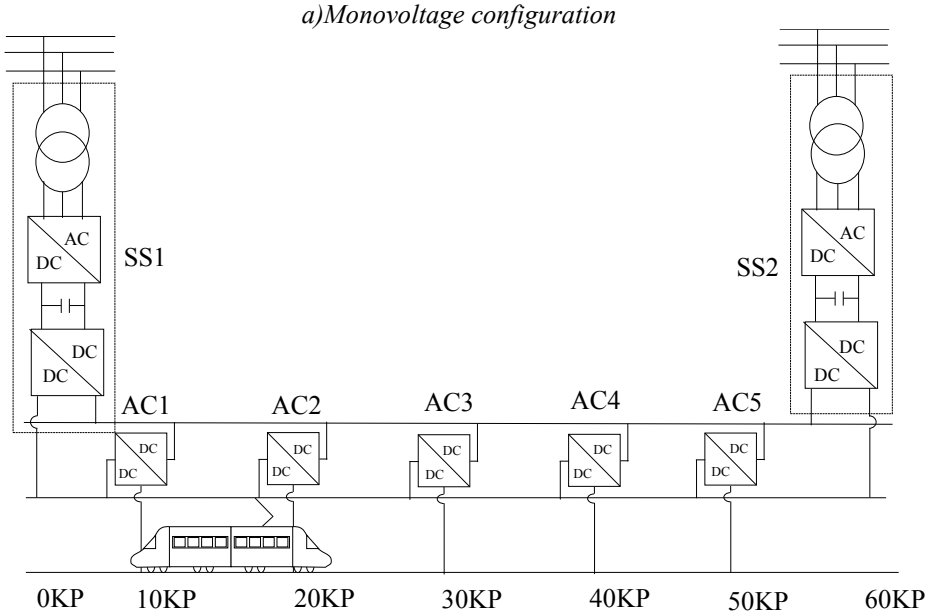

b)Bivoltage configuration

Figure 4.28. Advanved DC converter-based test cases definition.

Both cases are fed from the same utility grid used for the base test case through a three-phase transformer. For the monovoltage case, the transformer has winding connection of Ynd with a voltage ratio of 220/12 and a nominal power of 60MVA. For the bivoltage configuration, the transformer has a Ynd configuration with a voltage rate of 220/24 and nominal power of 60MVA. Both transformers have a short circuit impedance of 0.01jpu. The catenary configuration is the same but this time the two sections have joined.

4.6.1 Monovoltage catenary configuration

Figure 4.29 describes the voltage and current distribution obtained for the monovoltage DC catenary configuration. The distributions are very similar to the AC converter-based case. As it is observed, the voltage on the positive conductors decreases from the traction substation to the train and increases from this point to the other traction substation. The minimum voltage drop on each position of the conductor coincides when the train is located at this position. Alternately, the maximum values are obtained when the train are at the traction substations.

As it is described in Figure 4.29.b, the current demanded by the train is divided into two parts that corresponds to the current provided by each traction substation. The magnitude of this current decreases as the distance to the train increases. Accordingly, the maximum current for each point of the conductor coincides when the train is located at this position and the minimum when the train is placed at the opposite substation. It is noted that the minimum current registered never reaches the value zero.

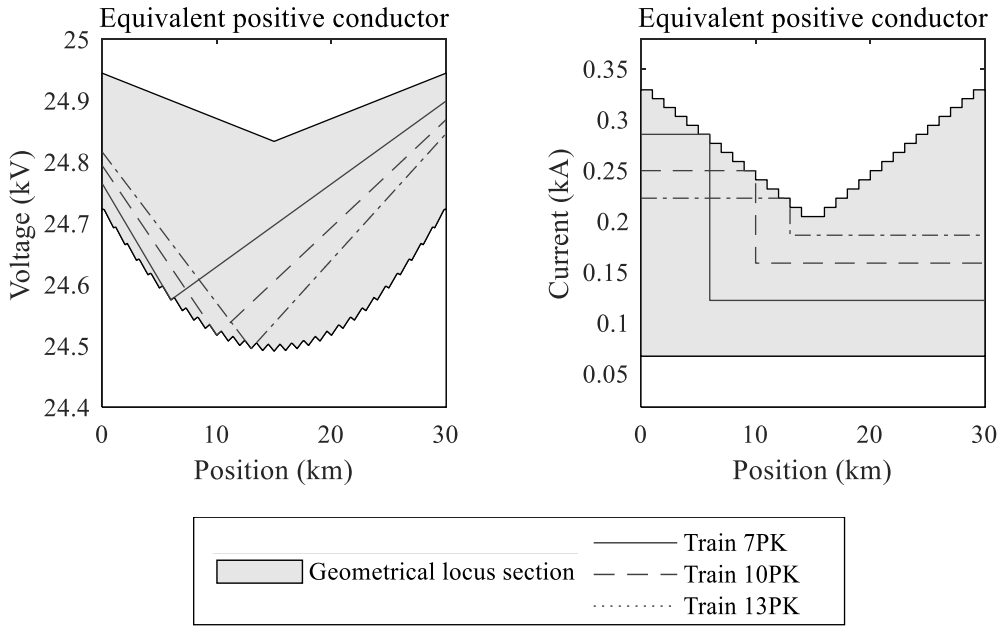

Figure 4.29. Voltage and current distribution. Advanced DC converter-based monovoltage system.

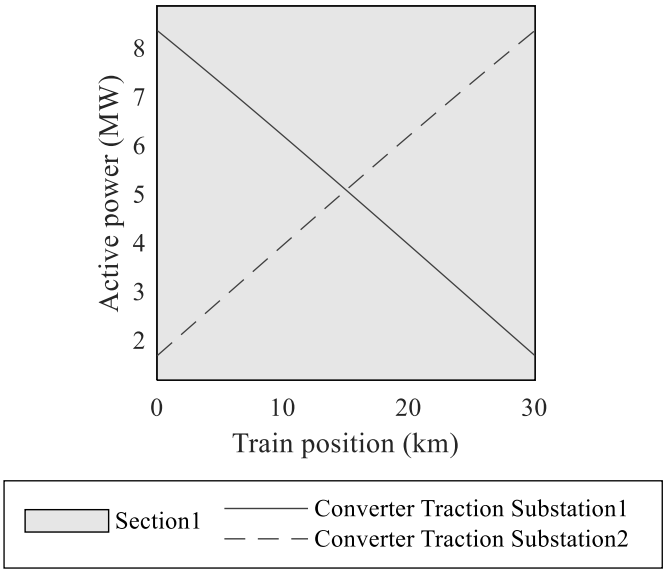

Figure 4.30. Power distribution. Advanced DC converter-based monovoltage system.

Figure 4.30, describes the active power delivered from the traction substation one, solid line, and from the traction substation two, dashed line, for all the train positions studied. According to these results, the power provided by each traction substation decreases as the train moves away from it. It is noted that when the train is placed at the middle position, both substations deliver the same power. Finally, it is important to highlight each traction substations always are loaded even when the train placed at the opposite one. This can be easily explained by the droop equation that demands a voltage drop to provide power.

4.6.2 Bivoltage catenary configuration

Figure 4.31 illustrates the voltage and current geometrical locus between the maximum and minimum values obtained for the equivalent positive and negative conductor over their length for all the train positions. The voltage distribution for the positive conductor is very similar to the AC bivoltage case and it is explained by the action of autoconverters. As it was previously explained, the minimum voltage describes a parabolic tendency between every two autoconverters. The maximum voltage levels are obtained when the train is located at the traction substations.

The current of the positive conductor has a slightly different behavior to the autotransformer case. In this case, the current is not balance every autoconverter. Due to the control imposed to the DC/DC converter of setting the same voltage on the positive and negative conductor, only the two adjacent autoconverter are working. This produces a better current distribution.

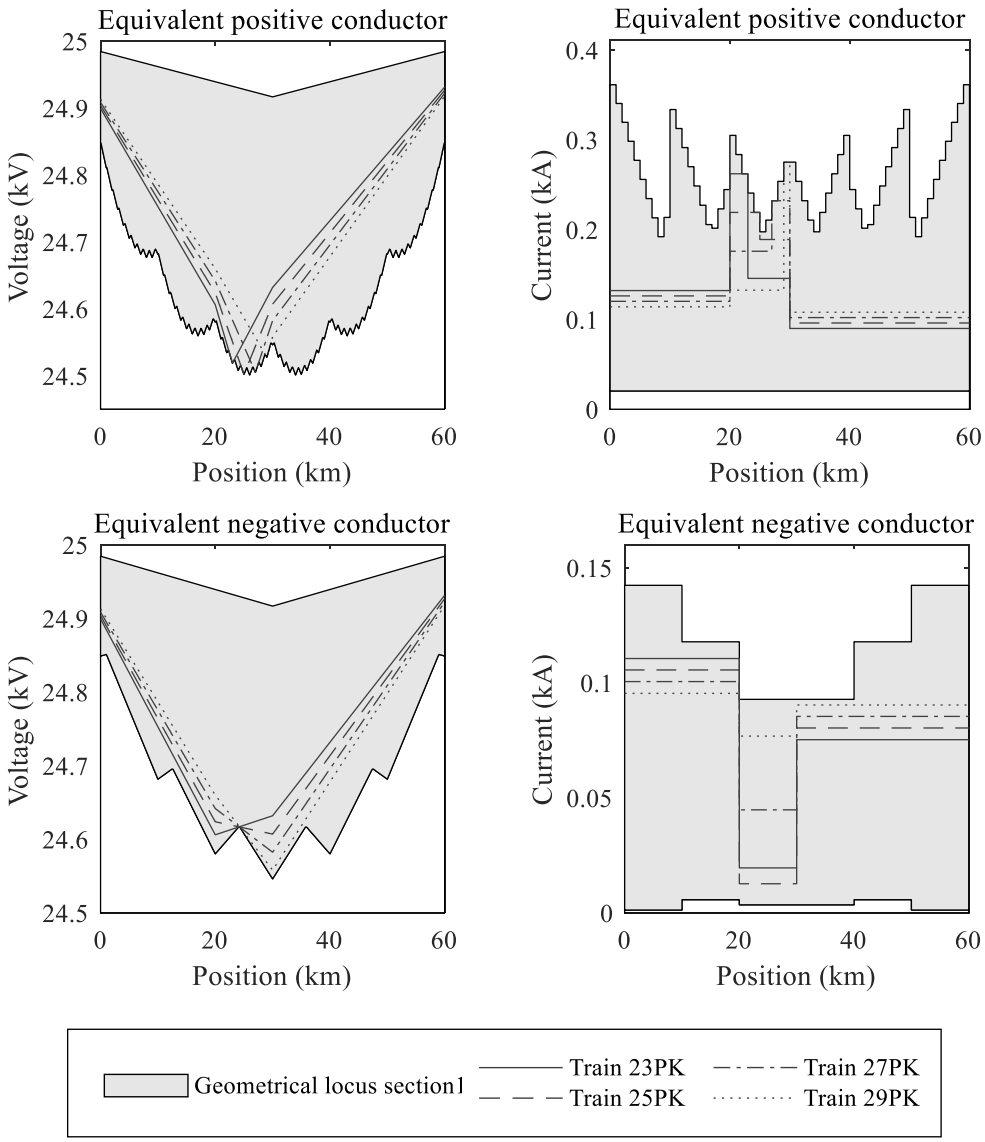

Figure 4.31. Voltage and current distribution. Advanced DC converter-based monovoltage system.

Figure 4.31.c shows the voltage distribution obtained for the equivalent negative conductor. As it is noted, the voltage on the equivalent negative conductor decreases from the traction substations to the autoconverters adjacent to the train. Depending on the relative position between the train and these two autoconverters, the voltage can increase or decreases. It is noted, that this time the voltage obtained does not change the tendency because the inexistence of electromagnetic coupling between the positive and negative conductors.

Finally, Figure 4.31.d describes the current distribution on the equivalent negative conductor. As it was previously appointed, the current is perfectly balance at the first autoconverter encountered, and thus it is maintained constant until the traction substations. These results validate the autoconverter model proposed.

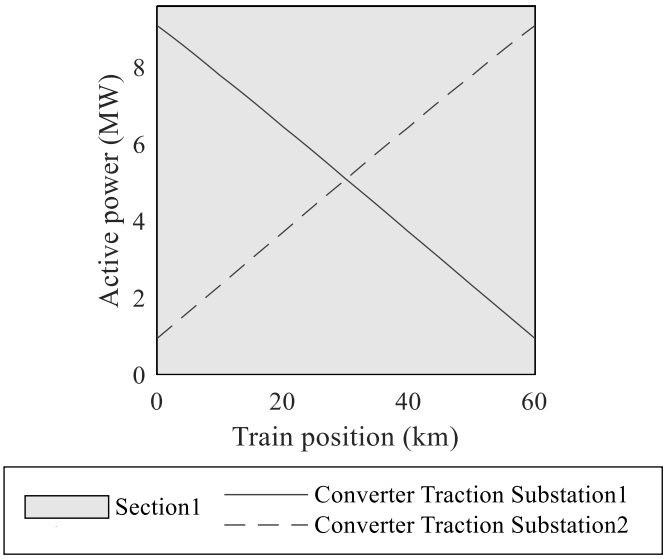

Figure 4.32. Power distribution. Advanced DC converter-based monovoltage system.

Figure 4.32 shows the active power delivered by each traction substation for tall the train position studied for the bivoltage catenary configuration. As in the monovoltage case, the power provided by the traction substation decreases as the train moves away from the substations.

4.6.3 Imbalance analysis

Figure 4.33 describes the quadratic mean square value of the active and reactive power for each phase of the utility grid. On the first hand, the converter performs a balance operation, distributing equally the active and reactive power among the three phases. On the other hand, both substations present the same quadratic mean square values since the power demanded by the train is the same for all the positions and the droop parameters set are the

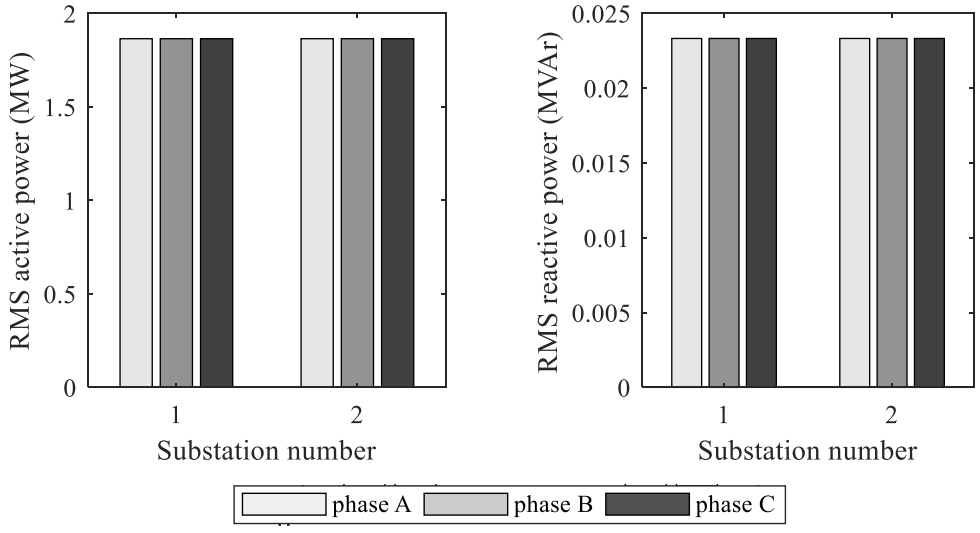

Figure 4.33. Utility grid power distribution. Advanced DC converter-based monovolatge system.

same as well. Finally, the reactive power consumption is clearly reduced from the conventional transformer system, reducing its value to the transmission line losses.

4.6.4 Power sharing analysis

This section analyzes the effectiveness of the control strategy proposed to increase the power cooperation between traction substations for advanced DC converter-based systems. In contrast to the advanced AC systems, where the active power cooperation between traction substations is principally governed by the angle droop parameter, in DC systems the active power control is governed by the voltage droop parameter. The conclusions obtained are the same for the monovoltage and bivoltage catenary configurations, and thus, only the bivoltage case is presented.

Figure 4.34.a describes the active power supplied by the traction substation one for the different train positions of the train for four different voltage droop parameters: 60/2000MW/V, 60/40000MW/V, 60/6000MW/V and 90/8000MW/V. As it is observed, the active power supplied by the traction substation one decreases as the distance between the traction substation and the train increases. On the other hand, the reduction of the value of the voltage droop parameter evidences a rise in the cooperation between the traction substations. According to Figure 4.34.b the maximum power ratio ranges from ten to almost three for the two extreme voltage droop parameters. As it is noted, all the curves intersect again at the middle of the section. In this case, the line impedance is the same for both converters and so that the active power sharing is equal to one.

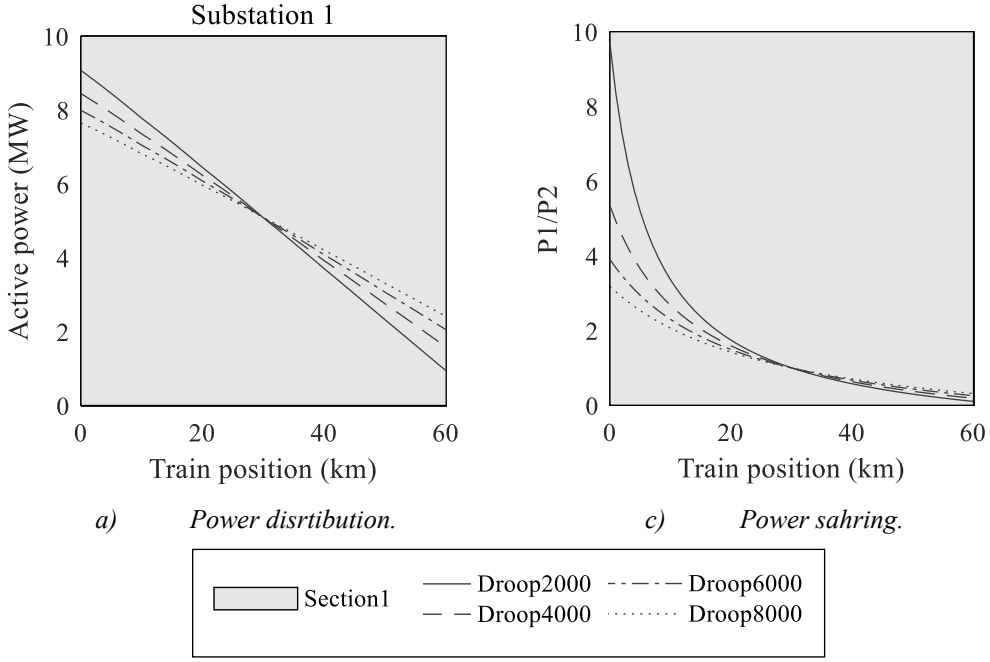

a) Power disrtibution. *c) Power sahring.*

Figure 4.34. Active power sharing analysis. Advanced DC converter-based bivoltage system.

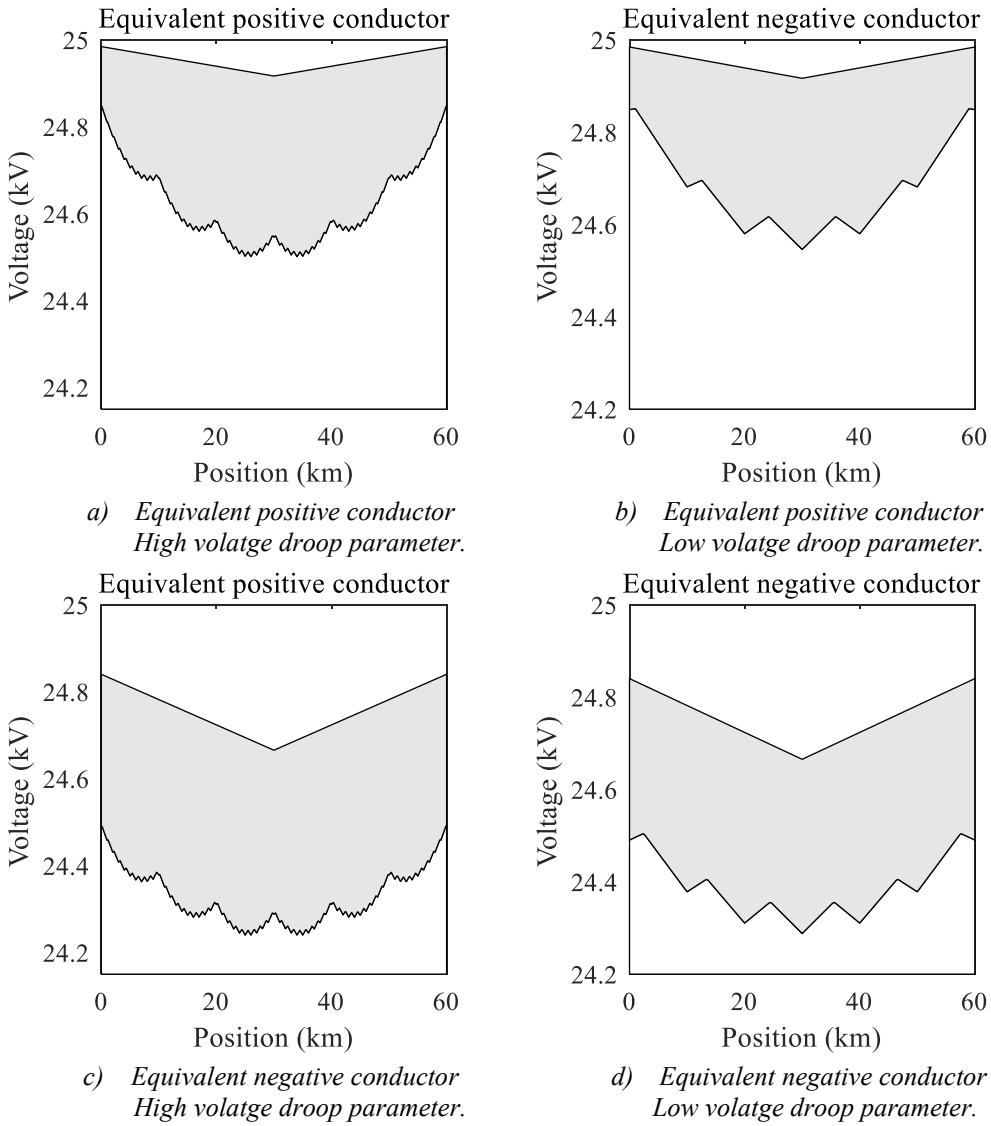

a) Equivalent positive conductor High volatge droop parameter.

b) Equivalent positive conductor Low volatge droop parameter.

c) Equivalent negative conductor High volatge droop parameter.

d) Equivalent negative conductor Low volatge droop parameter.

Figure 4.35. Voltage distrbution. Power sharing analysis. Advanced DC converter-based bivoltage system.

Finally, in order to validate the operation strategy, it is necessary to verify that the voltage levels are within the admissible levels defined by the standard. Figure 4.35 describes the voltage magnitude for the equivalent positive and negative conductor over their length for the two extreme angle droop parameters previously studied. According to these results, the variation of the voltage droop parameters modifies significantly the voltage distribution obtained. As it can be observed, it moved down the distribution. However, all the magnitudes values are within the admissible levels. In order to avoid this undesired effect, this thesis suggest implementing a secondary control that modifies the voltage references of the converters according to an average voltage of the whole line.

Chapter 5

High-speed railway line case study

5.1 Introduction

This chapter analyzes and compares the operation performance of transformer-based and advanced converter-based electrical railway power supply systems for a real traffic and electrical scenario. To this end, the high-speed railway line that connects the cities of Madrid and Valencia has been used as benchmark. This railway line has currently implemented a conventional transformer-based electrification scheme with a bivoltage catenary arrangement that will be adapted to obtain the corresponding AC and DC advanced converter-based configurations.

5.2 Traffic system

5.2.1 Input data

The simulation of the traffic system requires four different types of information: the topographic data of the railway line, the kinematic limitations of the sections, the dynamic characteristics of the trains and the railway operation timetable. The Madrid-Valencia high-speed railway line has a length of 384 km and four stations: Madrid (0 KP), Cuenca (181 KP), Utiel/Requena (314 KP) and Valencia (384 KP). The elevation profile of the railway line is depicted in Figure 5.1. In absent of more detailed data, these values have been obtained by simply interpolating the elevations of the stops and the tractions substations that are known values. Finally, the curvature of the line has been neglected due to the low effect observed in previous simulations.

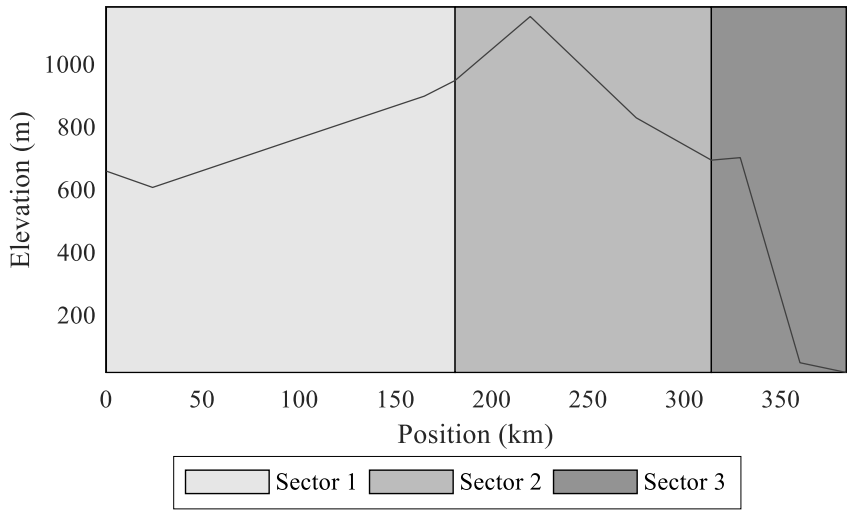

Figure 5.1. Topographic data represenation. Madrid-Valencia high-speed line.

The kinematic limitations aim to guarantee a safety and comfortable railway operation. In this case, the maximum velocity is set to 350km/h and the maximum acceleration and deceleration are limited to $1 m/s^2$ and $0.6 m/s^2$ respectively. These constrains are the same for all the sectors. On the other hand, the dynamic characteristics of the train are collected in Table 5.1. These data correspond to the train series 103 of Siemens®. It is assumed that this is the only train type circulating.

The train timetable data are listed in Table 5.2. They correspond to the normal operation conditions of the railway line according to the information provided by the railway Spanish operator [101]. As it can be observed, it consists of 13 trains for each direction distributed between the 6:45 and the 21:10. Finally, the stop time is set to two minutes.

Table 5.1. Train dynamic data.

Symbol(unit): description	*Value*
m (kg): train mass	*4.83e3*
μ: efficiency	*0.85*
cosφ: power factor	*0.95*
$F_{tr,max}$ *(N): maximum tractive force*	*283e3*
$P_{tr,max}$ *(W): maximum tractive power*	*8.8e6*
$F_{br,max}$ *(N): maximum braking force*	*-283e3*
$P_{br,max}$ *(W): maximum braking power*	*-8.8e6*
P_{aux} *(W):auxiliary services power*	*-8e3*
a (N): constant Davis coefficient	*0.0074*
b ($N \cdot s \cdot m^{-1}$)*: linear Davis coefficient*	*2.4815e-04*
c ($N \cdot s^2 \cdot m^{-2}$)*: quadratic Davis coefficient*	*1.4463e-05*

Table 5.2. Train timetable.

Towards Valencia	*Towards Madrid*
6:45	*6:45*
7:40	*7:10*
8:40	*8:00*
9:40	*9:15*
11:10	*10:40*
12:40	*12:40*
14:10	*14:10*
15:40	*15:10*
16:40	*16:15*
17:40	*17:10*
18:40	*18:10*
19:40	*19:10*
21:10	*21:10*

5.2.2 Simulation results

In the next subsections, the simulation results of the principal variables of the traffic system are comprehensively described. As it can be observed, the variable profiles are divided into three parts corresponding to the three sectors between stops. It is noted, that the sector order is increasing when the train is circulating towards Valencia and decreasing when the train is circulating towards Madrid. Finally, the time trip obtained is around one and a half hour being a little superior when the train is circulating towards Madrid. This value is very similar to the real time trip of one hour and forty-five minutes.

d) Velocity

Figure 5.2 shows the velocity profile described by the train for both circulating directions of the railway line. As it was explained in chapter three, the minimum time driving strategy presents three operation modes: acceleration, cruising and braking. During the acceleration mode, the train typically increases its velocity motivated by a positive force balance. However, this is not the only velocity behavior possible. When the train is facing a strong gradient against its motion, the tractive force available may not be sufficient to overcome the resistive force. In this case, two possible situations can be distinguished.

In the first situation, the maximum tractive force available has an equal and opposite sign value to the resistive force, and thus, the velocity of the train remains constant. This case is observed in the second sector when the train is circulating towards Madrid. In the second situation, the maximum tractive force available is lower than the value of the resistive force and the velocity of the train decreases. This case is seen in the first sector when the train is circulating towards Madrid.

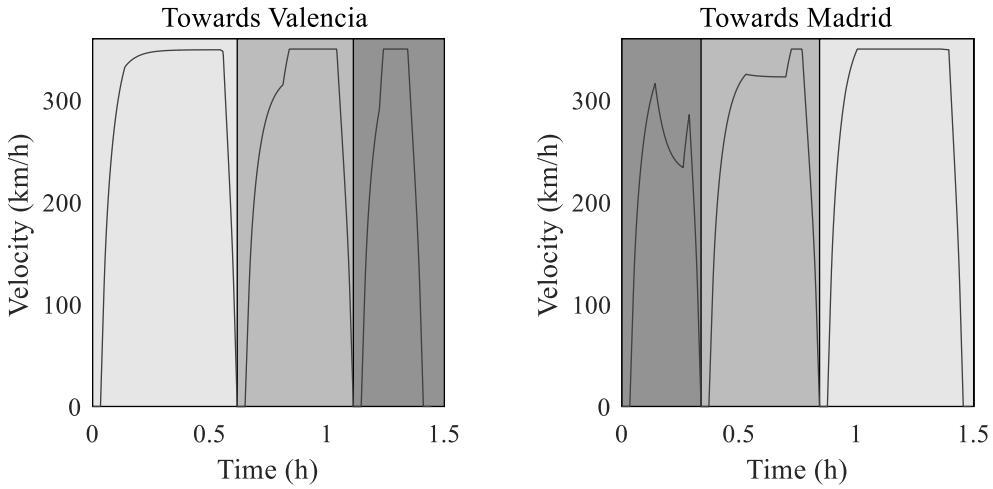

Figure 5.2. Train velocity simulation. Madrid-Valencia high-speed line.

During the cruising mode, the train maintains the velocity equals to the maximum velocity defined for each sector. To this end, the train must perform a force equals and opposite to the resistive force existing at each moment. As it can be observed this situation is reached in all the sectors for both circulating directions excepting in the first sector when the train is circulating towards Madrid. Finally, during the braking mode, all sectors evidence a steady reduction in the velocity of the train motivated by a negative force balance. However, as in the acceleration mode, it would have also been possible to have different velocity behaviors for other values of the gradient force.

e) Acceleration

Figure 5.3 illustrates the acceleration profile described by the train for both circulating directions. During the acceleration mode, the acceleration of the train typically describes a positive decreasing parabolic curve that produces the increase of the train velocity. The parabolic tendency is explained by the quadratic behavior of the aerodynamic and tractive forces. However, as it was explained in chapter three, the tractive force only shows a quadratic tendency for velocities greater than the breaking one, and thus for velocities lower to this value, the parabolic decreasing rate is only reduced to aerodynamic effect. Furthermore, as in the velocity case, the acceleration is altered with the changes in the gradient force. This effect can be observed as discontinuities in the acceleration profiles.

During the cruising mode, the acceleration turns zero because of the equivalence between the active and resistive forces. Finally, during the braking mode, the acceleration profile typically describes a negative decreasing parabolic curve. Nevertheless, due to the opposite behavior of the aerodynamic and braking forces with velocity, the acceleration profile can present and initial increasing part. It is noted that all maximum and minimum values obtained are within the admissible levels previously defined.

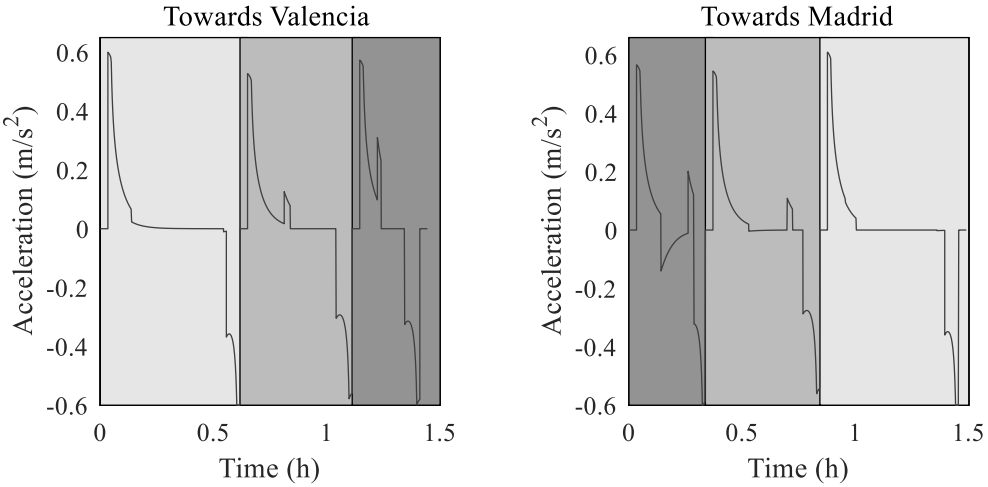

Figure 5.3. Train acceleration simulation. Madrid-Valencia high-speed line.

f) Forces

Figure 5.4 shows the resistive force experienced by the train for both circulating directions of the railway line. In general, the resistive force profile describes a negative parabolic curve due to the aerodynamic force that is moved up or down depending on the gradient of the line. Furthermore, it presents also intervals with constants values that corresponds to the cruising mode. As it is noted, the resistive force is more advantageous when the train is circulating towards Valencia, being especially adverse in the first sector when the train is circulating towards Madrid.

Figure 5.5 describes the tractive/braking force performed by the train for both circulating directions. During the acceleration mode, the train initially performs a constant effort until the breaking velocity is reached. After this point, the train reduces quadratically the value of this force in order not to exceed the power limit. The same analysis can be accomplished for the braking force. Finally, when the train is in cruising force, it performs a constant active force whose value is equal and opposite to the resistive force.

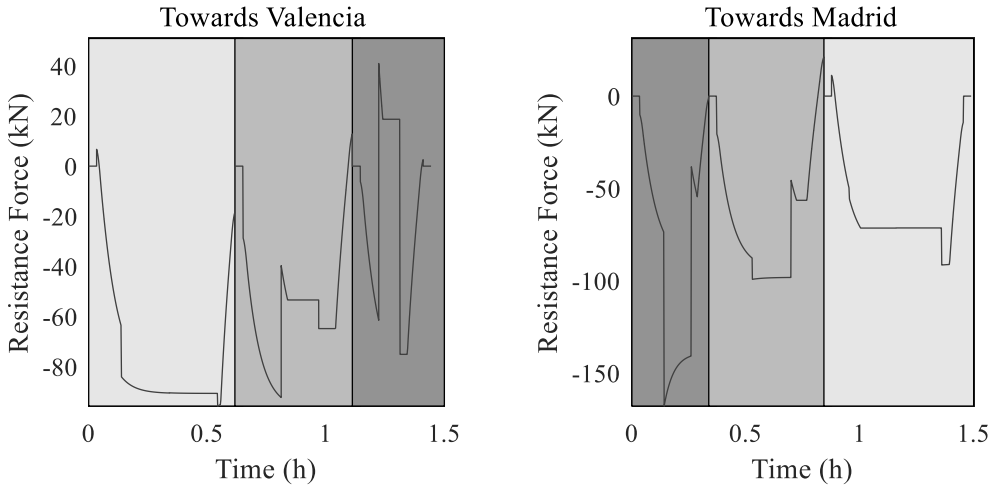

Figure 5.4 Train resistance force simulation. Madrid-Valencia high-speed line.

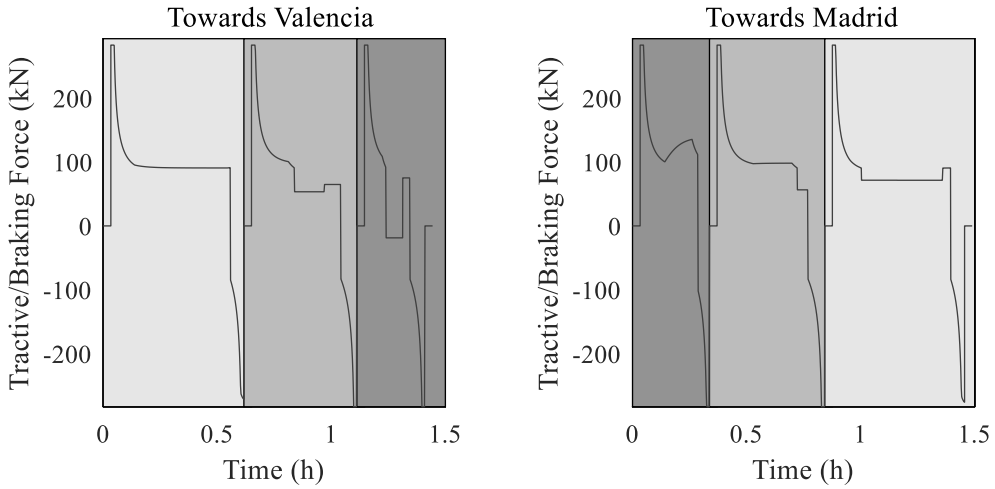

Figure 5.5. Tractive and braking force simulation. Madrid-Valencia high-speed line.

g) Power

Figure 5.6 describes the power demanded by the train from the catenary for both circulating directions of the railway line. During the acceleration mode, the power demanded depicts a negative decreasing curve until the maximum power available is reached. From this point, the train maintains the maximum consumption until the maximum velocity for the sector is reached. During the cruising mode, the power consumption is normally reduced because there is not any additional effort needed to increase the velocity. This situation is especially interesting in the third sector when the train is circulating towards Valencia. In this case, the train is able to maintain the maximum velocity without any electrical power from the catenary due to the positive effect of the gradient force. However, it is also possible that the train requires the maximum power to maintain the maximum velocity.

During the braking mode, the power demanded by the train turns zero. Since power regeneration is not permitted, all the values registered are negative. The maximum values observed coincide with the auxiliary services consumption, while the minimum values with the maximum power of the motor divided by the efficiency of the traction unit elements plus the consumption of the auxiliary services.

h) Traffic timetable

Figure 5.7 shows the traffic timetable obtained for the railway line for both circulating directions according to the train timetable provided by the operator. In solid lines, there are the trains circulating towards Valencia while in dash lines, the train circulating toward Madrid. According to these results, the current traffic timetable is not very heavy, being five the maximum number of trains that are simultaneously in the line.

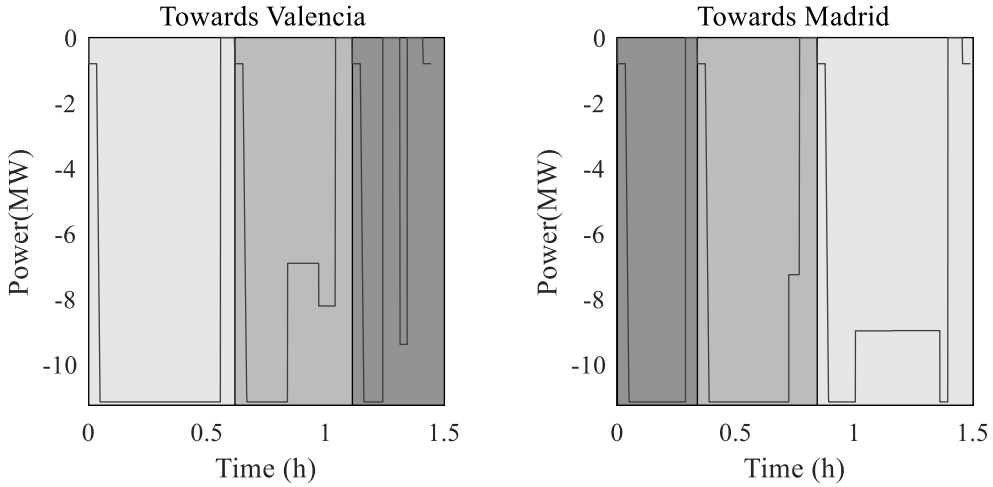

Figure 5.6. Train power simulation. Madrid-Valencia high-speed line.

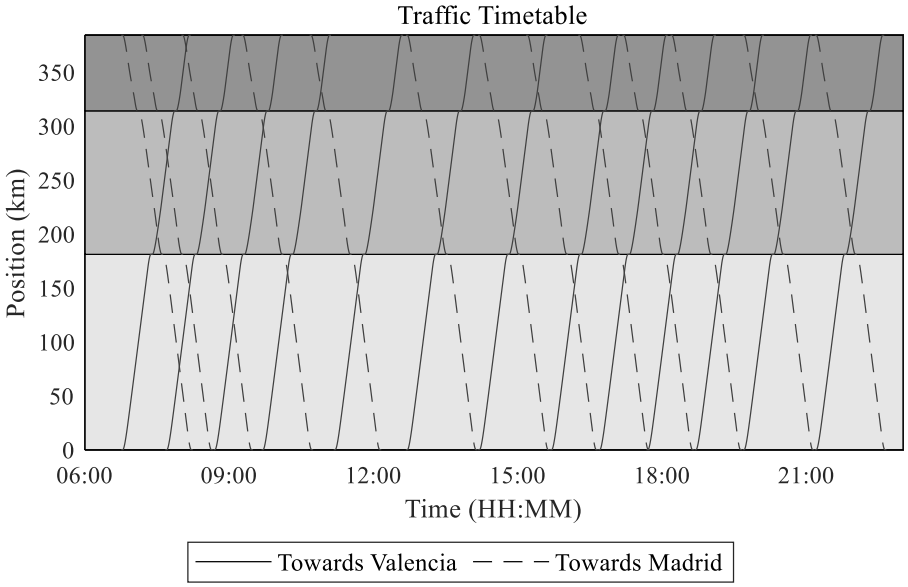

Figure 5.7. Traffic timetable simulation. Madrid-Valencia high-speed line.

5.3 Electrical system

This section analyzes and compares the electrical operation of the Madrid-Valencia high-speed line under three different electrification schemes for the traffic scenario previously calculated. To this end, the different electrical configurations are simulated every minute during the whole timetable according to the traffic condition existing.

5.3.1 Conventional transformer-based system

a) Input data

The Madrid-Valencia high-speed railway line is currently electrified using a conventional transformer-based scheme composed of thirteen independent electrical sections. The catenary presents a monovoltage catenary configuration for the first section and a bivoltage configuration for rest of the sections. However, in order to have the same catenary arrangement, the catenary of the first section has been transformed into a bivoltage configuration as well.

The distribution of the traction substations, the electrical sections and the autotransformers are shown in Figure 5.8, where ST denoted station, TS transformer substation and ATS autotransformer substation. Each substation has two traction transformers that are connected to different phases to minimize the voltage imbalance in the utility grid. All the parameters of the electrical elements are listed in Table 5.3.

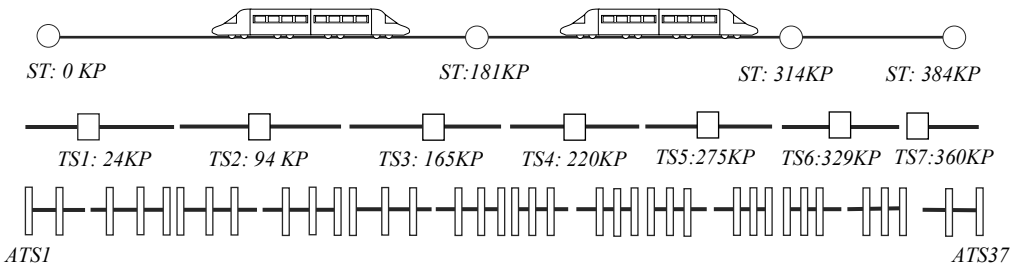

Figure 5.8. Madrid-Valencia high speed line. Conventional transformer-based configuration.

Table 5.3. Electrical parameters.Madrid-Valencia high-speed line. Conventional transformer-based bivoltage system.

Utility grid	
Nominal voltage(kV)	*220*
Short circuit power (GW)	*10*
R/X	*0*
Transformers	
Voltage Ratio	*220/25/25*
Nominal Power (MVA)	*60*
Short circuit impedance (pu)	*0.1j/0.1j/0.05j*
Auotransformers	
Voltage Ratio	*25/25*
Nominal Power (MVA)	*10*
Short circuit impedance (pu)	*0.05j*
Catenary	
Impedance (Ω/km)	$1e-3\begin{bmatrix} 0.11+0.28j & 0.07+0.12j \\ 0.07+0.12j & 0.13+0.31j \end{bmatrix}$

b) Operation analysis

Figure 5.9.a and Figure 5.9.b describe the geometrical locus of the voltage between the maximum and the minimum values obtained for the equivalent positive and negative conductors over their length during the whole traffic operation. These figures also include the mean voltage calculated for each position of the conductor during the whole time period. Due to the sectioning of the catenary, the voltage profiles are divided into thirteen intervals corresponding to the thirteen electrical sections existing.

As it can be observed in Figure 5.9.a, the lowest voltage magnitude for the equivalent positive conductor is obtained in the section number four with a value of 22.42kV, and the highest voltage magnitude is registered in the section number eleven with a value of 25.11kV. It is interesting to note that although regeneration is not considered, the voltage magnitude can present values greater than the nominal one. This is motivated by the phase

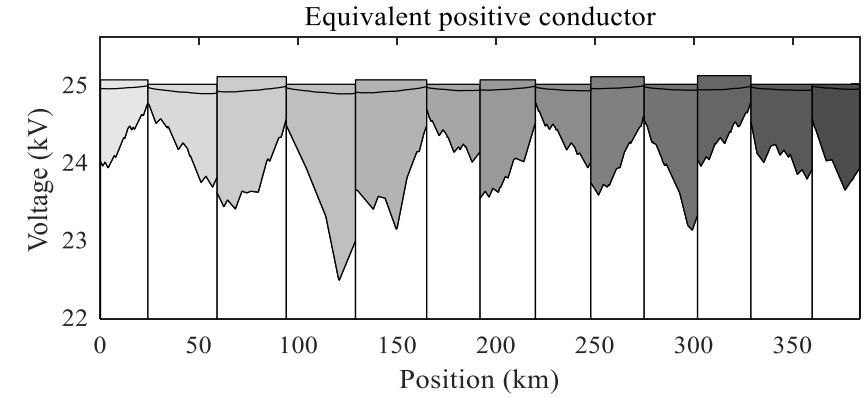

a) Equivalent positive conductor.Voltage distribution.

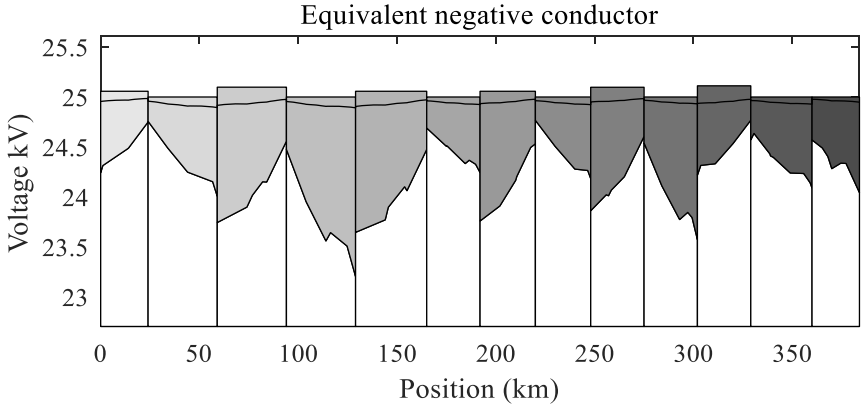

b) Equivalent negative conductor. Voltage distribution.

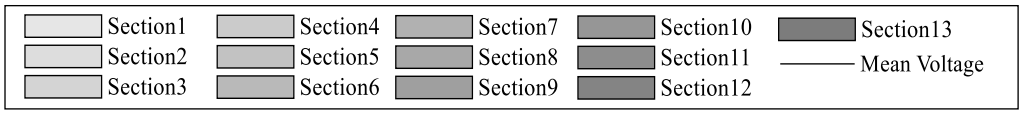

Figure 5.9. Voltage distribution. Madrid-Valencia high-speed line. Conventional transformer-based bivoltage system.

rotation performed on the traction transformers on the utility grid. Under such circumstances, when one of the transformer is loaded and the other not, the phase shift produced by the power consumption can lead to a voltage magnitude on the non-loaded transformer greater than the nominal one.

Regarding the equivalent negative conductor, the minimum and maximum voltage magnitude values are 23.2kV and 25.12kV respectively, and they are registered in the fourth and eleventh sections as well. In this case, the minimum and maximum values are greater than the ones obtained for the equivalent positive conductor due to the lower value of the current flowing through this conductor. Finally, it is noted that all the values are within the admissible voltage level defined in the standard EN50163:2004.

Figure 5.10.a and Figure 5.10.b describe the geometrical locus of the current between the maximum and the minimum values obtained for the equivalent positive and negative conductors over their length for the whole traffic operations. Furthermore, it has been included the mean quadratic current calculated for each position of the conductor during the whole time period. For the equivalent positive conductor, the maximum current is obtained in fifth electrical section with a value of 0.78kA. It is observed that the location of the minimum voltage does not coincide with the location of the maximum current.

For the equivalent negative conductor, the maximum current is registered in the fourth section with a value of 0.44kA. The current distribution of the negative equivalent conductor is more homogenous than the one obtained for the equivalent positive conductor since the current values can only change at the autotransformer positions. Finally, it is noted that for both conductors the minimum current registered is zero.

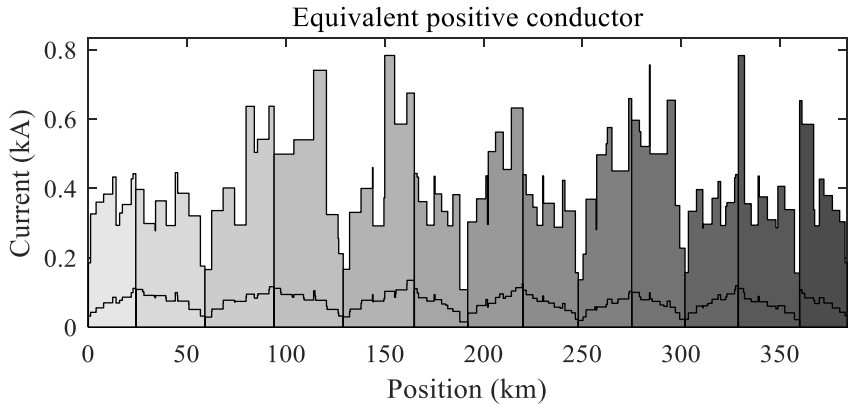

a) Equivalent positive conductor. Current distribution.

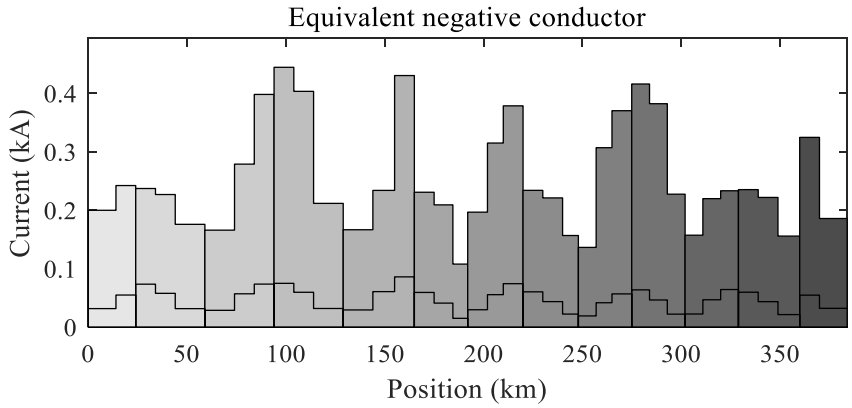

b) Equivalent negative conductor. Current distribution.

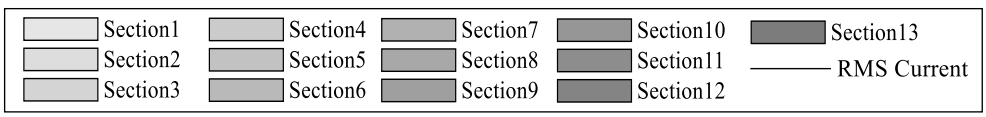

Figure 5.10. Current distribution. Madrid-Valencia high-speed line. Conventional transformer-based bivoltage system.

Figure 5.11.a and Figure 5.11.b show correspondingly the mean quadratic active and reactive power supplied by the traction substations during the whole traffic operation. According to the results obtained, the active power ranges from 6.67MW obtained for the third substation to 3.63MW registered for the seventh substation. On the other hand, the reactive power ranges from the 2.47Mvar of the third substation to the 1.31Mvar of the seventh substation. It is noted, that the active and reactive power distributions between the traction substations evidence an identical behavior. Finally, it is important to highlight the low power values obtained in comparison to the nominal power of 60MVA. This indicates an oversizing of the electrical installation for the current traffic.

Figure 5.12 shows the maximum voltage imbalance introduced in the utility grid for each traction substation during the whole traffic operation. As it observed, the maximum voltage imbalance value, 0.76% is obtained for the traction substation number three that coincide with the most loaded substation. Finally, all the maximum voltage imbalance factors are below the maximum imbalance permitted by the Spanish transmission system operator of 1%.

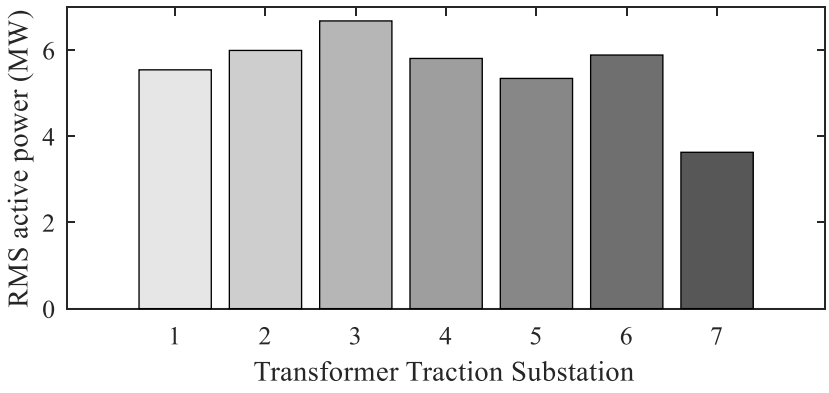

a) Active power distribution.

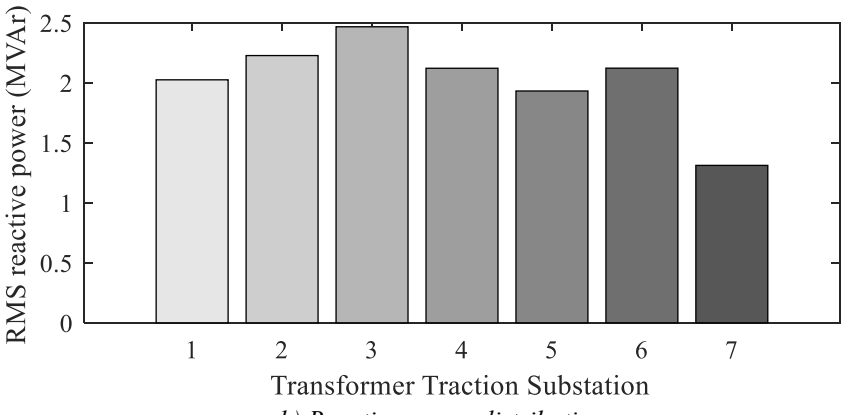

b) Reactive power distribution.

Figure 5.11. Power distribution. Madrid-Valencia high-speed line. Conventional transformer-based bivoltage system.

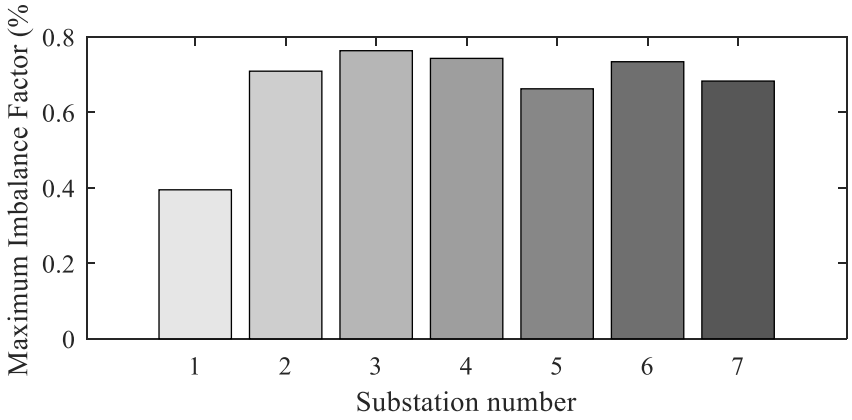

Figure 5.12. Voltage imbalance distribution. Madrid-Valencia high-speed line. Conventional transformer-based bivoltage system.

5.3.2 Advanced AC converter-based system

a) Input data

The advanced AC converter-based electrification scheme has been performed replacing the current transformer-based traction substations with the corresponding converter-based ones and connecting all the electrical sections. Furthermore, an additional autotransformer is added at the front of every traction converter substation and a three-phase transformer is connected to adapt the utility grid voltage level to the converter voltage level. According to this information, the system configuration is depicted in Figure 5.13, where the where ST denoted station, CS converter substation and ATS autotransformers substation. The parameters of the different electrical elements are listed in Table 5.4.

As it is observed, the angle and the voltage droop parameters of the traction converters are initially set to 60/0.1 MW/rad and 60/3000 MW/V respectively. According to the results obtained in chapter four, these values ensure and efficient distribution of the electrical power that it is the operation objective under normal grid conditions. However, these values will be modified in the subsection c in order to increase the power sharing between traction substations under an eventual utility grid contingency.

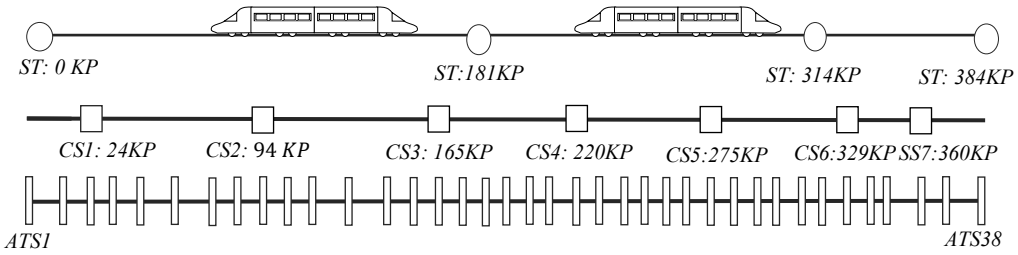

Figure 5.13. Madrid-Valencia high speed-line. Advanced AC converter-based bivoltage system.

Table 5.4. Electrical parameters.
Madrid-Valencia high-speed line. Advanced AC converter-based bivoltage system.

Utility grid	
Nominal voltage(kV)	*220*
Short circuit power (GW)	*10*
R/X	*0*
Transformers	
Voltage Ratio	*220/110*
Nominal Power (MVA)	*60*
Short circuit impedance (pu)	*0.1j*
Converter Stattions	
Nominal Power (MW)	*60*
Angle droop factor (MW/rad)	*60/0.1*
Magnitude drrop factor (MW/kV)	*60/3*
Auotransformers	
Voltage Ratio	*25/25*
Nominal Power (MVA)	*10*
Short circuit impedance (pu)	*0.05j*
Catenary	
Impedance (Ω/km)	$1e-3\begin{bmatrix} 0.11+0.28j & 0.07+0.12j \\ 0.07+0.12j & 0.13+0.31j \end{bmatrix}$

b) Operation analysis

Figure 5.14.a and Figure 5.14.b describe the geometrical locus of the voltage between the maximum and the minimum values obtained for the equivalent positive and negative conductors over their length for the whole traffic operation. These figures also include the mean voltage calculated for each position of the conductor during the whole time period. As it can be observed, the figures only present one section because the inexistence of neutral zones.

According to Figure 5.14.a, the lowest voltage magnitude has a value of 23.42kV and it is reached for the conductor positions of 120KP. This position corresponds to the fourth section of the conventional transformer-based configuration that it is also where the minimum value is registered. However, the minimum values obtained for the advanced AC converter-based system are significant superior to the conventional transformer-based systems. This can be explained principally by two factors. The first one is the better efficiency of the continuous catenary to transmit the power. The second one is the lowest voltage drop at the traction substation motivated by a high voltage droop parameter.

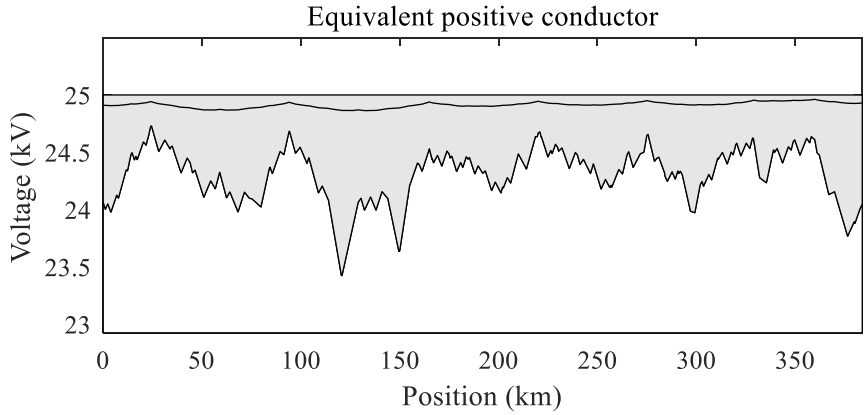

a) Equivalent positive conductor. Voltage distribution.

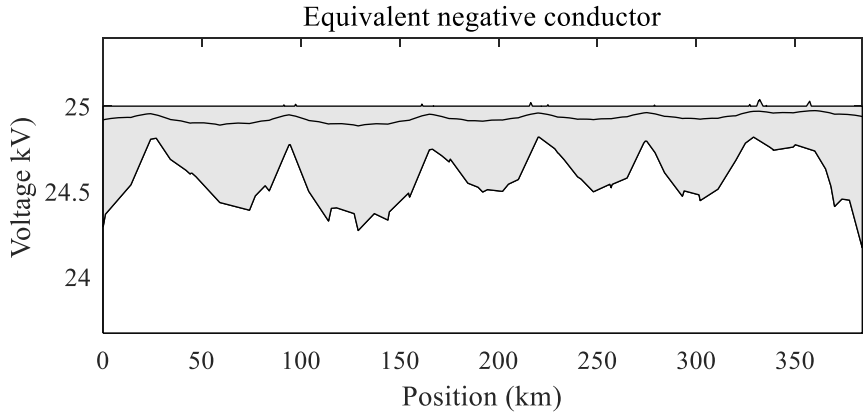

b) Equivalent negative conductor. Voltage distribution.

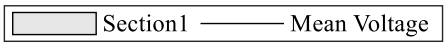

Figure 5.14. Voltage distribution. Madrid-Valencia high-speed line. Advanced AC bivoltage converterr-based system.

Regarding the voltage distribution on the equivalent negative conductor, the minimum voltage value is 24.17kV and it is registered at the position 384KP. It is observed, that there are some voltage values that are slightly higher that the nominal voltage of 25kV. As it was explained in chapter four, this is explained by the electromagnetic coupling existing between the equivalent positive and negative conductors. Finally, it is noted, that all the voltage values are again within the admissible level defined in the standard EN50163:2004.

Figure 5.15.a and Figure 5.15.b describe the geometrical locus of the current between the maximum and the minimum values obtained for the equivalent positive conductor over its length for the whole traffic timetable. It also includes the mean quadratic value of the current over all the conductor position for the whole traffic timetable. The maximum current value registered for the equivalent positive conductor is 0.63kA and it registered at the position 284KP, although there are some other locations with very similar values. It is interesting to note once again that the maximum voltage drop does not coincide with the maximum values of the current.

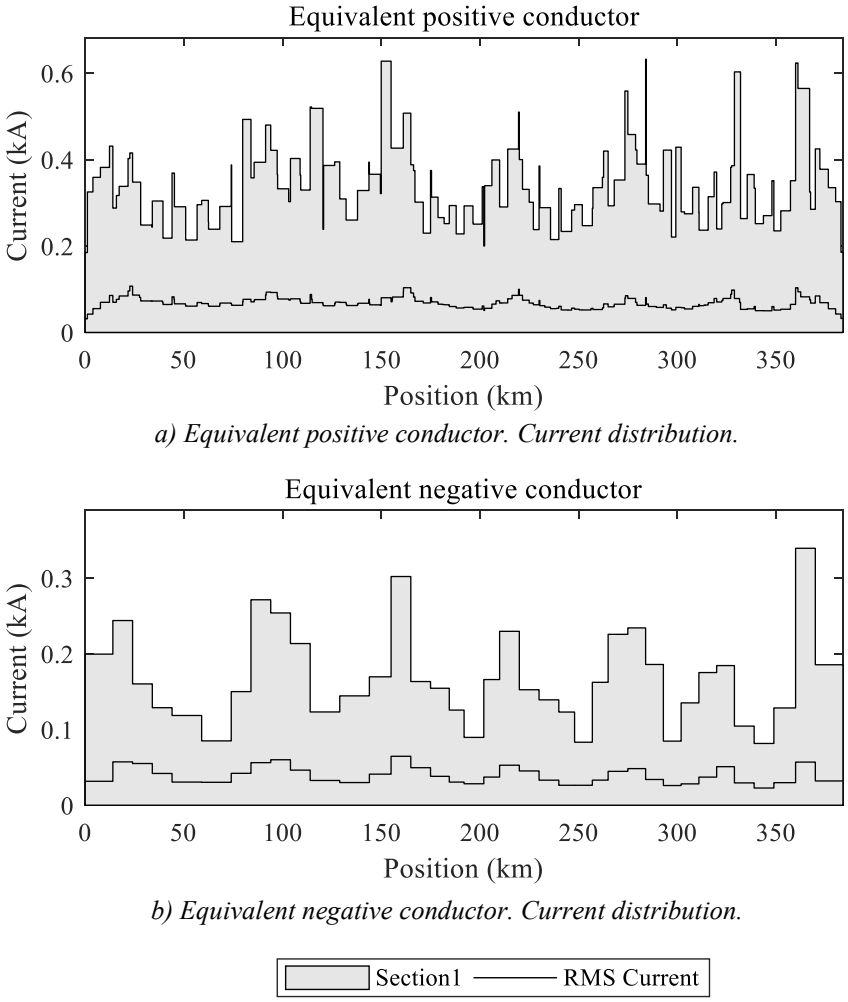

a) Equivalent positive conductor. Current distribution.

b) Equivalent negative conductor. Current distribution.

Figure 5.15. Current distribution. Madrid-Valencia high-speed line. Advanced AC bivoltage converter-based system.

Regarding the equivalent negative conductor, the maximum current value is 0.34kA and it is obtained for the conductor positions between the 360KP and 370KP. In this case, the value is not given for a specific point but for an interval. This is because of the conductor positions between two autotransformers have a constant current value.

Figure 5.16.a and Figure 5.16.b illustrates correspondently the mean quadratic active and reactive power supplied by the traction substations for the whole time period considered. According to the results obtained, the traction substation number three is the most loaded, with a quadratic mean active power of 4.82MW and reactive quadratic mean power of 3.5Mvar. On the other hand, the less loaded substation is the number six with a quadratic mean active and reactive power of 1.84MW and 1.31Mvar. It is noted, how the mean quadratic active and reactive power have been significantly decreased in comparison to the transformer-based configuration. Furthermore, the power difference between the traction substations have been also reduced.

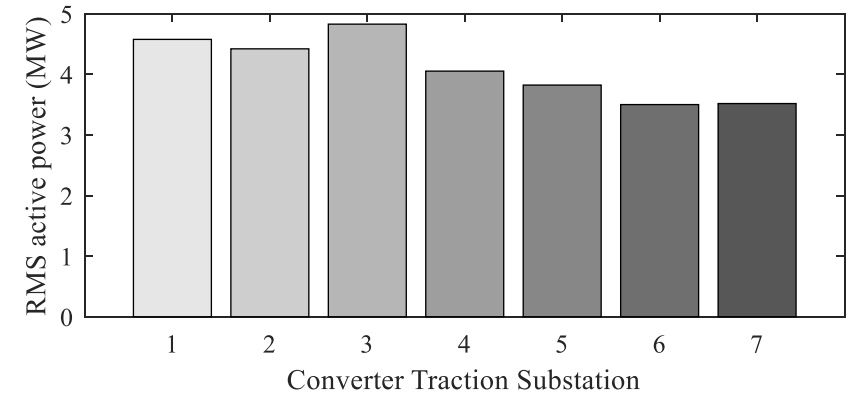

a) Active power distribution.

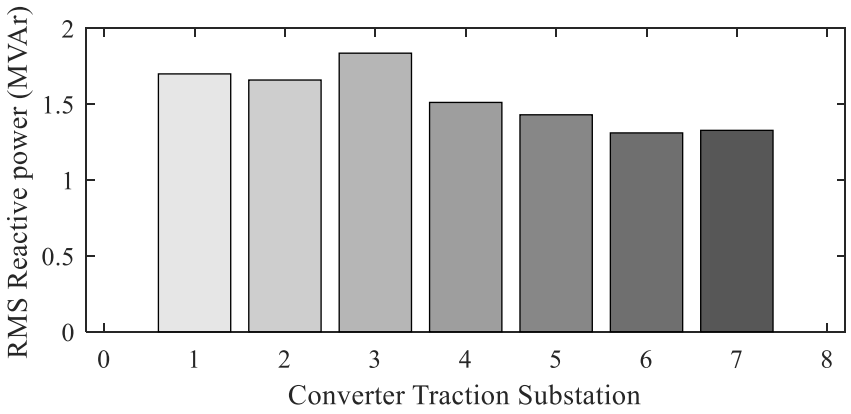

b) Reactive power distribution.

Figure 5.16. Power distribution. Madrid-Valencia high-speed line. Advanced AC bivoltage converter-based system.

c) Power sharing analysis

This subsection analyzes the effectiveness of control strategy proposed under a possible utility grid requirement of increasing the active power cooperation between the traction substations. Under normal grid conditions, the power demanded of the trains should be distributed according to their corresponding to the traction substations in order to increase the efficiency. However, it is also possible that the utility grid can be overloaded in some buses and the operator could ask for a consumption reduction in some points. Under such circumstances, the electrical railway system can increase the cooperation between the traction substations by simply decreasing the value of their droop parameters.

In order to study this effect, the angle droop parameters of the tractions substations are decreased to permit a maximum angle variation of 0.1rad, 0.3rad, 0.6rad and 0.9 rad. To facilitate the analysis the system has been simulated for a single time, 7:45. At this time, there are four trains placed at positions: 62,45KP, 91.66KP, 202,41KP and 315.65KP that are consuming an active power of 11,15MW, 8.96MW, 7.25 MW and 11,15MW.

Figure 5.17.a. shows the active power provided by each traction substation for the four angle droop parameters considered. As it can be observed, the active power sharing increases as the angle droop parameter decreases, and thus the active power supplied by each traction substation tends to converge. On the other hand, Figure 5.17.b describes the reactive power provided by each traction substation for the four angle droop parameters considered. In this case, the reactive power sharing has an opposite behavior, decreasing the reactive power sharing as the angle droop parameters is decreased. As it was explained in chapter four, the decrease in the angle droop parameter leads to a decrease in the reactive power cooperation. It is important to check that there is not any tractive substation consuming reactive power.

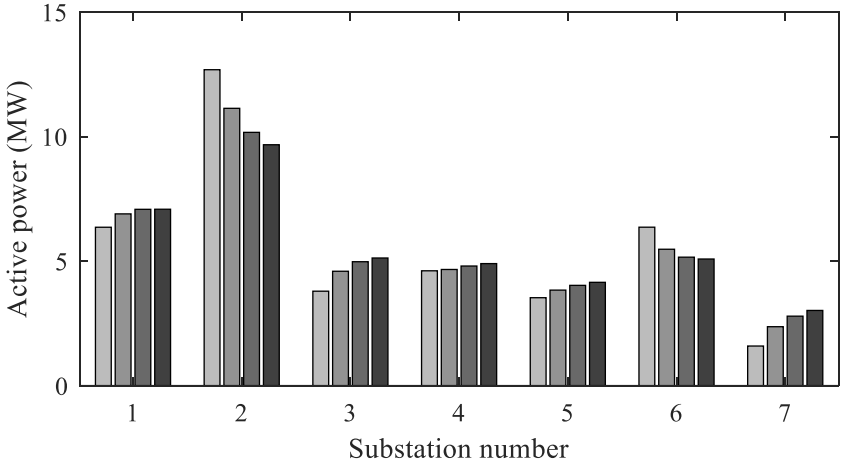

a) Active power sharing analysis.

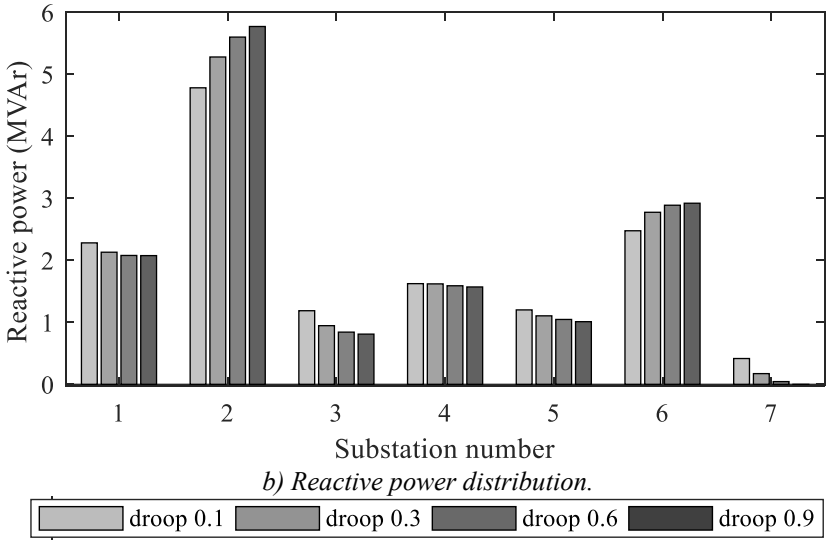

b) Reactive power distribution.

Figure 5.17. Power sharing analysis.
Madrid-Valencia high-speed line. Advanced AC bivoltage converter-based system.

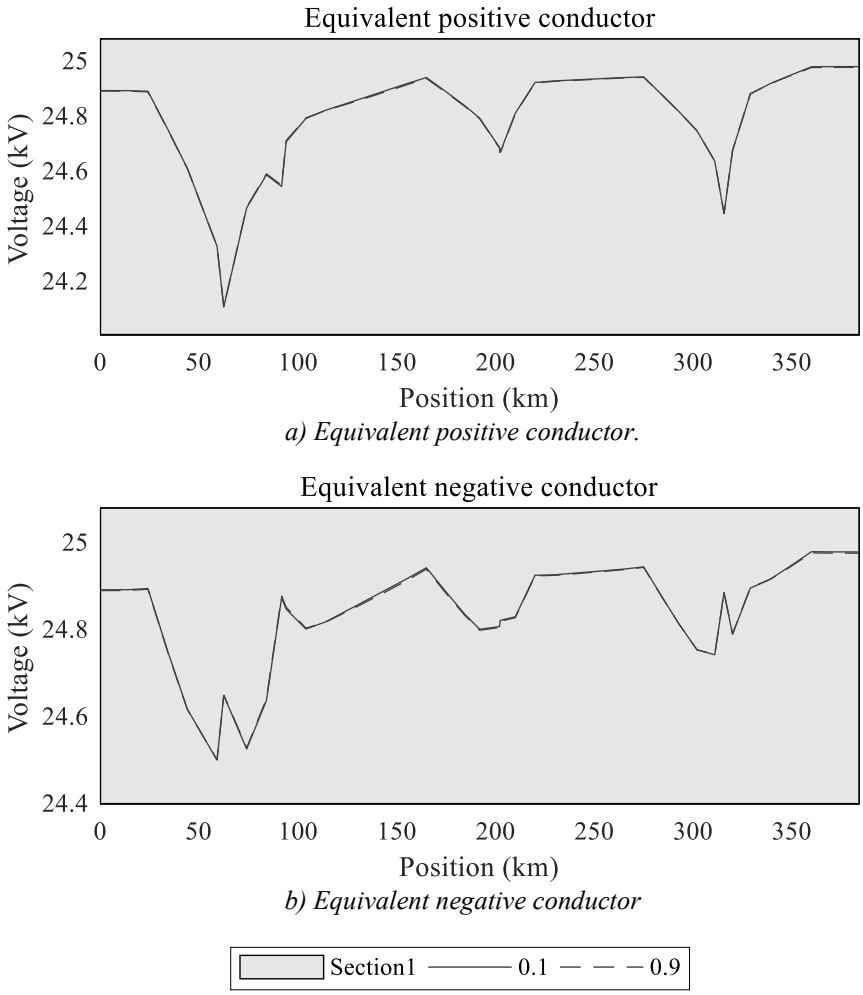

a) Equivalent positive conductor.

b) Equivalent negative conductor

Figure 5.18. Power sharing analysis.Voltage analysis.
Madrid-Valencia high-speed line. Advanced AC bivoltage converter-based system.

In order to validate the reliability of the new operation points, it is necessary to study the voltage magnitude of the equivalent positive and genitive conductor for the two extreme angle droop parameters: 60/0.1MW/rad and 60/0.9MW/rad. As it can be observed in Figure 5.18.a and Figure 5.18.b, the voltage magnitude for the equivalent positive and negative conductors for the two angle droop parameters are almost identical. This can be explained by the fact that the voltage droop is principally governed by the reactive power.

5.3.3 Advanced DC converter-based system

a) Input data

The advanced DC converter-based electrification scheme has been performed by simply replacing the current transformer-based traction substations with the corresponding converter-based ones and connecting all the electrical sections. Furthermore, the autotransformers have been substituted with equivalent DC/DC converters including an

additional one at the front of each traction substation in order to balance the current of the positive and negative conductors. Finally, a three-phase transformer is used to adapt the utility grid voltage to converter voltage level at each traction substation. The transformer voltage ratio has been selected to allow the converter to work in linear modulation zone under all possible conditions.

According to this information, the system configuration is depicted in Figure 5.19, where the where ST denoted station, CS converter substation and ACS autoconverter substation. The parameters of the different electrical elements are listed in Table 5.5. As it is observed, the voltage droop parameters of the traction converters are set to 60MW/2000V. According to results obtained in chapter four, this value ensures and efficient distribution of the electrical power that it is the operation goal under normal grid conditions.

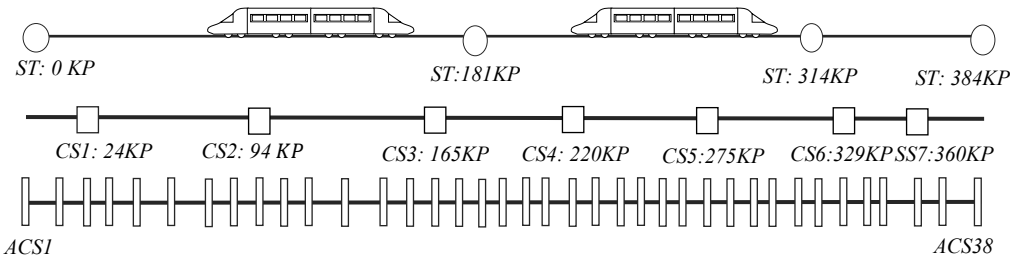

Figure 5.19. Madrid-Valencia high-speed line. Advanced DC converter-based bivoltage system.

Table 5.5. Eletrical parameters. Madrid-Valenia high-speed line. Advanced DC converter-based bivoltage system.

Utility grid	
Nominal voltage(kV)	*220*
Short circuit power (GW)	*10*
R/X	*0*
Transformers	
Voltage Ratio	*220/24*
Nominal Power (MVA)	*60*
Short circuit impedance (pu)	*0.1j*
Converter Stattions	
Nominal Power (MW)	*60*
Voltage droop factor (MW/V)	*60/3000*
Catenary	
Impedance (Ω/km)	$1e-3\begin{bmatrix} 0.11+0.28j & 0.07+0.12j \\ 0.07+0.12j & 0.13+0.31j \end{bmatrix}$

b) Operation analysis

Figure 5.20.a and Figure 5.20.b describe the geometrical locus of the voltage between the maximum and the minimum values obtained for the equivalent positive and negative conductors over their length during the whole traffic operation. These figures also include the mean voltage calculated for each position of the conductor during the whole time period. As in the advanced AC converter-based system, the figures only present a single electrical section due to the inexistence of neutral zones.

According to Figure 5.20.a, the minimum voltage for the equivalent positive conductor has a value of 23.83kV and it is obtained at the 120KP. This value is superior to the one obtained for the transformer-based and advanced AC converter-based systems. The comparison between AC and DC advanced converter-based system is not that easy because the difficulty of defining an equivalent droop angle that produces the same power

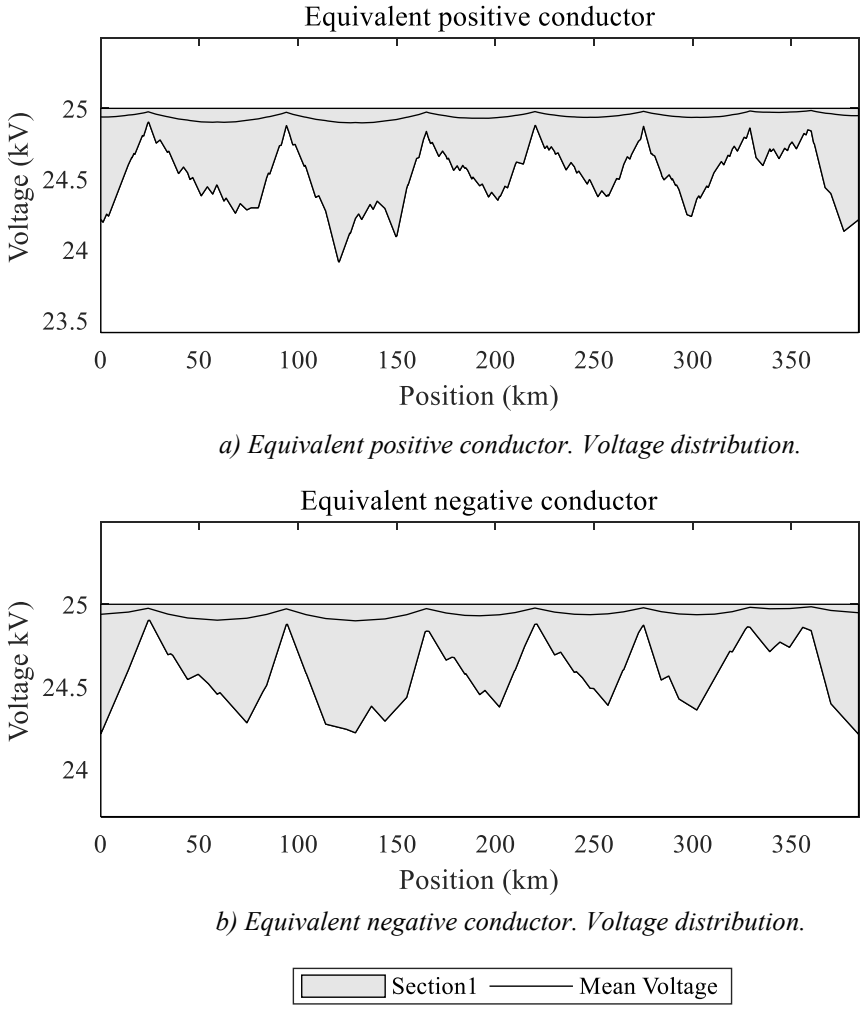

a) Equivalent positive conductor. Voltage distribution.

b) Equivalent negative conductor. Voltage distribution.

Figure 5.20. Voltage distribution. Madrid-Valencia high-speed line. Advanced DC bivoltage converterr-based system.

distribution. However, it also true that for the lowest possible angle and voltage droop parameters, the voltages drops are always lower for the DC systems because the reduction of the line losses. For the negative equivalent conductor, the minimum voltage level has a value of 24,08kV and it is obtained at the end of the last electrical section. Once again, the voltage drops are lower than for the two previous systems.

Figure 5.21.a describes the geometrical locus of the current between the maximum and the minimum values obtained for the equivalent positive conductor over its length for the whole traffic timetable. It has also been included the quadratic mean current calculated for each position of the conductor during the whole time period. The maximum current value is 0.66kA and it is reached at the 284KP. It is observed that this value its higher than the one obtained for the advanced AC case. This situation is motivated by the less power cooperation between tractions substations.

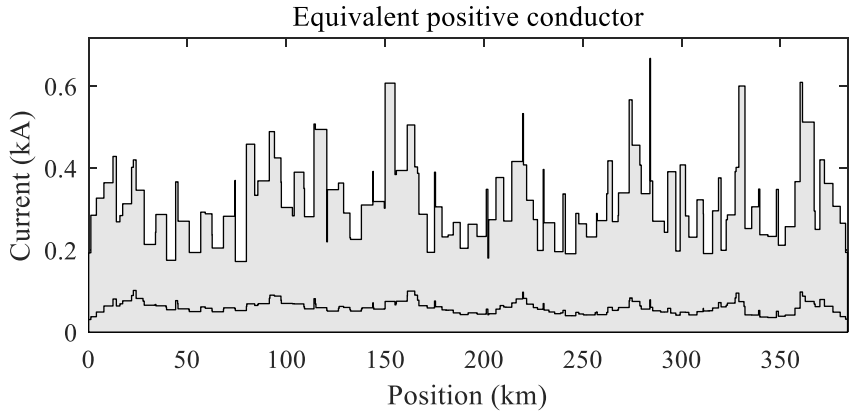

a) Equivalent positive conductor. Current distribution.

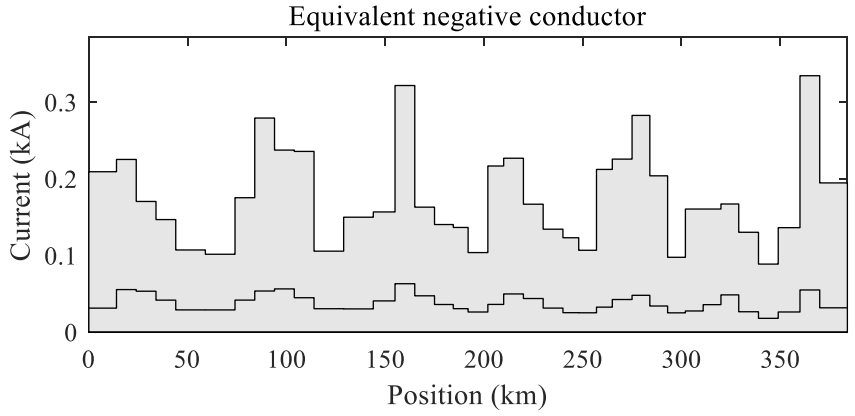

b) Equivalent negative conductor. Current distribution.

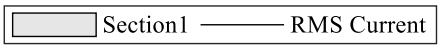

Figure 5.21. Current distribution. Madrid-Valencia high-speed line. Advanced DC bivoltage converter-based system.

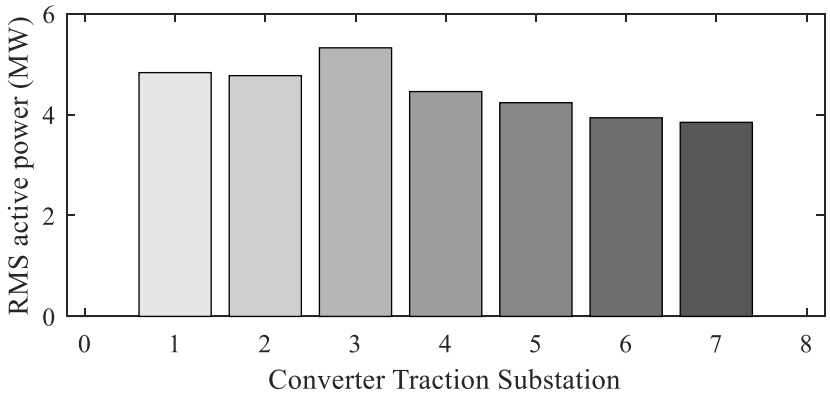

Figure 5.22. Power distribution. Madrid-Valencia high-speed line. Advanced DC bivoltage converter-based system.

On the other hand, Figure 5.21.b describes the same analysis but for the equivalent negative conductor. In this case, the maximum current observed has a value of 0.33kA and it is reached for the conductor positions between 360KP and 370KP. Finally, it is noted the less variability of the current distribution in this electrical scheme. This issue can be explained by the better performance of the DC/DC converters to distribute the current between the positive and negative conductors.

Figure 5.22 illustrates the mean square active power provided by each traction substation during the whole traffic timetable. As it is noted, the mean square values have been reduced in comparison to the ones obtained for the conventional transformer-based systems. In this case the highest quadratic mean value is 5.03 MW for the third substation and the lowest value, 3.66 MW for the seventh. It is observed, that these values produce a less cooperation between tractions substations as it was highlighted in the current analysis.

c) Power sharing analysis

This subsection analyzes the effectiveness of control strategy proposed under a possible utility grid requirement of increasing the active power cooperation between the traction substations. Following the same methodology used for the AC case, the voltage droop parameters of the tractions substations have been increasing to enable a maximum voltage drop of 1000 V, 2000 V and 3000 V. In order to facilitate the analysis and the comparison with the AC case, the same simulations instant have been studied.

Figure 5.23 shows the active power provided by each traction substations for the voltage droop parameters 60/1000 MW, 60/2000 MW/V and 60/3000 MW/V. As it can be observed, the power sharing increases as the voltage droop decreases, so that the difference between the most loaded and less loaded substations are reduced. However, these droop values do not allow to obtain a significant power cooperation as in the AC case. It has been

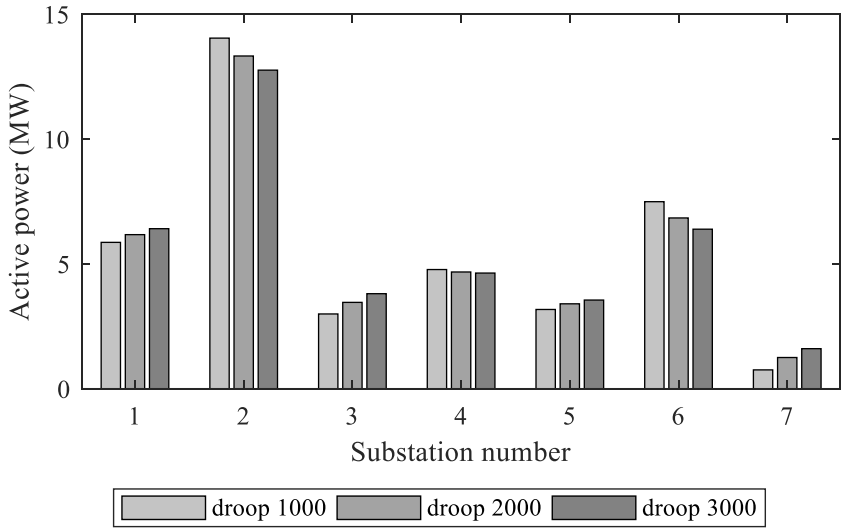

Figure 5.23. Power sharing analysis.
Madrid-Valencia high-speed line. Advanced DC bivoltage converter-based system.

simulated for lower voltage droop parameters, but the algorithm fails to converge. The reason behind this issue, is that the solution is approaching to a maximum as the voltage droop parameters is increased and so that the Jacobian matrix turns into singular. According to this information, this thesis suggests the investigation of alternative derivate-free based methods to solve the power flow for DC advanced-converter-based systems.

Finally, in order to analyze the reliability of the new operation points reached by the new droop parameters, the voltage magnitude distribution of the equivalent positive and negative conductors are shown in Figure 5.24.a and Figure 5.24.b respectively. As it was presented in chapter four, the increase of the droop voltage values leads to a higher voltage drops in the conductors.

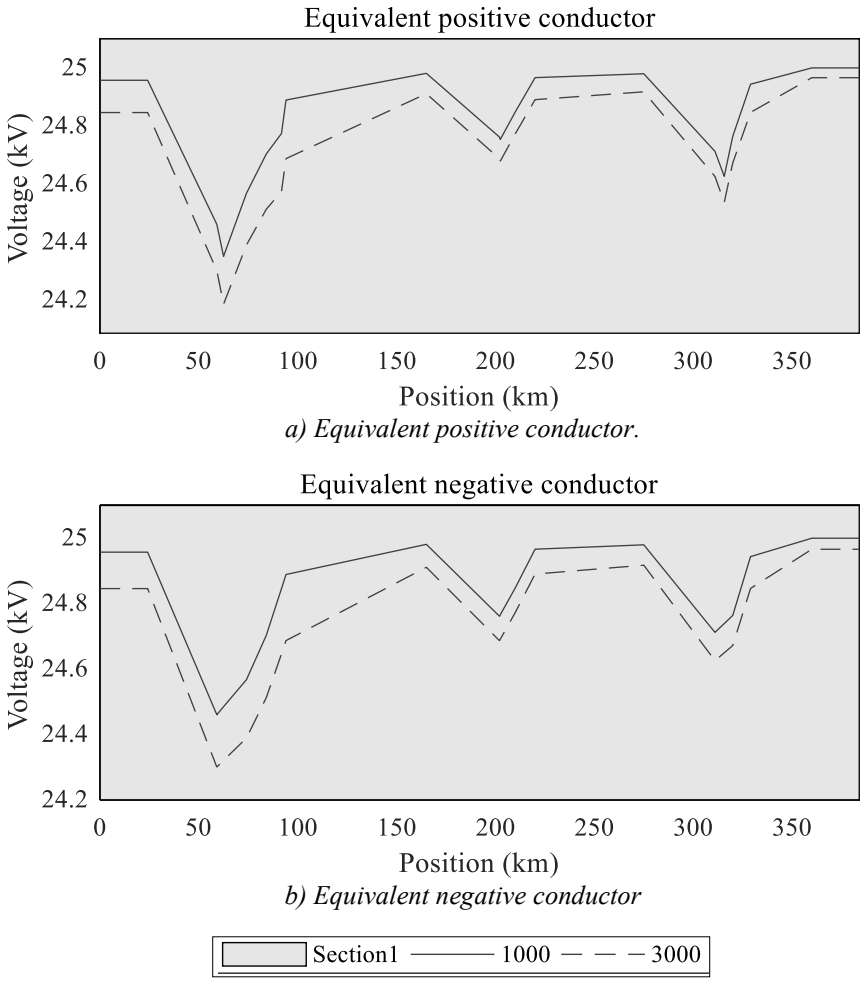

a) Equivalent positive conductor.

b) Equivalent negative conductor

Figure 5.24. Power sharing analysis. Madrid-Valencia high-speed line. Advanced AC bivoltage converter-based system.

Chapter 6

Closure

6.1 Conclusions

This section describes and summarizes the main conclusions drawn in this thesis. In order to facilitate their analysis, the conclusions have been organized according to the three main parts addressed in the dissertation, i.e. the analysis, simulation and operation of electrical railway power supply systems for high-speed lines.

- **Analysis of electrical railway power supply systems**

Electrical railway power supply systems can be classified into transformer-based systems and converter-based systems. Conventional transformer-based configurations are simple and reliable electrification schemes for high-speed lines, but they present strong drawbacks from the power quality point of view that reduce their potential and increases their cost. In order to minimize the impact of these drawbacks, new technological solutions have been proposed: balancing transformers and converter compensators.

Balancing transformers can solve the power imbalance, but they are only effective for dense traffic conditions. Converter compensators present a better performance, but their costs are still high with regard to the functionalities provided. Among the different converter compensators, the co-phase system deserves an especial attention since it enables to reduce the number of neutral zones by half. Despite all these enhancements, it is important to highlight that all these new configurations do not allow to perform an active control of the electrical power in the railway grid.

The use of converter-based systems for the electrification of high-speed lines has been traditionally very limited due to the high cost of the converter. However, they present some interesting characteristics that make this option very attractive: a continuous catenary and a balance operation. At the light of these advantages, researchers have proposed the

development of advanced converter-based systems that make use of modern power converters capable of using higher transmission voltage levels and performing a total controllable power management of the railway grid. This latter characteristic involves a real qualitative leap in railway electrification that modifies completely the way electrical railway systems are operated.

The utilization of AC or DC in advanced configurations is still a debate under discussion. The simple control and lower power losses of DC systems make this option very promising, but the doubts about the fault clearance capability and the necessity of rolling stock development turn AC systems a more realistic option at present.

- **Simulation of electrical railway power supply systems**

Railway simulation is a very powerful tool for the study of the electrical power supply system operation. It requires the simulation of two different systems, the traffic system and the electrical system. Depending on the interaction considered between them, there are two main simulation approaches: decoupled and coupled. When the focus of the study is on the electrical system, the decoupled simulation is the most extended option.

The simulation of the traffic system is normally divided into two parts. In the first part, the simulation of the movement of a single train for all circulating directions is determined. This simulation is based on a force balance analysis. Depending on how the active force performed by the train is used, different driving strategies can be defined. In the second part, the results obtained are extended to the rest of the trains according to the traffic timetable defined.

The simulation of the electrical system is typically performed by means of a steady state analysis. The steady state analysis of conventional transformer-based systems is more similar to the steady state analysis of distribution systems than transmission systems. According to literature, there are three principal distribution power flow methods used in the study of conventional transformer-based electrical railway systems: Gauss-Seidel, backward/forward sweep and current injection.

Conventional distribution power flow methods are not good candidates for the solution of advanced converter-based systems. The control strategies performed on the converter and their non-grounded connections in the bivoltage catenary configurations complicate enormously the implementation of these methods. Accordingly, they require the utilization of general power flow formulations such as the multiphase power flow. This method uses a modified nodal analysis and provides a systematic Jacobian formulation that can

reproduce any network topology and any control device law straightforwardly. Regarding the solution of hybrid AC/ DC systems, there are two methods depending on how the equations of AC and DC are solved: sequential and unified. Both approaches define different equations for AC and DC grids increasing the computational burden unnecessarily.

The system formulation depends on the power flow method used. In multiphase power flow method, the elements are represented by a combination of a passive network and active network. The passive grid is modelled using and admittance matrix, while the active network as branch constrains. While the representation of the catenary, transformers, utility grid and train models are comprehensively studied in literature, there representation of VSC converters in railway systems still need further development. This is especially critical for DC/DC converters where there is not any model reported so far.

The multiphase power flow is based on a Newton-Raphson solving algorithm. The formulation used so far involves the distinction between elements and phases complicating unnecessarily the notation and avoiding the utilization of general control equations. Due to the grid characteristic a full version of the method is needed. Furthermore, the solving algorithm needs a very accurate initial iteration point in order to avoid convergence issues. According to the literature review, there is not any initialization technique reported for this method that includes converters with droop control strategies.

- **Operation of advanced converter-based electrical railway power supply systems**

The enhancement of the reliability, efficiency and cost of the electrical operation of conventional transformer-based systems is very limited due to the radial configuration presented and the few number of controllable elements included. In this situation, all the measures undertaken so far are aimed to development of train control strategies that adapt their operation according to the catenary voltage condition existing. The introduction of advanced converter-based systems can change this situation radically. The utilization of a continuous catenary along with controllable converter substations enable to adapt the power distribution according to the traffic and utility grid conditions.

The operation of advanced converter-based configurations is essentially determined by the control system implemented. The operation of converter-based grids is now a hot topic on electrical engineering, but their application to railway grids is little explored. Among the control strategies, droop control methods are especially convenient for extended geographical systems such as railway grids, since they reduce the use communication channels between the traction substations.

Under normal utility grid conditions, the system should distribute the power according to the distance between the traction substations and the trains. To this end, it is necessary to incorporate the traffic information to the droop characteristics. The use of local variables, such as the angle and the voltage as control variables can perform this task due to the fact that they are affected by the line impedance. This effect depends on the value of the droop coefficients defined, so that for high droop values the power is distributed according to the distance and for low droop values the power is distributed according to droop coefficients ratio. This latter case can be used to enhance the grid stability.

The models and algorithms used and proposed in the thesis present coherent simulation results such as the voltage, the current and the power distributions for conventional transformer-based and advanced AC and DC converter-based railway systems. Furthermore, the results validate the control strategy proposed for AC and DC, obtaining an efficient power flow distribution for high droop values and a cooperation power distribution for low droop values. Finally, the DC/DC converter model proposed shows a perfect current balance performance.

The operation of the converter-based systems presents a more efficient power transmission than conventional transformer-based systems, enabling to reduce the quadratic mean power and the loading differences between the traction substations. Despite the lower line losses of DC systems, the control strategy proposed to increase the power cooperation between substations is more efficient for AC because the active power is principally regulated by the angle difference.

The results obtained for the whole complete high-speed line validates the robustness of the simulation tool and the effectiveness of the control system for larger and more complex systems. It also evidences the necessity of defining new solving algorithms for advanced DC converter-based system for low droop values. Secondly, the results prove the feasibility and potential of advanced converter-based systems over conventional transformer-based systems for the electrification of high-speed lines.

6.2 Contributions

This section presents the main contributions achieved in this thesis. Following the same analysis methodology used for the conclusions, the contributions have been organized according to the three main parts addressed in the dissertation, i.e. the analysis, simulation and operation of electrical railway power supply systems for high-speed lines.

- **Analysis of electrical railway power supply systems**

It has been proposed a new classification of the electrical railway power supply systems according to the type of traction substation used. In contrast to conventional classification based on the electrical current nature (AC industry frequency, AC low frequency and DC), this new aggrupation (transformer-based and converter-based) reflects clearer the two directions existing now in the electrification of high-speed lines.

It has been done a comprehensive review of the principal electrification schemes existing and proposed in literature. Although there are some other good reviews, they do not analyze their suitability for high-speed lines, the main focus of this thesis. Furthermore, they typically do not include intermediate solutions, such as balancing transformer or power conditioners.

- **Simulation of electrical railway power supply systems**

This work includes the definition of a generalized power flow formulation for conventional and advanced electrical railway power supply systems. The formulation is capable of including AC and DC elements in the same equations and it avoids to distinguish between phases and between elements, reducing the number of different equations needed.

A model for the DC/DC autoconverter stations has been developed. The implementation of bivoltage catenary configuration in DC electrification schemes requires the use of DC/DC power converters that play the role of the autotransformers in AC railway systems. To the author's knowledge, there is not any DC/DC autotransformer substation model reported in literature.

A novel initialization technique for the Newton-Raphson algorithm has been proposed. As it was explained, multiphase power flow requires of a good initial point to converge. The typical flat initial point tends to diverge for all the cases studied. To avoid this, this thesis suggests and initial linear system of equations capable of providing convergence for most of the cases studies.

- **Operation of advanced converter-based electrical railway power supply systems**

It has been done a thorough analysis of the operation of conventional transformer-based systems and a discussion of the possible operation control strategies applicable to the advanced converter-based systems. Although there are many reviews of converter-based systems, their application to railway grids is not addressed.

A new operation control system for AC and DC advanced converter-based system has been implemented and proposed. As it has been described before, the operation of advanced converter-based systems is essentially determined by the control system implemented. So far, all the control strategies proposed have been focused on the performance of individual converters avoiding to address the operation of the whole system. In this sense, this thesis has proposed a new operation control strategy capable of distributing efficiently the load among the traction based on the concept of droop control. For the AC case, an angle droop control is selected because it enables to incorporate the impedance effect on the power distribution.

6.3 Publications

This section includes the publications obtained during the thesis. They have been organized into journal and conference publications in reverse chronological order.

- Journal papers

D. Serrano-Jimenez, L. Abrahamsson, S. Castano-Solis, and J. Sanz-Feito, "Electrical railway power supply systems: Current situation and future trends," *Int. J. Electr. Power Energy Syst*., vol. 92, pp. 181–192, Nov. 2017.

- Conference papers

D. Serrano-Jimenez, J. Sanz-Feito, and S. Castano-Solis, "Modeling, Simulation and Analysis of an Advanced Mono-Voltage DC Converter-Based Electrical Railway Power Supply System for High Speed Lines," in *2017 IEEE Vehicle Power and Propulsion Conference (VPPC)*, 2017, pp. 1–5.

D. Serrano-Jimenez, M. Montilla-DJesus, E. Vergel-Medina, and J. Sanz-Feito, "Regenerative Braking Analysis of Conventional High Speed Railway Lines," in *2017 IEEE Vehicle Power and Propulsion Conference (VPPC)*, 2017, pp. 1–4.

L. Abrahamsson, D. Serrano-Jimenez, J. Laury, M. Bollen, "AC Cables Strengthening Railway Low Frequency AC Power Supply Systems" in 2017 *ASME/IEEE Joint Rail Conference, 2017*.

D. Serrano-Jimenez, J. Sanz-Feito, and S. Castano-Solis, "Advanced DC power supply system for high speed railways" in *11th World Congress on Railway Research (WCRR)*, Jun. 2016.

D. Serrano-Jimenez, S. Castano-Solis and , J. Sanz-Feito "Advanced power supply systems for high speed railways" in *17th edition of the European PhD School*, May. 2016.

6.4 Future works

This last section suggests some possible research directions in order to complete and enhance the work initiated in this thesis.

Regarding the electrical modeling, one possible first work can be the development of detailed mathematical expressions for the calculation of the converter power losses in steady state. As explained before, this issue has been widely discussed for single VSCs, but their application to combination of VSCs requires further investigations. The calculation of the converter power losses is a very important issue in order to perform a rigorous efficiency comparison between transformer-based and converter-based configurations.

Regarding the solving algorithm, one important work is the development of more robust resolution methods for DC advanced converter-based systems. As described before, the algorithm used fails to converge when the droop parameters of the converters are enough low. This is motivated by the proximity of the solution to a maximum that makes the Jacobian matrix singular. Accordingly, it would be interesting the utilization of derivative free approaches to overcome this undesired situation.

Another possible future work is the definition of power control strategies for advanced AC converter-based systems capable of decoupling the active and reactive power flow. As presented in chapter four, the modification of the active power sharing between traction substations is achieved by means of the angle droop parameter variations. However, due to the active and reactive power coupling existing, this variation not only affects the active power sharing but also the reactive one.

Finally, other further work is the development of a secondary control strategy for advanced converter-based DC systems that reduces the voltage drop motivated by the droop control. This issue is especially important when a high power sharing is required. In order to avoid it, this thesis suggest the possibility of including a secondary control that updates the voltage sets depending on the voltage condition of the whole railway grid.

References

[1] European Commission, “Roadmap to a Single European Transport Area - Towards a competitive and resource efficient transport system.” Brussels, p. 30, 2011.

[2] European Commission, “High-speed Europe. A sustainble link between citizens.” Luxembourg, p. 22, 2010.

[3] R. J. Hill, “Electric railway traction. Part 3: Traction power supplies,” *Power Eng. J.*, vol. 8, no. 6, pp. 275–286, Dec. 1994.

[4] T. Oura, Y. Mochinaga, and H. Nagasawa, “Railway Electric Power Feeding Systems,” *Japan Railw. Transp. Rev.*, no. 16, pp. 48–58, 1998.

[5] L. Abrahamsson, T. Schütte, and S. Östlund, “Use of converters for feeding of AC railways for all frequencies,” *Energy Sustain. Dev.*, vol. 16, no. 3, pp. 368–378, Sep. 2012.

[6] A. Steimel, “Power-electronic grid supply of AC railway systems,” in *2012 13th International Conference on Optimization of Electrical and Electronic Equipment (OPTIM)*, 2012, pp. 16–25.

[7] D. Serrano-Jiménez, L. Abrahamsson, S. Castaño-Solís, and J. Sanz-Feito, “Electrical railway power supply systems: Current situation and future trends,” *Int. J. Electr. Power Energy Syst.*, vol. 92, pp. 181–192, Nov. 2017.

[8] S. M. Mousavi Gazafrudi, A. Tabakhpour Langerudy, E. F. Fuchs, and K. Al-Haddad, “Power Quality Issues in Railway Electrification: A Comprehensive Perspective,” *IEEE Trans. Ind. Electron.*, vol. 62, no. 5, pp. 3081–3090, May 2015.

[9] Shi-Lin Chen, Fu-Chien Kao, and Tsung-Ming Lee, “Specification of minimum short circuit capacity for three-phase unbalance evaluation of high-speed railway power system,” in *Proceedings 1995 International Conference on Energy Management and Power Delivery EMPD ’95*, 1995, vol. 1, pp. 323–330.

[10] I. Saboya, I. Egido, E. Pilo, and L. Rouco, “Impact of high-speed trains in small isolated power system phase to phase imbalances,” in *WIT Transactions on The Built Environment*, 2012, vol. 127, pp. 615–626.

[11] J. E. Parton, “A general theory of phase transformation,” *Proc. IEE - Part IV Inst. Monogr.*, vol. 99, no. 2, pp. 12–23, Apr. 1952.

[12] Bin-Kwie Chen and Bing-Song Guo, “Three phase models of specially connected transformers,” *IEEE Trans. Power Deliv.*, vol. 11, no. 1, pp. 323–330, 1996.

[13] Zhiwen Zhang, Bin Wu, Jinsong Kang, and Longfu Luo, “A Multi-Purpose Balanced Transformer for Railway Traction Applications,” *IEEE Trans. Power Deliv.*, vol. 24, no. 2, pp. 711–718, Apr. 2009.

[14] T.-H. Chen, “Criteria to estimate the voltage unbalances due to high-speed railway demands,” *IEEE Trans. Power Syst.*, vol. 9, no. 3, pp. 1672–1678, 1994.

[15] T. H. Chen, “Network modelling of traction substation transformers for studying unbalance effects,” *IEE Proc. - Gener. Transm. Distrib.*, vol. 142, no. 2, p. 103, 1995.

[16] Hung-Yuan Kuo and T.-H. Chen, “Rigorous evaluation of the voltage unbalance due to high-speed railway demands,” *IEEE Trans. Veh. Technol.*, vol. 47, no. 4, pp. 1385–1389, 1998.

[17] Hu Yu, Yuan Yue, Chen Zhe, Chen Zhifei, and Tao Ye, “Research on the selection of railway traction transformer,” in *2010 Conference Proceedings IPEC*, 2010, pp. 677–681.

[18] H. E. Mazin and W. Xu, “Harmonic cancellation characteristics of specially connected transformers,” *Electr. Power Syst. Res.*, vol. 79, no. 12, pp. 1689–1697, Dec. 2009.

[19] M. H. Rashid, *Power electronics handbook: devices, circuits, and applications*, vol. 2nd; 2; 2. Burlington, MA: Academic Press.

[20] R. Grünbaum, “SVC for the Channel Tunnel Rail Link: providing flexibility and power quality in rail traction,” in *IEE Seminar on Power - it’s a Quality Thing*, 2005, pp. 3–3.

[21] G. Celli, F. Pilo, and S. B. Tennakoon, “Voltage regulation on 25 kV AC railway systems by using thyristor switched capacitor,” in *Ninth International Conference*

on Harmonics and Quality of Power. Proceedings (Cat. No.00EX441), 2000, vol. 2, pp. 633–638.

[22] Zhu Guiping, Chen Jianye, and Liu Xiaoyu, "Compensation for the negative-sequence currents of electric railway based on SVC," in *2008 3rd IEEE Conference on Industrial Electronics and Applications*, 2008, pp. 1958–1963.

[23] L. Sainz, L. Monjo, S. Riera, and J. Pedra, "Study of the Steinmetz Circuit Influence on AC Traction System Resonance," *IEEE Trans. Power Deliv.*, vol. 27, no. 4, pp. 2295–2303, Oct. 2012.

[24] P.-C. Tan, P. C. Loh, and D. G. Holmes, "A Robust Multilevel Hybrid Compensation System for 25-kV Electrified Railway Applications," *IEEE Trans. Power Electron.*, vol. 19, no. 4, pp. 1043–1052, Jul. 2004.

[25] A. Bueno, J. M. Aller, J. A. Restrepo, R. Harley, and T. G. Habetler, "Harmonic and Unbalance Compensation Based on Direct Power Control for Electric Railway Systems," *IEEE Trans. Power Electron.*, vol. 28, no. 12, pp. 5823–5831, Dec. 2013.

[26] Y. Mochinaga, Y. Hisamizu, M. Takeda, T. Miyashita, and K. Hasuike, "Static power conditioner using GTO converters for AC electric railway," in *Conference Record of the Power Conversion Conference - Yokohama 1993*, 1993, pp. 641–646.

[27] A. Luo, W. Wu, J. Shen, and S. Z., "Railway Static Power Conditioners for High-speed Train Traction Power Supply Systems Using Three-phase V/V Transformers," *IEEE Trans. Power Electron.*, vol. 26, no. 10, pp. 2844–2856, Oct. 2011.

[28] F. Ma, A. Luo, X. Xu, H. Xiao, C. Wu, and W. Wang, "A Simplified Power Conditioner Based on Half-Bridge Converter for High-Speed Railway System," *IEEE Trans. Ind. Electron.*, vol. 60, no. 2, pp. 728–738, Feb. 2013.

[29] Z. Sun, X. Jiang, D. Zhu, and G. Zhang, "A Novel Active Power Quality Compensator Topology for Electrified Railway," *IEEE Trans. Power Electron.*, vol. 19, no. 4, pp. 1036–1042, Jul. 2004.

[30] C. Wu, A. Luo, J. Shen, F. J. Ma, and S. Peng, "A Negative Sequence Compensation Method Based on a Two-Phase Three-Wire Converter for a High-Speed Railway Traction Power Supply System," *IEEE Trans. Power Electron.*, vol. 27, no. 2, pp. 706–717, Feb. 2012.

[31] S. Hu *et al.*, "A New Integrated Hybrid Power Quality Control System for Electrical Railway," *IEEE Trans. Ind. Electron.*, vol. 62, no. 10, pp. 6222–6232, Oct. 2015.

[32] F. Ma *et al.*, "A Railway Traction Power Conditioner Using Modular Multilevel Converter and Its Control Strategy for High-Speed Railway System," *IEEE Trans. Transp. Electrif.*, vol. 2, no. 1, pp. 96–109, Mar. 2016.

[33] Z. Shu, S. Xie, and Q. Li, "Single-Phase Back-To-Back Converter for Active Power Balancing, Reactive Power Compensation, and Harmonic Filtering in Traction Power System," *IEEE Trans. Power Electron.*, vol. 26, no. 2, pp. 334–343, Feb. 2011.

[34] N.-Y. Dai, M.-C. Wong, K.-W. Lao, and C.-K. Wong, "Modelling and control of a railway power conditioner in co-phase traction power system under partial compensation," *IET Power Electron.*, vol. 7, no. 5, pp. 1044–1054, May 2014.

[35] M. Chen, Q. Li, and G. Wei, "Optimized Design and Performance Evaluation of New Cophase Traction Power Supply System," in *2009 Asia-Pacific Power and Energy Engineering Conference*, 2009, pp. 1–6.

[36] K.-W. Lao, N. Dai, W.-G. Liu, and M.-C. Wong, "Hybrid Power Quality Compensator With Minimum DC Operation Voltage Design for High-Speed Traction Power Systems," *IEEE Trans. Power Electron.*, vol. 28, no. 4, pp. 2024–2036, Apr. 2013.

[37] K.-W. Lao, M.-C. Wong, N. Dai, C.-K. Wong, and C.-S. Lam, "A Systematic Approach to Hybrid Railway Power Conditioner Design With Harmonic Compensation for High-Speed Railway," *IEEE Trans. Ind. Electron.*, vol. 62, no. 2, pp. 930–942, Feb. 2015.

[38] A. Nabae, I. Takahashi, and H. Akagi, "A New Neutral-Point-Clamped PWM Inverter," *IEEE Trans. Ind. Appl.*, vol. IA-17, no. 5, pp. 518–523, Sep. 1981.

[39] T. A. Meynard and H. Foch, "Multi-level conversion: high voltage choppers and voltage-source inverters," in *PESC `92 Record. 23rd Annual IEEE Power Electronics Specialists Conference*, 1992, pp. 397–403.

[40] H. Richard and B. Baker, "Electric power converter," 3867643, 1974.

[41] H. Akagi, "Classification, Terminology, and Application of the Modular Multilevel Cascade Converter (MMCC)," *IEEE Trans. Power Electron.*, vol. 26, no. 11, pp.

3119–3130, Nov. 2011.

[42] M. Glinka and R. Marquardt, “A new AC/AC multilevel converter family,” *IEEE Trans. Ind. Electron.*, vol. 52, no. 3, pp. 662–669, Jun. 2005.

[43] J. Ranneberg, “Transformerless topologies for future stationary AC-railway power supply,” in *2007 European Conference on Power Electronics and Applications*, 2007, pp. 1–11.

[44] X. He *et al.*, “Advanced Cophase Traction Power Supply System Based on Three-Phase to Single-Phase Converter,” *IEEE Trans. Power Electron.*, vol. 29, no. 10, pp. 5323–5333, Oct. 2014.

[45] Z. Shu, X. Xie, and Y. Jing, “Advanced Co-phase Traction Power Supply Simulation Based on Multilevel Converter,” in *Proceedings of the 2011 2nd International Congress on Computer Applications and Computational Science SE - 63*, vol. 145, F. L. Gaol and Q. V. Nguyen, Eds. Springer Berlin Heidelberg, 2012, pp. 459–465.

[46] X. He, A. Guo, X. Peng, Y. Zhou, Z. Shi, and Z. Shu, “A Traction Three-Phase to Single-Phase Cascade Converter Substation in an Advanced Traction Power Supply System,” *Energies*, vol. 8, no. 9, pp. 9915–9929, Sep. 2015.

[47] E. Pilo de la Fuente, S. K. Mazumder, and I. G. Franco, “Railway Electrical Smart Grids: An introduction to next-generation railway power systems and their operation.,” *IEEE Electrif. Mag.*, vol. 2, no. 3, pp. 49–55, Sep. 2014.

[48] D. Laousse, C. Brogard, H. Caron, and C. Courtois, “Direct current- A future under which conditions,” *elektrische bahnen*, vol. 114, pp. 260–275, 2016.

[49] M. L. Erlangen, “High voltage DC power supply - Part 1: Basics ans systems,” *Elektrische bahnen*, vol. 109, pp. 271–275, 2011.

[50] M. L. Erlangen, “High Voltage DC power supply- Part 2: Technology and migration strategies,” *elektrische bahnen*, vol. 109, pp. 672–679, 2011.

[51] A. Gomez-Exposito, J. M. Mauricio, and J. M. Maza-Ortega, “VSC-Based MVDC Railway Electrification System,” *IEEE Trans. Power Deliv.*, vol. 29, no. 1, pp. 422–431, Feb. 2014.

[52] H. Kakigano, Y. Miura, and T. Ise, “Low-Voltage Bipolar-Type DC Microgrid for

Super High Quality Distribution," *IEEE Trans. Power Electron.*, vol. 25, no. 12, pp. 3066–3075, Dec. 2010.

[53] H. Dong, B. Ning, B. Cai, and Z. Hou, "Automatic Train Control System Development and Simulation for High-Speed Railways," *IEEE Circuits Syst. Mag.*, vol. 10, no. 2, pp. 6–18, 2010.

[54] S. N. Talukdar and R. L. Koo, "The analysis of electrified ground transportation networks," *IEEE Trans. Power Appar. Syst.*, vol. 96, no. 1, pp. 240–247, Jan. 1977.

[55] M. Coto, P. Arboleya, and C. González-Morán, "On the Use of Graph Theory for Railway Power Supply Systems Characterization," *Intell. Ind. Syst.*, vol. 1, no. 2, pp. 127–139, Aug. 2015.

[56] A. Stephan, "OpenPowerNet – simulation of railway power supply systems," in *WIT Transactions on The Built Environment*, 2008, vol. 103, pp. 449–459.

[57] S. Hillmansen, R. White, P. Weston, T. Fella, and Y. Chen, "Multi-conductor model for AC railway train simulation," *IET Electr. Syst. Transp.*, vol. 6, no. 2, pp. 67–75, Jun. 2016.

[58] L. Abrahamsson, "Railway Power Supply Models and Methods for Long-term Invement Analysis," School of Electrical Engineering and Computer Science, KTH, 2008.

[59] E. Pilo, L. Rouco, A. Fernandez, and A. Hernandez-Velilla, "A simulation tool for the design of the electrical supply system of high-speed railway lines," in *2000 Power Engineering Society Summer Meeting (Cat. No.00CH37134)*, vol. 2, pp. 1053–1058.

[60] T. Kulworawanichpong, "Multi-train modeling and simulation integrated with traction power supply solver using simplified Newton–Raphson method," *J. Mod. Transp.*, vol. 23, no. 4, pp. 241–251, Dec. 2015.

[61] J. Jong and S. Chang, "Algorithms for generating speed train profiles," *J. East. Asia Soc. Transp. Stud.*, vol. 6, pp. 356–371, 2005.

[62] J. A. Martinez and J. Mahseredjian, "Load flow calculations in distribution systems with distributed resources. A review," in *2011 IEEE Power and Energy Society General Meeting*, 2011, pp. 1–8.

[63] K. Balamurugan and D. Srinivasan, "Review of power flow studies on distribution

network with distributed generation," in *2011 IEEE Ninth International Conference on Power Electronics and Drive Systems*, 2011, pp. 411–417.

[64] M. A. Laughton, "Analysis of unbalanced polyphase networks by the method of phase co-ordinates. Part 1: System representation in phase frame of reference," *Proc. Inst. Electr. Eng.*, vol. 115, no. 8, p. 1163, 1968.

[65] B. Stott, "Review of load-flow calculation methods," *Proc. IEEE*, vol. 62, no. 7, pp. 916–929, 1974.

[66] T.-H. Chen, M.-S. Chen, K.-J. Hwang, P. Kotas, and E. A. Chebli, "Distribution system power flow analysis-a rigid approach," *IEEE Trans. Power Deliv.*, vol. 6, no. 3, pp. 1146–1152, Jul. 1991.

[67] R. C. Dugan and T. E. McDermott, "An open source platform for collaborating on smart grid research," in *2011 IEEE Power and Energy Society General Meeting*, 2011, pp. 1–7.

[68] C. J. Goodman and T. Kulworawanichpong, "Sequential Linear Power Flow Solution For AC Electric Railway Power Supply Systems," *WIT Trans. Built Environ.*, vol. 61, 2002.

[69] T.-Q. Zhao, H.-D. Chiang, and K. Koyanagi, "Convergence analysis of implicit Z-bus power flow method for general distribution networks with distributed generators," *IET Gener. Transm. Distrib.*, vol. 10, no. 2, pp. 412–420, Feb. 2016.

[70] D. Shirmohammadi, H. W. Hong, A. Semlyen, and G. X. Luo, "A compensation-based power flow method for weakly meshed distribution and transmission networks," *IEEE Trans. Power Syst.*, vol. 3, no. 2, pp. 753–762, May 1988.

[71] C. S. Cheng and D. Shirmohammadi, "A three-phase power flow method for real-time distribution system analysis," *IEEE Trans. Power Syst.*, vol. 10, no. 2, pp. 671–679, May 1995.

[72] K. P. Schneider, D. Chassin, Y. Chen, and J. C. Fuller, "Distribution power flow for smart grid technologies," in *2009 IEEE/PES Power Systems Conference and Exposition*, 2009, pp. 1–7.

[73] P. Arboleya, B. Mohamed, C. Gonzalez-Moran, and I. El-Sayed, "BFS Algorithm for Voltage-Constrained Meshed DC Traction Networks With Nonsmooth Voltage-Dependent Loads and Generators," *IEEE Trans. Power Syst.*, vol. 31, no. 2, pp.

1526–1536, Mar. 2016.

[74] S. V. Raygani, A. Tahavorgar, S. S. Fazel, and B. Moaveni, “Load flow analysis and future development study for an AC electric railway,” *IET Electr. Syst. Transp.*, vol. 2, no. 3, p. 139, 2012.

[75] P. A. N. Garcia, J. L. R. Pereira, S. Carneiro, V. M. da Costa, and N. Martins, “Three-phase power flow calculations using the current injection method,” *IEEE Trans. Power Syst.*, vol. 15, no. 2, pp. 508–514, May 2000.

[76] L. R. de Araujo, D. R. R. Penido, S. C. Júnior, J. L. R. Pereira, and P. A. N. Garcia, “Comparisons between the three-phase current injection method and the forward/backward sweep method,” *Int. J. Electr. Power Energy Syst.*, vol. 32, no. 7, pp. 825–833, Sep. 2010.

[77] T. Kulworawanichpong, “Optimising AC electric railway power flows with power electronics control,” University of Birminghan, 2003.

[78] G. Diaz, J. Gomez-Aleixandre, and J. Coto, “Direct Backward/Forward Sweep Algorithm for Solving Load Power Flows in AC Droop-Regulated Microgrids,” *IEEE Trans. Smart Grid*, vol. 7, no. 5, pp. 2208–2217, Sep. 2016.

[79] F. Mumtaz, M. H. Syed, M. Al Hosani, and H. H. Zeineldin, “A Novel Approach to Solve Power Flow for Islanded Microgrids Using Modified Newton Raphson With Droop Control of DG,” *IEEE Trans. Sustain. Energy*, vol. 7, no. 2, pp. 493–503, Apr. 2016.

[80] W. Xu, J. R. Marti, and H. W. Dommel, “A multiphase harmonic load flow solution technique,” *IEEE Trans. Power Syst.*, vol. 6, no. 1, pp. 174–182, 1991.

[81] J. J. Allemong, R. J. Bennon, and P. W. Selent, “Multiphase power flow solutions using EMTP and Newtons method,” *IEEE Trans. Power Syst.*, vol. 8, no. 4, pp. 1455–1462, 1993.

[82] J. Beerten, S. Cole, and R. Belmans, “A sequential AC/DC power flow algorithm for networks containing Multi-terminal VSC HVDC systems,” in *IEEE PES General Meeting*, 2010, pp. 1–7.

[83] M. Baradar and M. Ghandhari, “A Multi-Option Unified Power Flow Approach for hybrid AC/DC Grids incorporating Multi-Terminal VSC-HVDC,” *IEEE Trans. Power Syst.*, vol. 28, no. 3, pp. 2376–2383, 2013.

[84] Chung-Wen Ho, A. Ruehli, and P. Brennan, "The modified nodal approach to network analysis," *IEEE Trans. Circuits Syst.*, vol. 22, no. 6, pp. 504–509, Jun. 1975.

[85] W. H. Kersting, *Distribution system modeling and analysis*. Taylor & Francis, 2012.

[86] I. Dzafic, R. A. Jabr, and H.-T. Neisius, "Transformer Modeling for Three-Phase Distribution Network Analysis," *IEEE Trans. Power Syst.*, vol. 30, no. 5, pp. 2604–2611, Sep. 2015.

[87] M. Bazrafshan and N. Gatsis, "Comprehensive Modeling of Three-Phase Distribution Systems via the Bus Admittance Matrix," *IEEE Trans. Power Syst.*, pp. 1–1, 2017.

[88] J. Beerten, S. Cole, and R. Belmans, "Generalized Steady-State VSC MTDC Model for Sequential AC/DC Power Flow Algorithms," *IEEE Trans. Power Syst.*, vol. 27, no. 2, pp. 821–829, May 2012.

[89] X.-P. Zhang, "Multiterminal Voltage-Sourced Converter-Based HVDC Models for Power Flow Analysis," *IEEE Trans. Power Syst.*, vol. 19, no. 4, pp. 1877–1884, Nov. 2004.

[90] E. Acha, C. R. Fuerte-Esquivel, H. Ambriz-Pérez, and C. Angeles-Camacho, *FACTS : modelling and simulation in power networks*. Chichester, UK: John Wiley & Sons, Ltd, 2004.

[91] Q. Zhao, J. García-González, O. Gomis-Bellmunt, E. Prieto-Araujo, and F. M. Echavarren, "Impact of converter losses on the optimal power flow solution of hybrid networks based on VSC-MTDC," *Electr. Power Syst. Res.*, vol. 151, pp. 395–403, Oct. 2017.

[92] CENELEC, "European Standard EN50163-Railway Applications-Supply voltages of traction systems." 2004.

[93] CENELEC, "European Standard EN50388 -Railway applications -Power supply and rolling stock - Technical criteria for the coordination between power supply (substation) and rolling stock to achieve interoperability." 2005.

[94] D. E. Olivares *et al.*, "Trends in Microgrid Control," *IEEE Trans. Smart Grid*, vol. 5, no. 4, pp. 1905–1919, Jul. 2014.

[95] T. Dragicevic, X. Lu, J. Vasquez, and J. Guerrero, "DC Microgrids–Part I: A Review of Control Strategies and Stabilization Techniques," *IEEE Trans. Power Electron.*, pp. 1–1, 2015.

[96] J. M. Guerrero, J. C. Vasquez, J. Matas, L. G. de Vicuna, and M. Castilla, "Hierarchical Control of Droop-Controlled AC and DC Microgrids—A General Approach Toward Standardization," *IEEE Trans. Ind. Electron.*, vol. 58, no. 1, pp. 158–172, Jan. 2011.

[97] J. Rocabert, A. Luna, F. Blaabjerg, and P. Rodríguez, "Control of Power Converters in AC MicrogridsRocabert, J., Luna, A., Blaabjerg, F., & Rodríguez, P. (2012). Control of Power Converters in AC Microgrids. IEEE Transactions on Power Electronics, 27(11), 4734–4749. http://doi.org/10.1109/TPEL.2012.2199334," *IEEE Trans. Power Electron.*, vol. 27, no. 11, pp. 4734–4749, Nov. 2012.

[98] R. Teixeira Pinto, P. Bauer, S. F. Rodrigues, E. J. Wiggelinkhuizen, J. Pierik, and B. Ferreira, "A Novel Distributed Direct-Voltage Control Strategy for Grid Integration of Offshore Wind Energy Systems Through MTDC Network," *IEEE Trans. Ind. Electron.*, vol. 60, no. 6, pp. 2429–2441, Jun. 2013.

[99] R. Majumder, A. Ghosh, G. Ledwich, and F. Zare, "Angle droop versus frequency droop in a voltage source converter based autonomous microgrid," in *2009 IEEE Power & Energy Society General Meeting*, 2009, pp. 1–8.

[100] T. Tereid, "Active control of reactive power in a modern electrical rail vehicle," Norwegian University of Science and Technology, 2011.

[101] RENFE, "www.renfe.es." .